

772-19298c
CR-128546



THE JOHNS HOPKINS UNIVERSITY

DEPARTMENT
OF
PHYSICS

TECHNICAL LIBRARY
BUILDING 45

NOV 8 1972

Manned Spacecraft Center
Houston, Texas 77058

SPECIAL REPORT

NASA/MSC Contract NAS 9-11528

Task I. Principal Investigator Services

DIFFUSE REFLECTIVITY OF THE
LUNAR SURFACE

Submitted by
Wm. G. Fesie
Principal Investigator

January 15, 1972

Baltimore, Maryland 21218

THE JOHNS HOPKINS UNIVERSITY

DEPARTMENT OF PHYSICS
HOLTHOOD CAMPUS
BALTIMORE, MARYLAND 21218

January 15, 1972

To: Distribution

From: Wm. G. Fastie, Principal Investigator

Subject: Special Report on the Diffuse Reflectivity of the Lunar Surface.
NASA/MSC Contract NAS 9-11528. Task I - Principal Investigator Services.

We submit herewith a special Principal Investigator's report, prepared with the aid of Richard C. Henry (co-investigator), giving our study of previous work on lunar reflectivity and the steps we are taking to obtain lunar samples for the purpose of measuring their ultraviolet diffuse reflectivity.



Wm. G. Fastie

WGF:ec

Distribution:

10 copies NASA/MSC, L. McFadin
1 copy " " , D. D. Clayton
1 " " " , E. Jones
1 " " " , N. Hardee
1 " " " , E. Smith
1 " " " , H. Harvey
1 " ONRRR/JHU, W. B. Girkin
1 " APL/JHU, T. Wyatt
1 " APL/JHU NASARR, D. Beeman
1 " JHU, A. Ashton
1 " NASA, E. Esenwein, Jr.
1 " NASA/GSFC, J. Diggins
1 " Henry J. Smith
1 " John Pomeroy
1 " C. A. Barth, Univ. of Colorado
1 " G. Thomas, Univ. of Colorado
1 " T. M. Donahue, Univ. of Pittsburgh
1 " R. Henry, JHU
1 " • P. Feldman, JHU
22 copies File

SPECIAL REPORT

DIFFUSE REFLECTIVITY OF THE LUNAR SURFACE

Submitted by

**Wm. G. Fastie
Principal Investigator**

**The Johns Hopkins University
Department of Physics
Baltimore, Maryland 21218**

NASA/MSC Contract NAS 9-11528

Task I. Principal Investigator Services

January 15, 1972

I. INTRODUCTION

The Technical Supporting Studies Plan DRD No. MA-091T under NASA/MSC Contract NAS 9-11528, "Task I. Principal Investigator Services," calls for "acquisition of information about the UV albedo of the moon in the spectral region 1175 to 1675 in order to make it possible to roughly predict the observed signal during the Apollo 17 UVS observations of the lunar surface." This special report gives the initial result of that search.

II. RESULT OF SEARCH

Search of the literature, and inquiry among knowledgeable scientists, indicates that no data at all are available concerning the UV reflectivity of the moon in the spectral range of interest. Therefore, we are, in a separate action, proposing to the National Aeronautics and Space Administration that we be provided with samples of lunar dust material with which we can make our own laboratory measurements of the albedo. This proposal is attached as Appendix A.

When the samples have been obtained, and the measurements made, a further special report will be made giving the results.

A considerable body of literature exists concerning the diffuse reflectivity of the lunar surface in other spectral regions; particularly relevant papers are reproduced as appendices to this report. Of special interest is Appendix B, which reports the ultraviolet albedo of the far side of the moon above 1900 A. This is the nearest in wavelength to our region of any report we have located.

III. CONCLUSION

By obtaining lunar samples and performing the measurements described in Appendix A, we will be able to acquire the information required.

APPENDIX A

ts

A Proposal to the
National Aeronautics and Space Administration
for
DETERMINATION OF THE FAR-ULTRAVIOLET ALBEDO
OF LUNAR DUST SAMPLES

Submitted by The Johns Hopkins University

Principal Investigator:

Richard C. Henry
Department of Physics
The Johns Hopkins University
Charles and 34th Streets
Baltimore, Maryland 21218
(301) 366-3300, Ext. 459

January 1972

Introduction

This proposal has been prepared by Dr. Richard C. Henry, Assistant Professor of Physics, The Johns Hopkins University, Homewood Campus. It is submitted in conjunction with Technical Support Studies Plan DRD No. MA-091T under NASA/MSC Contract NAS 9-11528.

Mr. William G. Fastie, Adjunct Professor of Physics, The Johns Hopkins University, has agreed to serve as co-investigator for this experiment. Professor Fastie is Principal Investigator under the above-mentioned contract.

Facilities used will be the Spectroscopy Laboratory of The Johns Hopkins University, and the Apollo Calibration Facility of the Johns Hopkins University. The latter is described in DRD JHU-I-UVS "Calibration Plan for Ultraviolet Spectrometer Experiment S169", which represents Contract NAS 9-11528 Task I, and "Response to NASA/MSC Contract Change Authorization No. 5" to the above contract.

This is a no-cost proposal.

I. Summary

We propose to determine the far ultraviolet diffuse reflectivity of samples of lunar dust material. This proposal is specifically for the purpose of obtaining appropriate samples. Equipment for measuring the diffuse reflectivity of materials (e. g. paint samples) is already in existence at this university (as described above) and would need only minor modification for the proposed experiment which will include the measurement of the polarizing properties of the lunar samples. Measurements can be made as a function of both illumination angle and angle of observation.

II. Background

NASA/MSC Contract NAS 9-11528 calls for the study of the lunar surface and lunar atmosphere using a far ultraviolet spectrometer on board Apollo 17. The spectrometer will be in the Apollo command module, and normally will be pointed at the lunar surface. Additional modes allow observation of the galactic background. The conditions when the lunar surface is examined may be summarized as follows:

- a) moon dark (dark current measurement)
- b) surface dark, atmosphere illuminated (measurement of the lunar atmosphere)
- c) surface illuminated (measurement of lunar albedo)

It is in connection with operation c) above, that the present proposal is made. Measurement of far-ultraviolet albedo (reflectance) of laboratory samples of lunar dust material will allow the in-orbit measurements to be interpreted much more completely. Knowledge of the albedo of the lunar material is also essential in planning the time-line for the use of the spectrometer in lunar orbit; thus it is very important that our measurements be made without delay. The Apollo 17 landing site will be measured from orbit, and samples from that site also are requested for measurements in the laboratory.

III. Previous Work

An excellent general summary of the optical properties of the lunar surface is given in "The Nature of the Lunar Surface" (The Johns Hopkins Press, Baltimore), which summarizes the 1965 IAU-NASA symposium. Chapters particularly relevant are "Optical Properties of the Moon's Surface" by B. W. Hapke (p. 141), "The Application of Polarized Light for the Study of the Moon's Surface" by A. Dollfus (p. 155), and "Radio Measurements of the Moon," by F. Drake (p. 277). At that time, no data on the ultraviolet reflectivity of the moon had been published.

More recent work is cataloged in Appendix A, attached. Measurements in the far ultraviolet, particularly to wavelengths short of

1900 Å, have not been made; this is the gap that we propose to fill. Lebedinsky et al. measured the albedo of the moon in the 1900-2750 Å range with 14 Å resolution using an ultraviolet spectrometer on the Zond-3 space probe. They obtained an albedo of 1 to 1.5%; the result is shown in detail in Figure 1. We expect to extend these measurements down to about 1000 Å. We have made an informal inquiry among lunar scientists and we find apparently no measurement in this range (1000 to 1900 Å) has been made.

IV. Instrumentation

The ultraviolet reflectometer as it presently exists at the Apollo 17 Calibration Facility of the Johns Hopkins University is illustrated in Figure 2. Briefly, it consists of a hydrogen light source, giving strong emission lines at 1216 Å and molecular band emissions throughout the region below 2000 Å. This light enters an Ebert spectrometer, which disperses it and passes it into the reflectometer. The monochromatic diverging beam is collimated and directed onto the sample for which the reflectivity is desired. A photomultiplier tube is placed on a movable mount and can be swung (from outside) to observe the reflected intensity as a function of angle. Provision is made for directly observing the beam that impinges on the sample, so that the observations can be placed on an absolute basis.

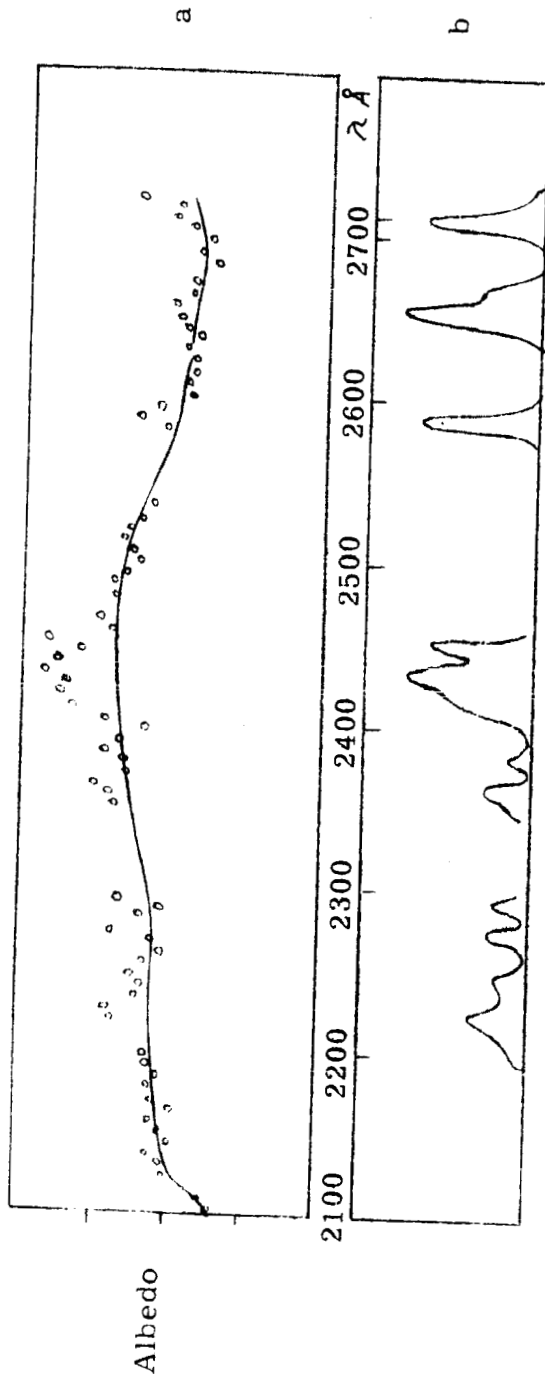


Figure 1. a) Lunar albedo according to Lebedinsky et al. The curve represents the albedo of terrestrial rocks.
 b) Proposed lunar fluorescence bands (Lebedinsky et al.)

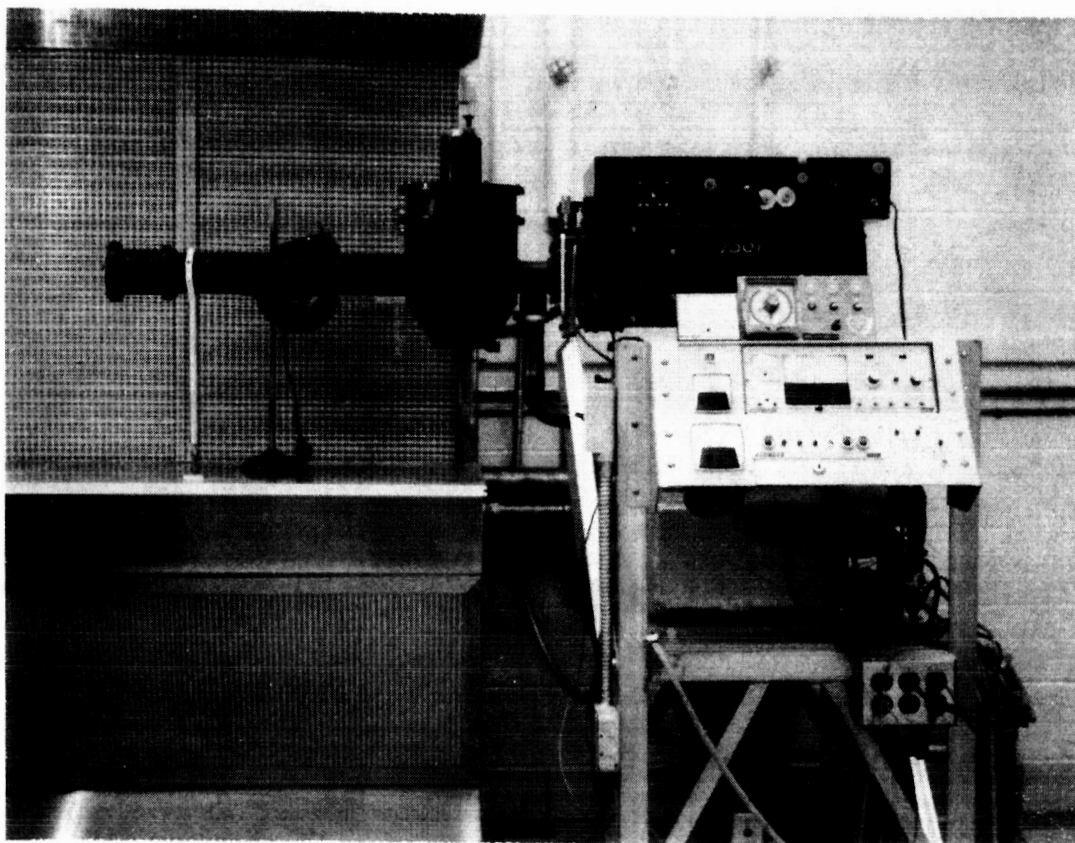


Figure 2. .- Far ultraviolet reflectometer for measurement of the reflectivity of mirrors, paint samples, and lunar dust samples.

Two modifications will be made before making lunar dust sample measurements:

- a) A Triple Reflection Polarizer will be constructed and inserted in the system just outside the exit slit of the spectrometer. This is to allow determination of the polarization properties of the instrumental system and of the lunar samples. The polarizer is described in Applied Optics, volume 8, no. 3, page 667 (V. G. Horton, et al.)
- b) A right-angle bend in the system will be introduced following the polarizer. This will offer the advantage that a dust sample can be measured: in the present configuration the sample must be solid, but with the right-angle introduced the sample can always lie on a plate that is perpendicular to the direction of the earth's gravitational field and will be held in position by that field.

V. Procedures

It is proposed that measurements of the diffuse spectral reflectivity of lunar samples be obtained, as a function of the following parameters:

- a) angle of incidence: various values between 0° and 90° ,
- b) angle of reflection: various values between 0° and 90° , for each of the angles of incidence under a).

- c) polarization: to be studied for each situation under a) and b) above.
- d) wavelength: a range of wavelengths from about 1000 Å to about 2200 Å ; this would allow some overlap with previous work.

About five samples are requested, and should be from any Apollo landing sites up to the present. As great a variety as possible in optical appearance is requested. Additional samples should be provided from the landing site of Apollo 17. The latter is important as we have proposed to study the albedo of the lunar surface from orbit during Apollo 17, and will make concentrated observations from lunar orbit of the landing site for that mission. Comparison of the laboratory and orbital measurements will be essential in understanding the meaning of the orbital observations for other positions on the moon.

VI. Samples Requested

It is requested, therefore, that the following lunar samples be provided to the Principal Investigator for the experimentation described above:

- a) About five 1/10 ounce specimens of lunar surface dust obtained on any Apollo missions. These samples are needed immediately, as preliminary determination of

the far-ultraviolet albedo of the dust is urgently needed in the Apollo 17 engineering planning.

- b) About three 1/10 ounce specimens of lunar surface dust obtained on Apollo 17, to be delivered to the Principal Investigator as soon as possible after the Apollo 17 mission is completed.

These samples will be retained by the Principal Investigator until July 1, 1973, at which time it is anticipated that the work described will be completed.

VII. Sample Care

The Physics Department at the Johns Hopkins University owns two substantial safes, one of which contains "medium security" items and the other "high security" items. The combination of the latter safe is known only to the Department Chairman, Dr. George Owen, and the Administrative Assistant, Mr. J. A. O'Brien. It is proposed that the lunar samples be stored in the high-security safe, under the Principal Investigator's supervision.

During the investigative run, portions of the sample would be left inside the reflectometer, inside the Apollo calibration facility.

This facility is a "white room" with access limited to authorized persons.

The tests proposed are non-destructive. The samples, however, are dust, and some loss will be inevitable. We judge that no more than 5% of the samples will be lost during the entire period of testing.

Budget

No funds required.

Appendix A to Proposal

References on the Lunar Albedo

A) Ultraviolet

Johnson, M. C., Vacuum Ultra-violet Scattering Distributions, Applied Optics, 7, 5, p. 879-881, May 1968.

Lebedinsky, A. I., V. A. Krasnopolsky, and M. U. Aganina, "The Spectral Albedo of the Moon's Surface in the Mid Ultraviolet according to data from the Zond-3 space probe,) Moon and Plants II, North Holland Publishing Company, Amsterdam, p. 47-54, 1968.

B) General

Birkebak, R. C., Cremers, C. J., and Dawson, J. P., "Directional Spectra and Total Reflectance of Lunar Material," Proceedings of the Apollo 11 Lunar Science Conference, Volume 3, p. 1993-2000.

Conel, J. E., and Mash, D. B., "Spectral Reflectance and Albedo of Apollo 11 Lunar Samples: Effects of Irradiation and Vitri-fication and Comparison with Telescopic Observations," *ibid*, p. 2013-2024.

Gold, T., Campbell, M. J., and O'Leary, B. T., "Optical and High-frequency Electrical Properties of the Lunar Sample," *ibid*, pp. 2149-2154.

Appendix B to Proposal

Currently-Approved Reflectivity

Measurement Experiments,

Apollo 14-17

September 1971

<u>Investigator</u>	<u>Institution</u>	<u>Approved Investigation</u>
Adams, J. B. Johnson, T. V. McCord, T. B.	College of the Virgin Is. M. I. T. M. I. T.	Visible and Near-Infrared Reflection Spectroscopy
Burns, R.	M. I. T.	Optical Absorption and Specular Reflectivity
Perry, C. H. Anastassakis, E. Lowndes, R.	Northwestern University Northwestern University Northwestern University	Infrared Absorption and Light Scattering Spectra

APPENDIX B

MOON AND PLANETS II-NORTH-HOLLAND PUBLISHING COMPANY, AMSTERDAM

Foster

THE SPECTRAL ALBEDO OF THE MOON'S SURFACE IN THE MID-ULTRAVIOLET ACCORDING TO DATA FROM THE ZOND-3 SPACE PROBE

A. I. LEBEDINSKY, V. A. KRASNOPOLSKY and M. U. AGANINA

USSR

Abstract. Fourteen spectra of the Moon's surface have been obtained in the 1900 - 2750 Å wavelength range with 14 Å resolution using an ultraviolet spectrophotometer flown on the Zond-3 space probe. Examination of the spectra has shown that the Moon's mean albedo in the above spectral range is about 1 - 1.5%. A sharp increase in brightness in the 2420 - 2470 Å range was found in all the spectrograms which is likely to be connected with the Moon's surface luminescence. This effect is different in various spectrograms and results in a 10 - 50% excess of brightness. The spectra obtained relate mainly to the continental regions on the remote side of the Moon as photographed with the Zond-3 phototelevision camera. The optical axes of both instruments were aligned and the monochromator viewing field was about 2.5° in diameter, which corresponded to the resolution on the ground of the order of 500 km. The determined optical characteristics should therefore be considered as being a result of very significant averaging, and the possibility is not excluded that the Moon's surface luminescence within small regions proves to be more intensive. The results of the laboratory studies on terrestrial rocks are known from previously published data. None of this data, however, corresponds to the reflecting characteristics of the Moon's surface. It is possible that these differences are connected not with the chemical or mineralogical composition of the lunar rocks but with the features of the surface appearing as a result of long "treatment" of the surface in vacuum by various specific factors such as micrometeorites, solar wind, hard corpuscular and electromagnetic radiation.

Резюме: С помощью ультрафиолетового спектрофотометра, установленного на АМС "Зонд-3", получено 14 спектров лунной поверхности в интервале длин волн 1900-2750 Å с разрешающей способностью 14 Å. Изучение спектров показало, что среднее альbedo обратной стороны Луны в указанной спектральной области составляет около 2%. Резкое повышение яркости обнаружено на всех спектрограммах в нескольких интервалах, что можно полагать связанным с люминесценцией лунной поверхности. Этот эффект различен на различных спектрограммах и дает от 10 до 50% избытка яркости.

Полученные спектры в основном относятся к материковым районам обратной стороны Луны, сфотографированным фототелевизионной камерой станции "Зонд-3". Оптические оси этих приборов были установлены параллельно, а поле зрения монохроматора имело диаметр около 3,0 градусов, что соответствовало разрешающей способности на местности порядка 500 км. Поэтому определение оптические характеристики следует рассматривать как результат очень сильного осреднения, и не исключена возможность, что в пределах малых участков люминесценция лунной поверхности окажется наиболее интенсивной.

По опубликованным данным известны результаты исследований в лабораторных условиях различных образцов земных пород. Отражательные характеристики лунной поверхности не похо-

ли ни на один из них. Возможно, что эти отличия связаны не с химическим или минералогическим составом лунных пород, а с особенностями поверхности, возникающими при длительной ее "обработке" в вакууме различными специфическими факторами, как-то: микрометеоритами, солнечным ветром, жесткой корпускулярной и электромагнитной радиацией.

The lunar surface reflectivity was measured photoelectrically in the 1900 - 2750 Å wavelength range with a resolution of 14 Å, and the Moon was also measured spectrographically in the 2800 - 3550 Å range, from the Zond 3 spacecraft which passed by the Moon on 17 July 1965. The equipment, calibration, and initial treatment of the material obtained have been described in refs. [1,2]. The dependence of the Moon's mean albedo on the wavelength has also been obtained in the above-mentioned ranges, the absolute standardization of the spectrographic measurements being carried out according to the data of Moon observations from the Earth in the near ultraviolet range [3,4] which agreed well with the measurement of the excess of the Moon's color [5,6]. The Moon's photoelectric spectra were averaged, ref. [1], omitting the indicatrix of reflection for the Moon and mutual orientation of the optical axis of the instrument, solar ray and measured site. The coincidence of the calculated values of the albedo on the long-wave edge of the photoelectric data and at the short-wave edge of the photographic spectrum, however, indicated that the result did not manifest a great error.

For more accurate averaging and for further treatment of the material, it was necessary to obtain the trajectory of the optical axis of the instrument over the lunar disc. This trajectory was reconstructed for nine of fifteen photoelectric spectra. For this purpose the telemetric data on the performance of various systems aboard Zond 3, the photographs of the lunar surface and the map of the Moon's remote side plotted on the basis of these photographs [7] were used.

Assuming that the indicatrix of reflection for the lunar surface in the middle ultraviolet is the same as that for visible light, we recalculated further the monochromatic brightness of each measured area of the lunar surface at the full Moon, when this brightness should not depend on the location of such an area on the lunar disc. It was assumed in this recalculation that the brightness distribution along the equator of the Moon is determined by the group of the curves obtained for various lunar phases by Orlova [8] and, more precisely defined, by Minnaert [9,10] and that the brightness meridians, i.e. large circles perpendicular to the brightness equator are the isophotes.

The spectral intensities so recalculated were averaged, i.e. the average spectrum of the Moon's remote side was obtained during the full Moon and is shown in fig. 1a by the solid line. The dotted line in the same figure represents the energy distribution in the solar spectrum [12,13] averaged in 15 Å intervals with an increment of 5 Å, the intensities being divided by π . In other words, fig. 1a is the comparison of the Moon's ultraviolet spectrum at full Moon, I , with the spectrum of the white surface, I_0/π , represent-

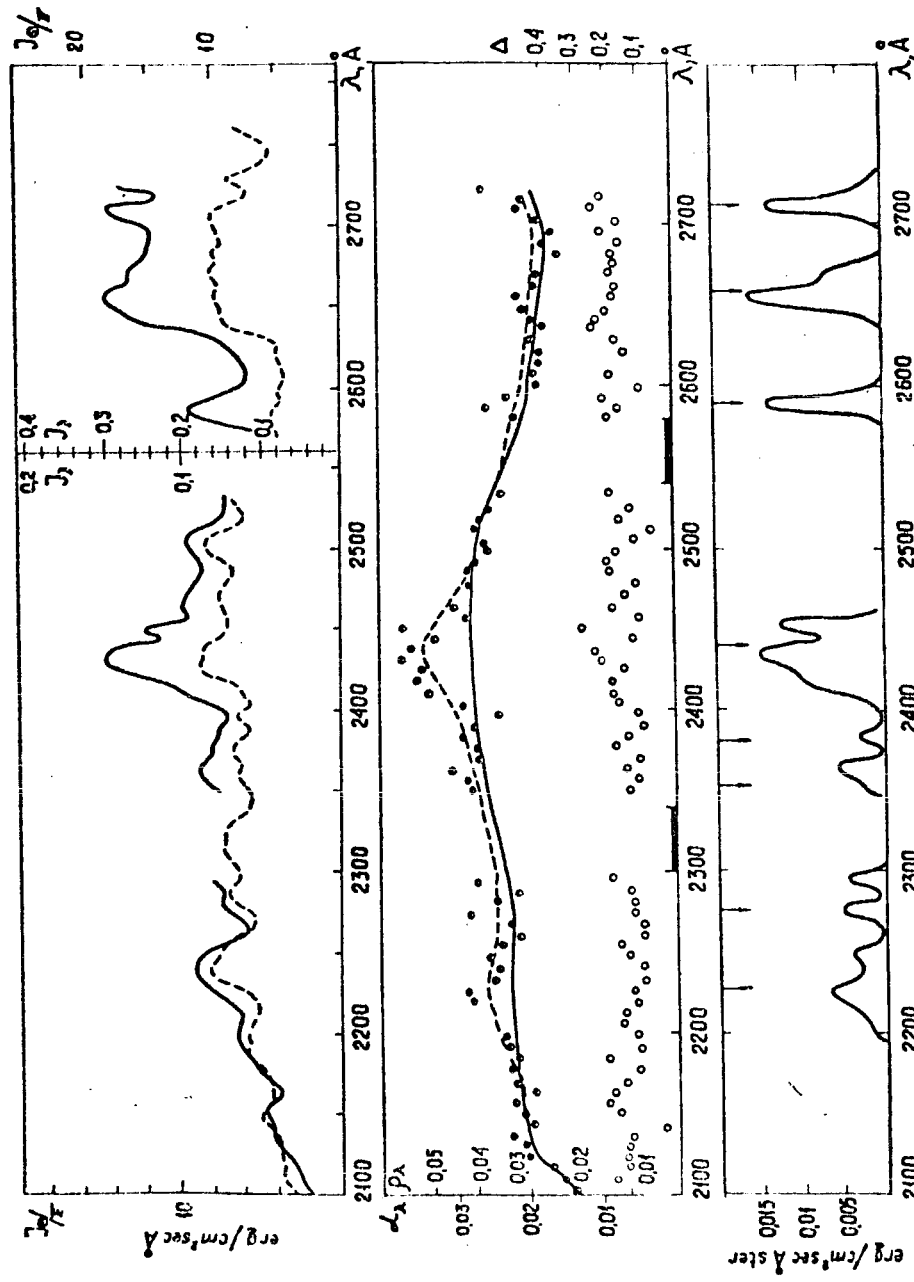


Fig. 1.

ing the solar curve according to Lambert's law. The white surface is two orders brighter than the lunar surface. The scale of the ordinate is different at the right and left sides of the plot. The scale for the lunar surface is indicated at the right and left of the vertical line which divides the plot; that for the white surface is indicated at the sides of the plot.

The black circles in fig. 1b indicate the values of the mean factor of the monochromatic brightness of the lunar surface (the spectral albedo),

$\rho_\lambda = \frac{\pi I_\lambda}{I_\odot \lambda}$, i.e. the ratio of the ordinates of the curves in fig. 1a. If the value ρ_λ is multiplied by the factor $q = 0.66$ [13] then α_λ (the monochromatic spherical lunar albedo) is obtained. The factor q is determined by the physical structure of the lunar surface and it is therefore reasonable to assume that this factor is the same for the ultraviolet radiation as for the visible part of the spectrum.

The line drawn through all the points gives the dependence of the lunar albedo with wavelengths; the curve is very remarkable. The preliminary study which we carried out of the spectra of some rocks as well as those treated in the atlas compiled by the IIT Research Institute in Chicago [11] of the spectra of 37 rocks show that the wavelength dependence of the albedo of minerals is represented in the ultraviolet range by a smooth curve with the absence of appreciable details in intervals smaller than 100 Å.

The examination of possible systematic errors in the measurements shows that these errors should not adversely affect the smoothness of the averaged curves. One may speculate that these errors could result in a rise of the albedo curve in one interval and in a lowering in other intervals. The same applies to possible errors in the measurements of the solar spectrum. Thus, only the statistical errors of averaging may be of great importance in the formation of small details of the lunar albedo curve.

In fact, the Moon was observed from Zond 3 as a disc having a diameter of about 18°. The viewing field of the instrument was about 3°. Nine measurements localized on the disc were carried out in each wavelength. Hence, about one-fourth of the lunar disc observed from Zond 3 was studied in each wavelength.

The photographs obtained from Zond 3 have shown a fairly high degree of homogeneity of the area studied on the remote side of the Moon which has mainly a continental structure. However, in the ultraviolet light, the lunar surface appears to be much less homogeneous and this property of the lunar surface may be a means of studying its finer characteristics.

In each wavelength of the studied spectral range, the measurements were carried out at nine points of known selenographic coordinates. The scatter of these 9 values will be denoted as Δ_λ . This scatter is shown in fig. 1b (the right scale, empty circles). The scatter was calculated as follows. Let $x_{i\lambda}$ be the observed monochromatic intensity in the i th spectrum at the wavelength λ and $y_{i\lambda}$ be the intensity reduced to the conditions of observation of the same area of the lunar surface at full Moon, i.e. under the conditions which might take place at a certain moment at the appropriate trajectory of Zond 3.

The values Δ_λ presented in fig. 1b have been calculated using the formula

$$\Delta_{\lambda} = \frac{1}{9} \frac{1}{y_{\lambda}} \sum_{i=1}^9 |y_{i\lambda} - y_{\lambda}|,$$

where y_{λ} is the average of nine values of $y_{i\lambda}$ shown as the black circles in fig. 1b.

The value of the scatter of Δ_{λ} characterizes the degree of the lunar inhomogeneity in various wavelengths, but it does not show a systematical change with the wavelength. On the average $\Delta_{\lambda} = 16.5\%$ which corresponds to the mean square root deviation $\sigma = 22\%$ for the normal distribution of probabilities. Since our selection included ten values, then the accuracy is $\sigma \approx 8\%$. These values make it possible to evaluate not only the contribution of the statistical errors but to also give the characteristics of the lunar surface inhomogeneity.

The complicated form of the curve of the spectral albedo, ρ_{λ} may be interpreted as the result of superposition of the bright bands with a width of tens of \AA onto the smooth energy distribution in the spectrum. The origin of the bands may be of two kinds. They are either the spectral bands of the albedo of lunar minerals or the bands of fluorescence occurring under the influence of the external factors, for example the solar ultraviolet radiation or corpuscular streams. Generally speaking, these two possibilities may be distinguished according to the presence or absence of the dependence of the intensity of the bands with time, but this problem is not included in the present report. Without analyzing the physical mechanics of luminescence, we shall simply consider the observed spectrum as the sum of the smooth spectrum plotted within the change errors along the lower edge of the scatter of the black circles in fig. 1b (thick curve) and the spectral bands which will be conditionally named emission bands. For comparison, fig. 1b shows the curve (dotted line) corresponding to the averaging of the values of Δ_{λ} in the 60 \AA interval carried out with a 7.5 \AA increment.

The calculation of the probability of the statistical deviations of individual values from the curve which approximates these values shows that the point scatter observed in fig. 1b cannot be explained statistically. This forces the assumption that some groups of the points which protrude outside of the average curve or do not reach it are the existing details connected with either the spectral bands of the increased albedo or the luminescence of the lunar surface.

Since an appreciable dependence of Δ_{λ} on the wavelength is absent within the studied spectral range, it is possible to plot a single distribution function for Δ_{λ} which characterizes the degree of the color diversity of the lunar surface in the studied range of the middle ultraviolet. This function is presented in fig. 2. The observed values are shown by the points, and the curve of normal law with a dispersion of 22% is plotted as the solid line. The deviations from the curve of the normal distribution law are most likely due to the fact that on the remote side of the Moon there exist an ultimate number of areas having a dimension of the order of that of the field of view of our instruments, between which transient regions exist.

As was indicated above, the thick line in fig. 1b is drawn approximately along the bottom edge of the distribution of the individual values of ρ_{λ} , tak-

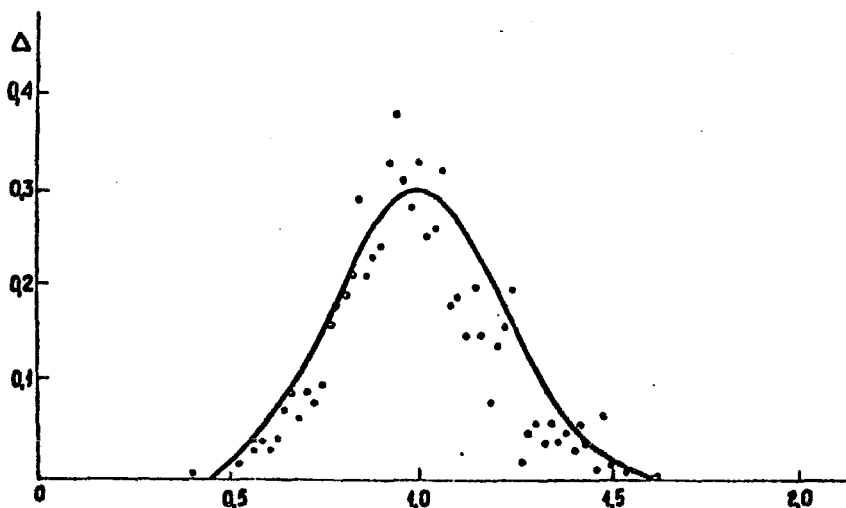


Fig. 2.

ing into account the probable statistical scatter. The statistically unlikely excesses over this curve will be considered as the emission bands. The spectrum of the bands so obtained is shown in fig. 1c.

It is likely that about 15 emissions are present here, some of which overlap and form broader bands. One or two of these bands may be produced by statistical scatter. On the other hand, it is likely that the curve of the true albedo is even lower and in this event the luminescent emissions will increase but a continuous background between the emissions and the new bands will appear.

The emission bands in fig. 1c have equivalent widths of the order of 15 - 30 Å at a mean intensity of about 0.01 erg/cm²sec.Å. ster. which is two - three orders lower than the solar ultraviolet energy which is capable of producing the luminescence in these wavelengths, and is also lower than the energy of the corpuscular streams and solar wind.

When examining the 15 spectra available to us, one may clearly see the recurrence of emission bands in individual spectra.

In order to judge the emission distribution over the lunar disc, eight wavelengths marked with arrows in fig. 1c have been selected. For these wavelengths, λ , the differences $z_{\lambda i} = y_{\lambda i} - y_{\lambda}$ ($i = 1, \dots, 9$) have been formulated the spectra bound to coordinates. The values of $z_{\lambda i}$ were plotted on the lunar map and averaged inside a circle with a radius of 10 degrees of the selenographical latitude, i.e. the circles corresponding to the area were about half the viewing field of our instrument. The obtained averages $z(b, l)$ were plotted on one of the photographs obtained from Zond 3 which is presented in fig. 3.

As can be seen from fig. 3 the distribution of $z(b, l)$ has its peak at the point with the following coordinates: 20° latitude and 110° longitude. The values of $z(b, l)$ are decreased when approaching that edge of the lunar disc where the Oceanus Procellorum is located.

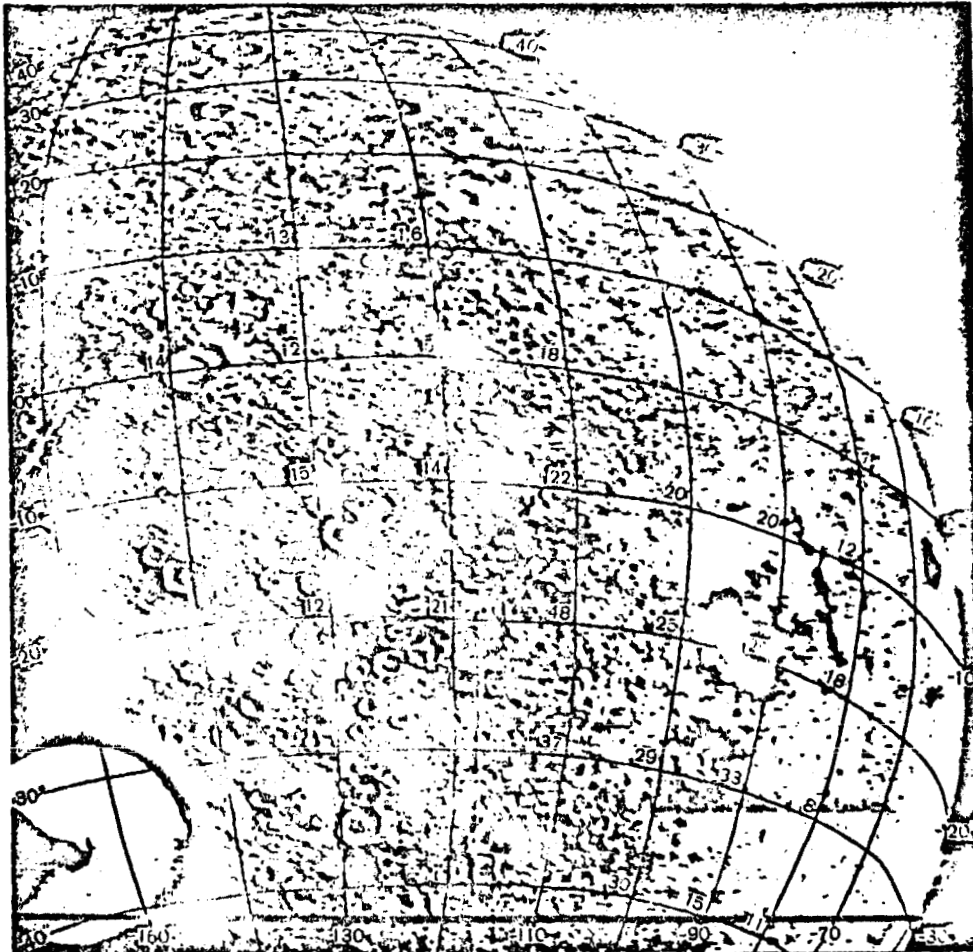


Fig. 3.

When comparing the spectral albedo obtained by us for the middle ultraviolet with the data of the observations from the Earth in the near ultraviolet, one should bear in mind the fact that a purely continental region of the lunar surface was observed by Zond 3 and that the disc visible from the Earth is occupied mostly by the seas. Therefore in order to obtain comparable data, it is necessary to increase the albedo determined as a result of the telescopic observations by a factor of about one and a half.

The comparison of the smooth portion of the spectral lunar albedo with the laboratory spectra of the terrestrial rocks obtained both by us and by Watts in Chicago [11], has not yet permitted identification to be made.

REFERENCES

- [1] V. A. Krasnopolsky, A. A. Krysko and A. I. Lebedinsky, in: Moon and Planets, ed. A. Dollfus (North-Holland, Amsterdam, 1967) p. 55.
- [2] G. M. Aleshin, V. A. Iosenas, V. A. Krasnopolsky, A. I. Lebedinsky, A. S. Selivanov and V. V. Zasetky, in: Moon and Planets (North-Holland, Amsterdam, 1967) p. 65.
- [3] N. P. Barabashov and A. T. Chekirda, Proceedings of the Kharkov Astronomical Observatory, 3, No. 11 (1954) 13.
- [4] N. N. Petrova, Astronom. Zhur. 43, No. 1 (1966).
- [5] V. V. Sharonov, Astronom. Tsirk. Akad. Nauk SSSR, No. 157 (1955) 19.
- [6] A. V. Markov (ed.), Luna (Moscow, 1960).
- [7] Yu. N. Lipsky, Astronom. Zhur. 43 (1966) 1111.
- [8] N. S. Orlova, Astronom. Zhur. 33 (1965) 93.
- [9] M. Minaert, Astrophys. J. 93 (1941) 403.
- [10] G. P. Kuiper and B. M. Middlehurst (eds.), Planets and Satellites (University of Chicago Press, 1961) p. 228.
- [11] H. V. Watts, Reflectance of Rocks and Minerals to Visible and Ultraviolet Radiation, Technical Letter NASA-32 (1966).
- [12] N. L. Wilson et al., Astrophys. J. 119 (1954) 590.
- [13] H. H. Malison et al., Astrophys. J. 132 (1960) 746.
- [14] C. W. Allen, Astrophysical Quantities (London, 1955).

7.

Optical Properties of the Moon's Surface*

B. W. Hapke

Center for Radiophysics and Space Research, Cornell University, Ithaca, New York

I would like to discuss the optical properties of the moon's surface and what can be deduced concerning the outermost millimeter or so of the lunar surface when these properties are combined with appropriate laboratory studies. I believe that the optical evidence gives very strong indications that the lunar surface is covered with a layer of fine dust of unknown thickness.

The moon's surface is characterized by a number of rather unusual optical properties, which are summarized in Figure 7-1. The brightness peaks at full moon, when the source is directly behind the observer, that is, when the sun is directly behind the earth. The brightness decreases sharply as the phase angle increases from 0 degrees. This is true no matter what part of the lunar disk one is observing. The upper part of Figure 7-1 gives two typical curves illustrating how the brightness of two areas vary as the angle of incidence i changes. The upper left curve is for an area on the 0-degree meridian of longitude, ϵ being the angle of observation. The upper right curve corresponds to an area on the 60-degree meridian of longitude as the angle of incidence changes. The shape of the curves is apparently independent of latitude; one gets a similar sort of photometric function for any lunar latitude as long as the longitude remains the same. There is some scatter about these mean curves for various areas on the lunar surface, but the departures from the mean curves are not nearly as significant as the range of values which the reflec-

tion law for a variety of different kinds of surfaces can take.

In the lower left of Figure 7-1 are shown curves of polarization as a function of phase angle ϕ . The shape of the curve is very nearly independent of position on the lunar surface. The polarization is negative for phase angles less than about 23 degrees, and goes through a negative maximum of about 1.0 per cent. Then at 23 degrees or so, the polarization becomes zero and the plane of polarization rotates 90 degrees. The polarization then goes through a positive maximum, when the phase angle is around 90 to 110 degrees, depending on the area observed. The brighter areas, such as the highlands, generally have lower positive polarization and the darker areas, such as the maria, have higher polarization. The position of the maximum may be shifted a little bit toward larger phase angles for the darker areas.

The color of the moon is rather significant: it is redder than sunlight. The lower right part of Figure 7-1 shows color differences on a magnitude scale versus wavelength for various areas on the lunar surface. These data have been corrected to a color difference of zero at a wavelength of 5,600 Å, which is the wavelength of the green filter we use.

It is convenient to characterize these photometric curves by a number of parameters. The first parameter is the normal albedo A_n , which is the brightness of the surface relative to the brightness of a perfectly reflecting, perfectly diffusing surface, both areas viewed and illuminated normally. The

* This research has been sponsored by a grant from the National Aeronautics and Space Administration.

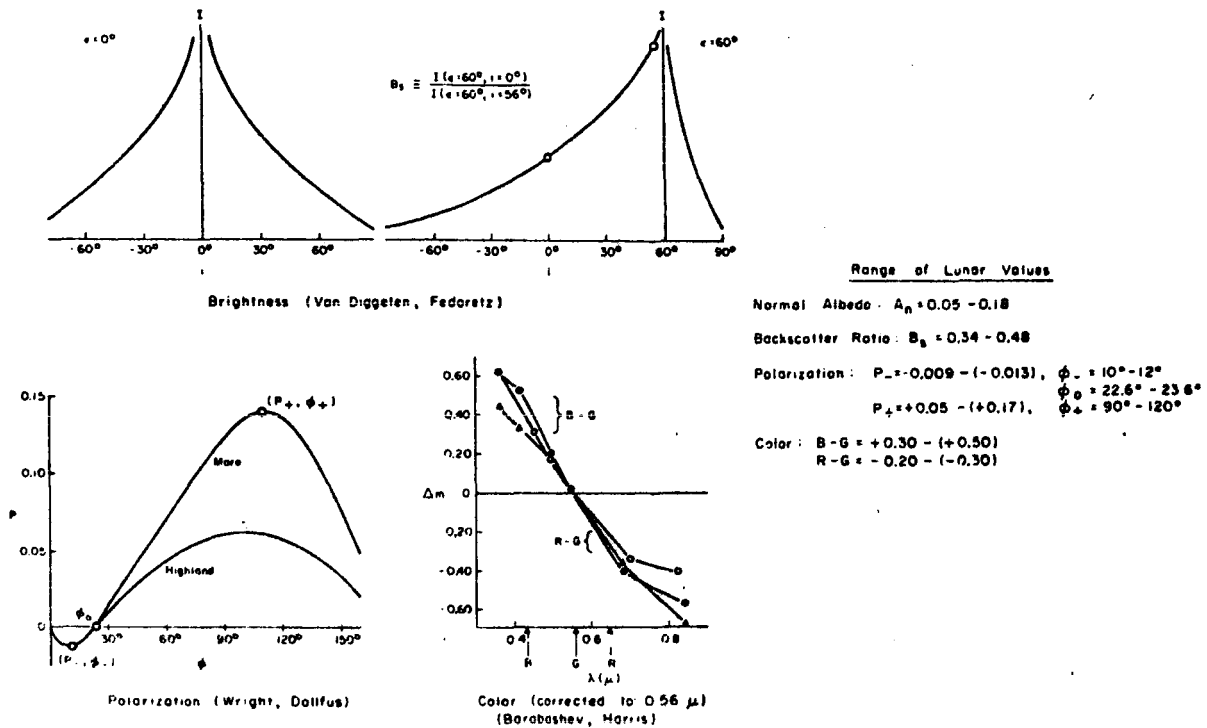


FIGURE 7-1: Photometric characteristics of the lunar surface.

range of normal albedo on the moon is from 5 per cent to about 18 per cent.

The shape of the backscatter curve can be characterized by the backscatter ratio, B_s , which is the ratio of the brightness at $\epsilon = 60$ degrees and $i = 0$ degrees to the ratio of the brightness at $\epsilon = 60$ degrees and $i = 56$ degrees. These two points are shown in the upper right curve of Figure 7-1. The backscatter ratio for the moon is about 0.34 to 0.48.

The polarization can be characterized by three parameters: the point of negative maximum, the inversion angle, and the point of the positive maximum. On the moon the negative maximum has the range of about 0.9 to 1.3 per cent, the inversion angle from 22.5 to 23.5 degrees; the value of polarization at positive maximum ranges from about 5 to 17 per cent, and the position of the positive maximum is 90 to 120 degrees.

We measured the color of our laboratory surfaces at 4,250 Å, 5,600 Å, and 6,450 Å. $B-G$ refers to the brightness of the surface at the position of the blue filter on a magnitude scale relative to the brightness at 5,600 Å, and similarly for $R-G$, which refers to the red filter. Lunar values of $B-G$ are from

about +0.30 to +0.50, and of $R-G$, from -0.20 to -0.30.

The fact that every area on the lunar surface possesses these unusual optical characteristics shows that they must be exogenous and are not due to some peculiar property of lunar lavas or to some other internal cause. I suggested a few years ago that these rather remarkable lunar photometric properties could be explained as the result of micrometeorites impacting the lunar surface and pulverizing it to a very high degree. The resulting dust would be acted upon by the solar wind, darkening and otherwise altering the optical characteristics of the dust. If this suggestion is correct, then if we take a rock of the proper composition, grind it up, and irradiate it with protons of a few kilovolts energy to simulate the solar wind hitting the moon, the resulting material should possess the proper photometric properties.

Figure 7-2 shows the photometric properties of hydrogen-ion-irradiated dunite powder. If the solar wind is impacting the moon at the same flux as measured by Mariner II, the radiation dose which this powder has received would be equivalent to something like 100,000 years on the moon.

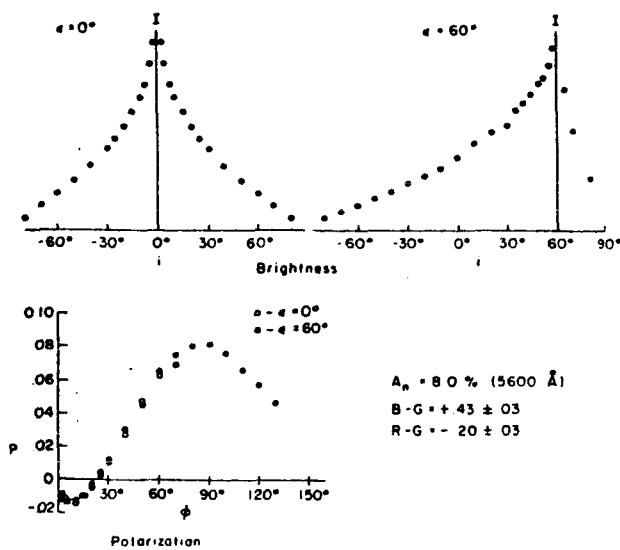


FIGURE 7-2: Photometric properties of dunite powder (size $< 7\mu$) after 65 coul/cm² of H-ion irradiation.

The photometric properties of the dunite powder reproduce those of the moon quite well.

The remainder of this paper is devoted to a discussion of some of the properties of surfaces that affect their photometric characteristics; whether one can deduce that other types of surfaces could not have these photometric properties; and the composition of the lunar surface. In the laboratory studies about to be described, I have been helped by Hsiu Yung Chow and Eddie Wells, graduate students at Cornell University.

Figure 7-3 is a schematic diagram of the process which I believe is responsible for the darkening of the lunar surface by the solar wind. Ions from the solar wind strike the particles that make up the lunar surface and sputter atoms off these particles. Assuming that the moon is composed of a silicate rock material, the sputtered atoms will consist of oxygen, silicon, and various kinds of metals. Some of these sputtered atoms will leave the surface completely. However, when one has a rather complex surface, some of these sputtered atoms may fly over and stick to the undersides of adjacent rock particles. Because oxygen is a more volatile element it will have a lower sticking coefficient than the other types of atoms and fewer oxygen atoms than the silicon or metal atoms will stay on the undersides of these particles. This process results in a coating of a dark material on the underside of a rock particle; the coating is probably a non-

stoichiometric silicate compound (or glass) which is deficient in oxygen.

The sputtering action of the solar wind, of course, will also make etch pits in the surfaces of the particles and it will generally clean their upper surfaces. But the primary mechanism responsible for the darkening is the coating of the underside of the particles with a thin, absorbing, nonstoichiometric compound. Lattice vacancies in such compounds would be highly efficient in producing absorbing effects.

Figure 7-4 shows an experiment we did in the laboratory. We put an aluminum oxide ball inside an aluminum oxide crucible and bombarded it from above with 2 kev He ions. The middle photo shows the bombarded ball and the unirradiated ball. The unirradiated ball is shiny and the upper surface of the irradiated ball has been cleaned and roughened by sputtering but the underside is darkened. The right hand photo is a photomicrograph of the interface between the dark and light areas of the irradiated ball. Dark streaks were formed under the little asperities sticking out from the ball. These streaks are the geometric shadows of the asperities to the ion beam.

Figure 7-5 shows how the ion bombardment affects the photometric properties of some large materials, rocks and chunks of rocks. As in Figure 7-3, the darkening is much more efficient on a rough surface than on a smooth surface.

In many of the following figures a white disk appears on a black square as an albedo reference. The dark square is black velvet, which has an

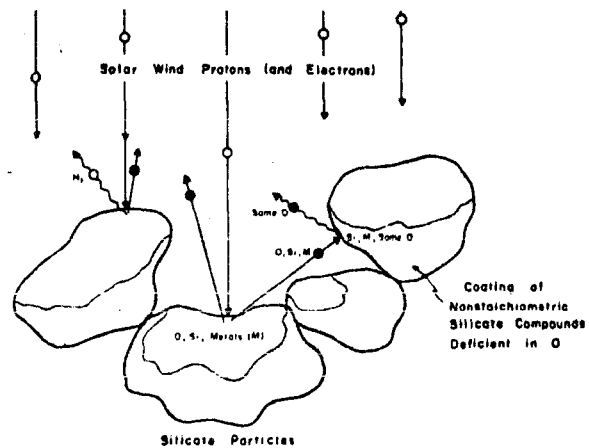


FIGURE 7-3: Schematic diagram of process responsible for darkening of lunar surface by solar wind.

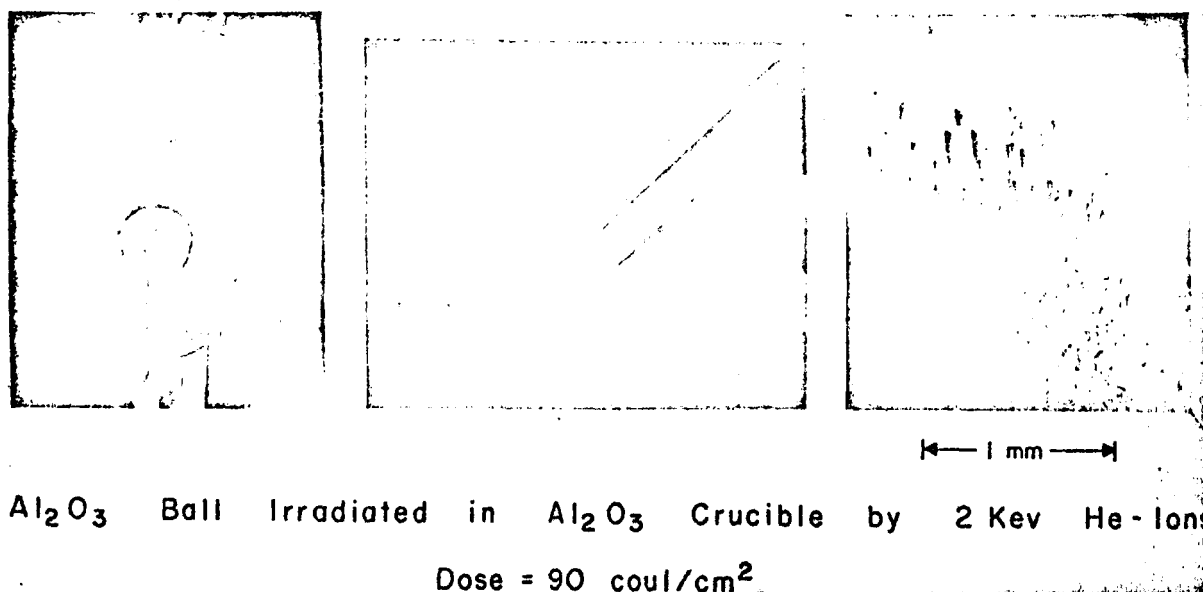


FIGURE 7-4: Effect of ion bombardment on aluminum oxide ball (laboratory experiment).

albedo of about 1 per cent; the disk is magnesium oxide powder, which has an albedo close to unity.

Figure 7-6 is a photo of some coarse olivine basalt powders, showing the effects of particle size and different types of irradiation on the appearance of a rock powder. The top row is the unirradiated material. The middle row is after 10^6 roentgens of gamma ray irradiation from Co⁶⁰. The bottom row is after hydrogen ion irradiation. The gamma radiation had no effect at all, nor were the color, albedo, or other photometric properties appreciably affected. In contrast, the hydrogen ion radiation is very efficient for changing the photometric properties. Observe that the coarser materials darken less than the finer materials.

Finer particles are much more efficiently darkened than coarser particles by the mechanism shown in Figure 7-3 because there are so many more free surfaces. All naturally occurring rocks and minerals are partially absorbing. Large particles, whether or not they are bombarded, have their optical properties dominated by the absorbing and reflecting properties of the rock itself. But, when finely ground, the particles become translucent, and if an absorbing coating is put on the undersides the optical properties are controlled by the coating rather than by the optical properties of the rock itself.

Figure 7-7 is a photo of fine olivine basalt powders, which were handled somewhat before the

picture was taken. When first taken out of the vacuum system they were quite uniformly darkened. Again the gamma irradiation had no effect at all; however, the hydrogen ion bombardment had a remarkable effect. Also shown is a sample bombarded with helium ions. The effect of helium ion irradiation is about the same as hydrogen ion irradiation, except the efficiency is better. The same dose of helium ions will produce the same effects in a much shorter time than an equivalent dose of hydrogen ions.

It is important to show that the darkening effects of ion irradiation are not due to cracked pump oil or to some other spurious effect. We have several independent indications that the effects are real, but the most dramatic proof is shown in Figure 7-8.

The materials in each row of Figure 7-8 were irradiated simultaneously side by side in the vacuum system. The top row is untreated material; the center row was irradiated by hydrogen ions; the lower row by helium ions. The powders are pure magnesium oxide, aluminum oxide, and silicon dioxide, plus mixtures of these three powders. The mixtures are physical only and not chemically combined. Note that the two mixtures of SiO₂ with Al₂O₃ and with MgO both darkened appreciably under hydrogen ion irradiation, whereas the pure materials darkened only very slightly. This figure illustrates the nonlinear effect, so to speak, of the ion irradiation, in that one cannot deduce from

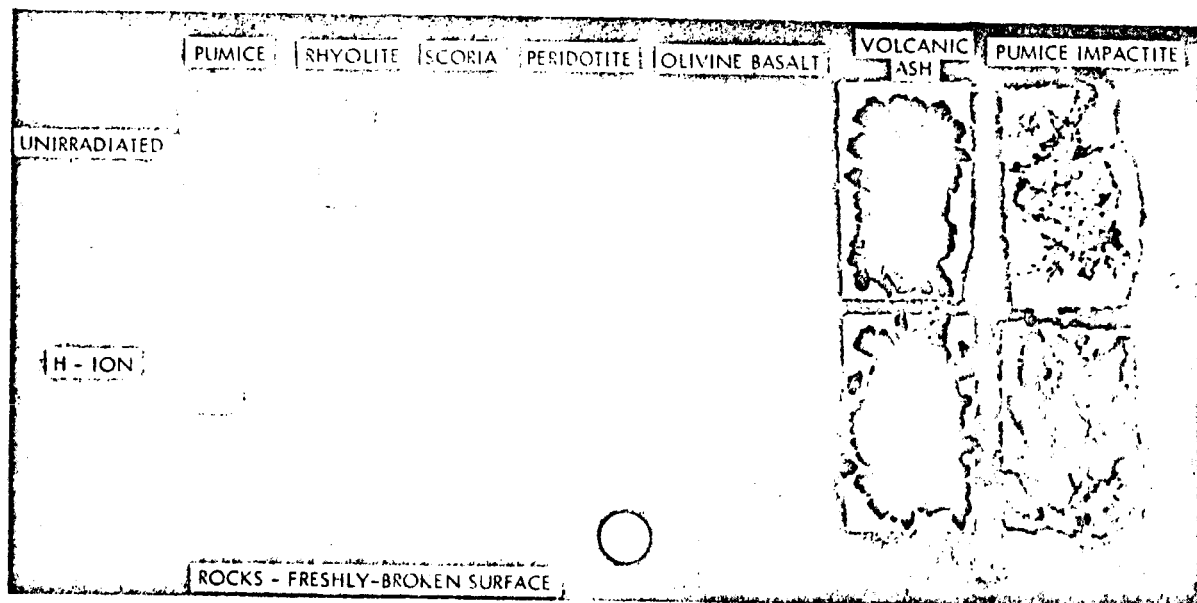


FIGURE 7-5: Effect of ion bombardment on the photometric properties of rocks and chunks of rocks.

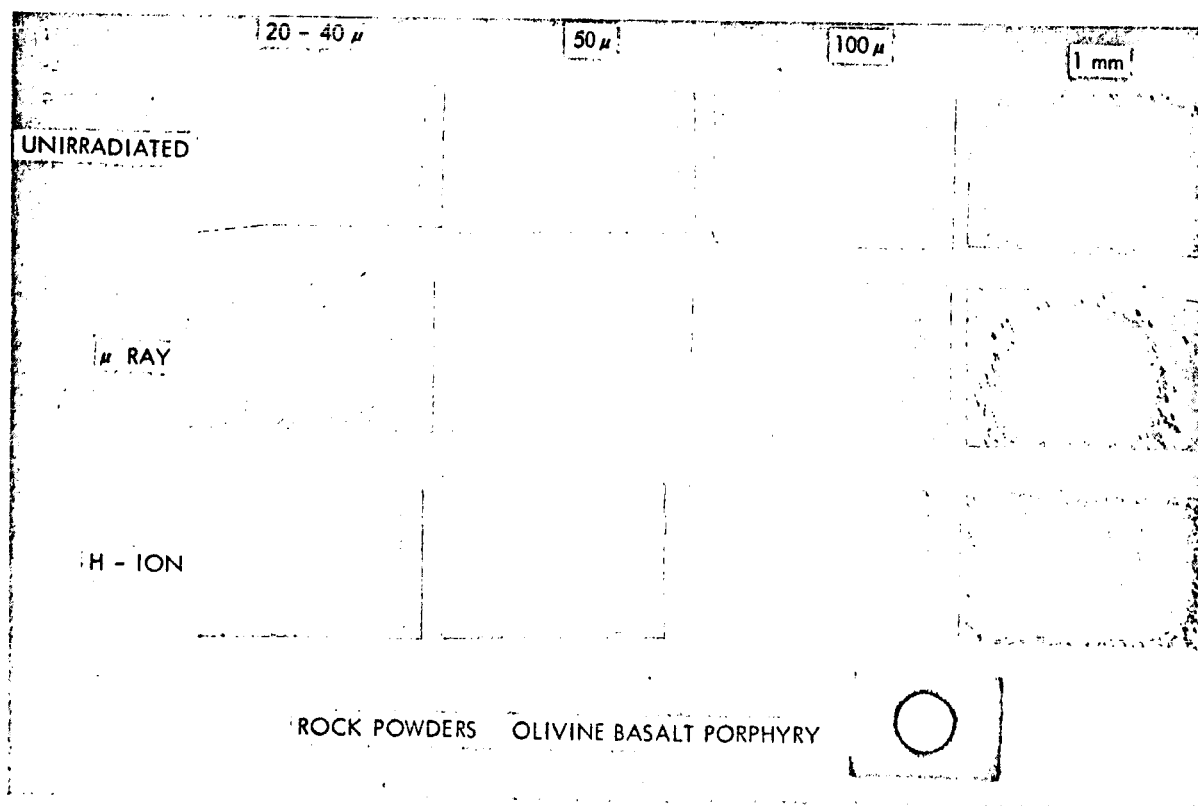


FIGURE 7-6: Effects of particle size and different types of irradiation on the appearance of a rock powder.

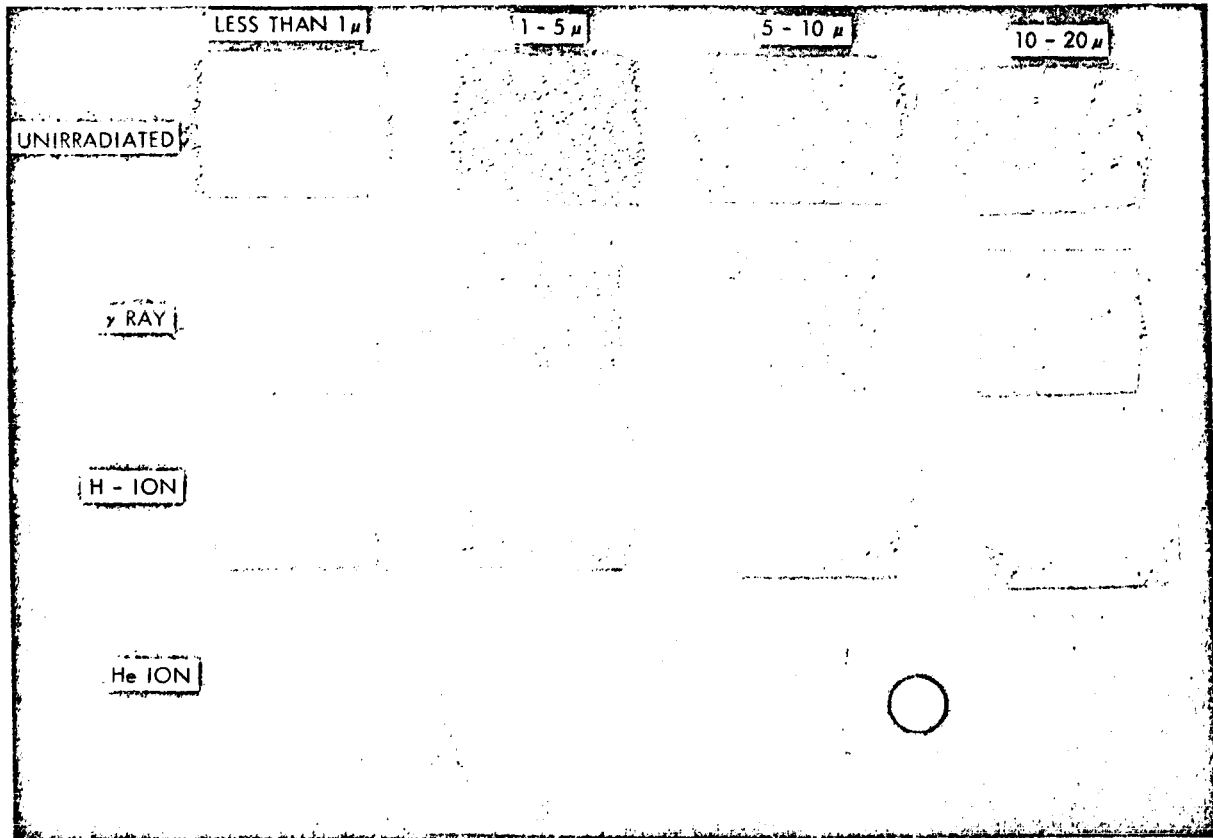


FIGURE 7-7: Effect of hydrogen-ion bombardment on fine olivine-basalt powders.

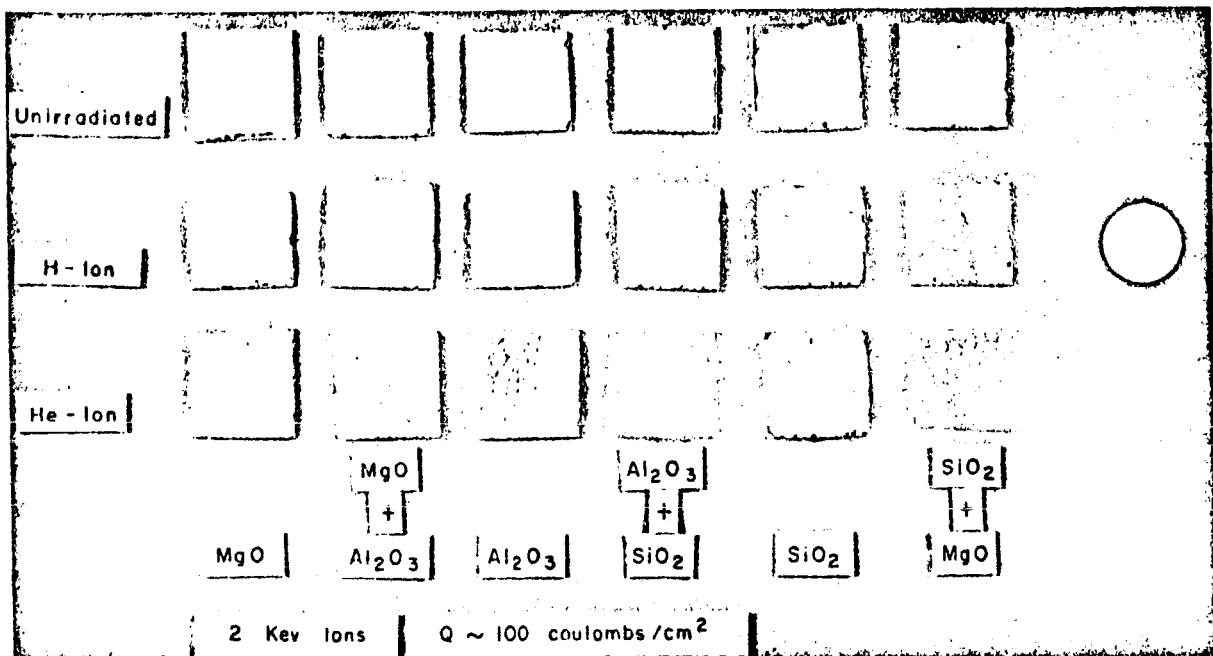


FIGURE 7-8: Effect of irradiation on mineral oxide powders.

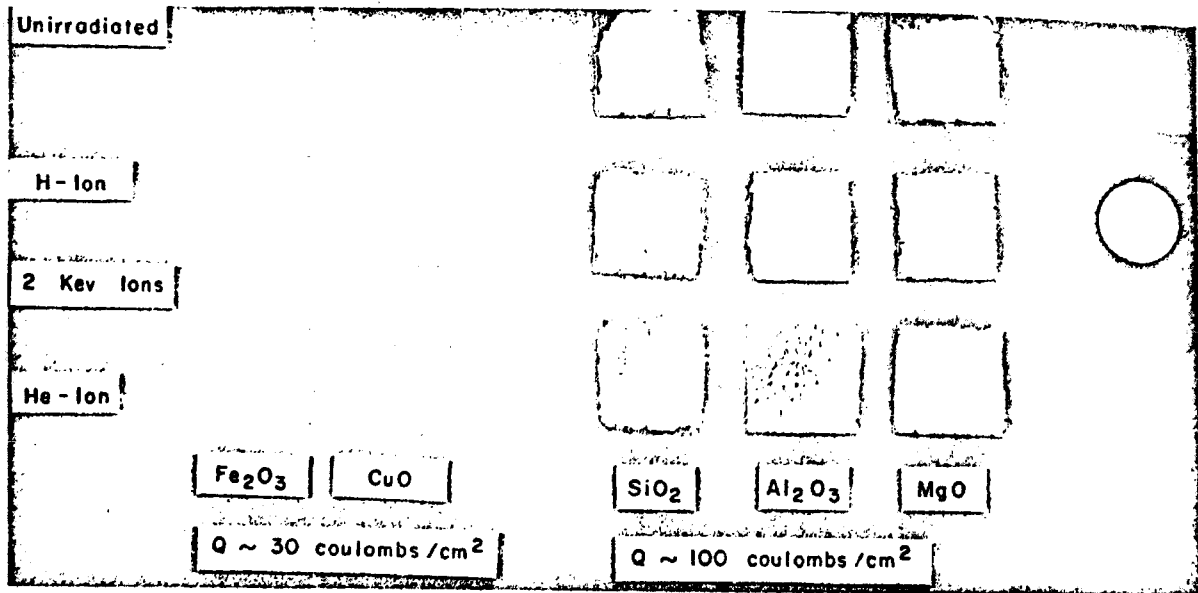


FIGURE 7-9: Effect of irradiation on mineral oxide powders.

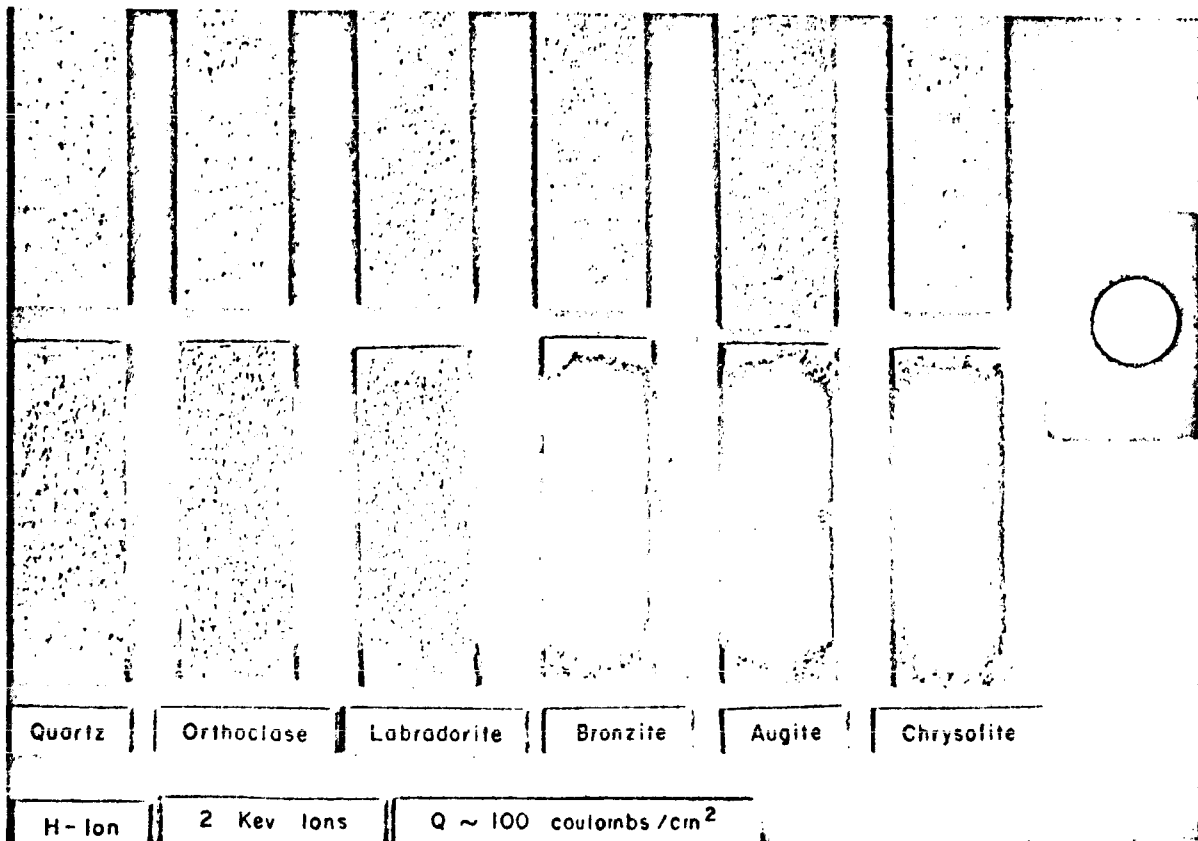


FIGURE 7-10: Effect of irradiation on mineral powders.

bombarding pure materials what the optical properties of a mixture of materials would be. Bombardment by helium ions darkened all the powders quite a bit, with the exception of the magnesium oxide which darkened very little. Even so, the mixtures have a lower reflectivity than the pure materials.

This figure also illustrates that the SiO_2 lattice has a strong role to play in this phenomenon since the mixture of the aluminum oxide and magnesium oxide did not darken nearly as much as did the mixtures which contained the silicon dioxide.

Figure 7-9 shows some pure metal oxides which were bombarded. The ferric oxide was darkened in both cases by both hydrogen and helium ion irradiation to about the same extent. Hydrogen ion irradiation reduced cupric oxide to pure metal but helium ion irradiation did not greatly affect it. This illustrates that, particularly in the case of copper oxide, there evidently are some chemical effects

occurring which are important for certain pure materials, in addition to the mechanical effects of sputtering. The other oxides were affected only slightly by irradiation.

Figure 7-10 shows some rock-forming mineral powders before and after hydrogen irradiation. Quartz is not changed much. There is a strong correlation between composition and the amount of darkening. Basic materials generally turn darker and bluer than acidic materials.

Figure 7-11, also illustrating the effect of composition, shows enstatite, which is mainly magnesium silicate, and hypersthene, in which some of the magnesium atoms are replaced by iron. The hypersthene is darker and bluer than the enstatite. In other words, the iron content has an effect on the optical properties of an irradiated mineral. This probably has something to do with the fact that iron is a transition metal and itself forms non-stoichiometric compounds.

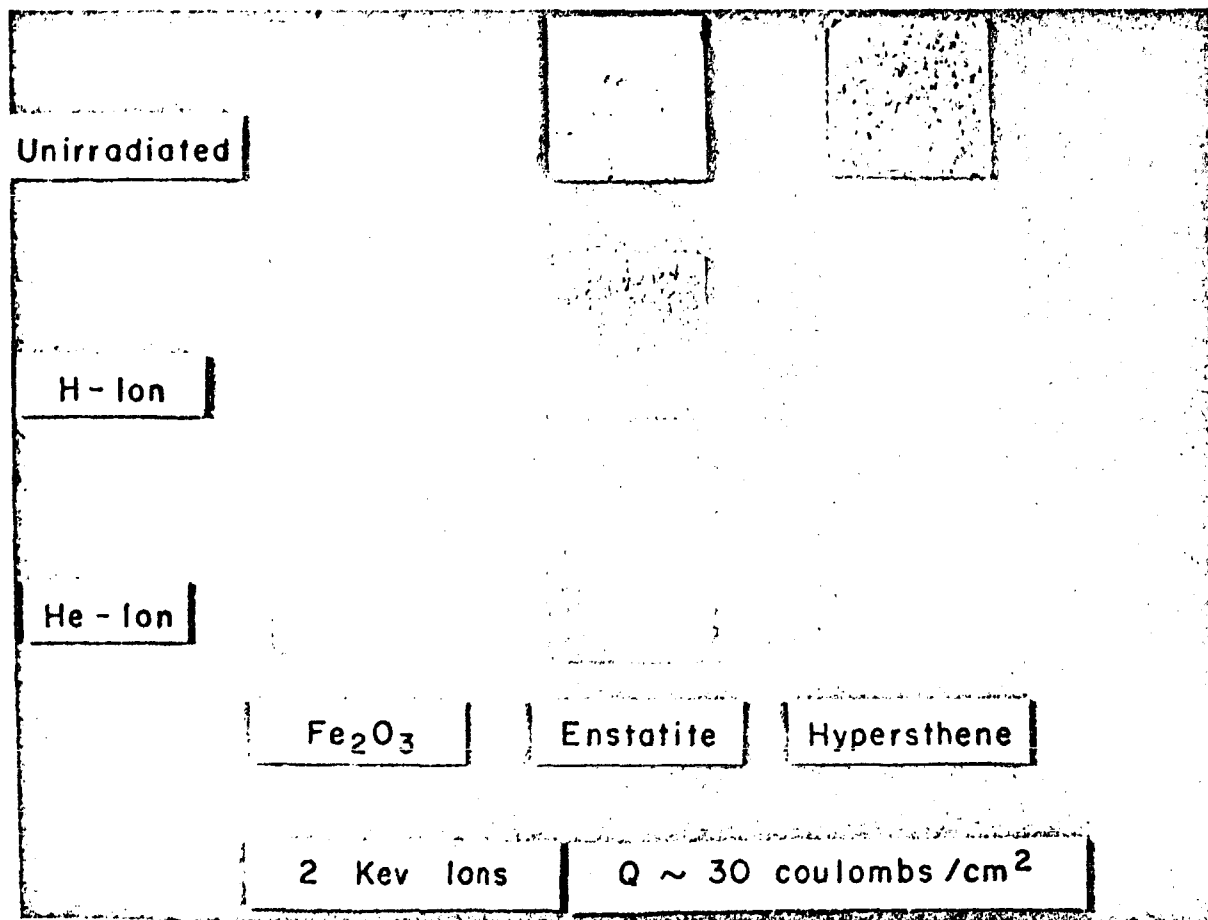


FIGURE 7-11: Effect of irradiation on Fe mineral powders.

Figure 7-12 shows some irradiated igneous rock powders. Again the effect of composition is striking—the basic materials are generally darkened and less red than the acidic materials. Note that the irradiated chondrite is much darker than any of the igneous rocks.

Figure 7-13 gives the effect of particle size on the quantitative photometric properties of olivine basalt powder; these are the photometric characteristics which were defined in connection with Figure 7-1. The gray bands on all the curves are the range of lunar values.

The normal albedo of the unirradiated material increases as the particle size decreases, but for the irradiated material the albedo is roughly constant. The backscatter ratio decreases drastically with particle size. The amount of positive polarization is a strong function of particle size and decreases in a very striking manner as particle size decreases. For large materials the polarization is far too great for the moon. For large particles the phase angle of the positive polarization peak is shifted to much higher values than is true for the moon. In our apparatus we can measure only up to a maximum phase angle of 130 degrees and the ϕ_+ curve is still

rising at 130 degrees for the particles which are labeled with an arrow. Thus the polarization provides another indication that large chunks of material are not exposed at the lunar surface. This has been emphasized by Dollfus. The material labeled as being one centimeter in size on the figure actually refers to the freshly broken surface of solid rock and is not pulverized material.

It is clear from this figure that only particles which are of the order of 1 to 10 μ in size can simultaneously reproduce all the lunar photometric characteristics. It is possible, however, to reproduce one or two of the lunar photometric properties in other ways. For instance, a high backscatter ratio can be obtained by using chunks of vesicular rock formed into a jumbled surface that is riddled with tunnels pointing in all directions. However, in general, such large chunks will have a high polarization, far too high for the moon, and the phase angle of the maximum polarization has too large a value. Also, Lyot and Dollfus found in their investigations that certain varieties of volcanic ash would have the correct polarization curves, but these ashes do not have the correct brightness functions. It may be inferred that the size distribu-

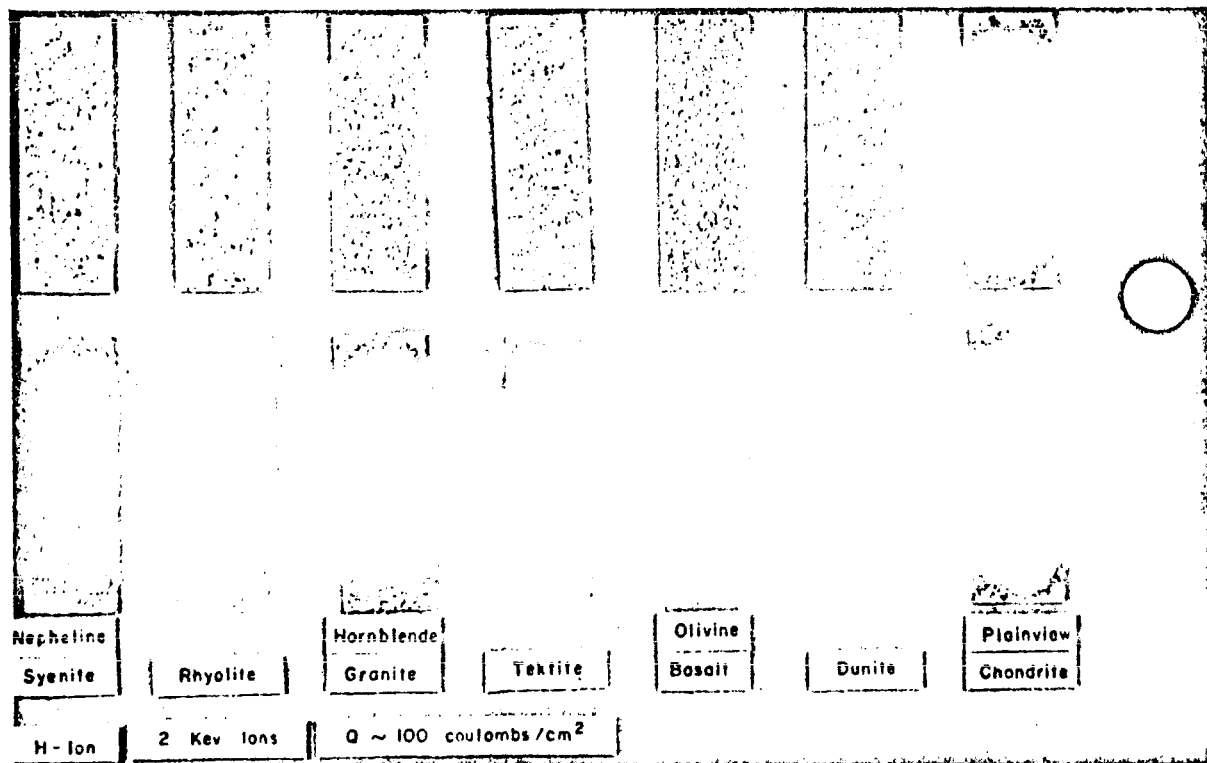


FIGURE 7-12: Effect of irradiation on rock powders.

THE NATURE OF THE LUNAR SURFACE

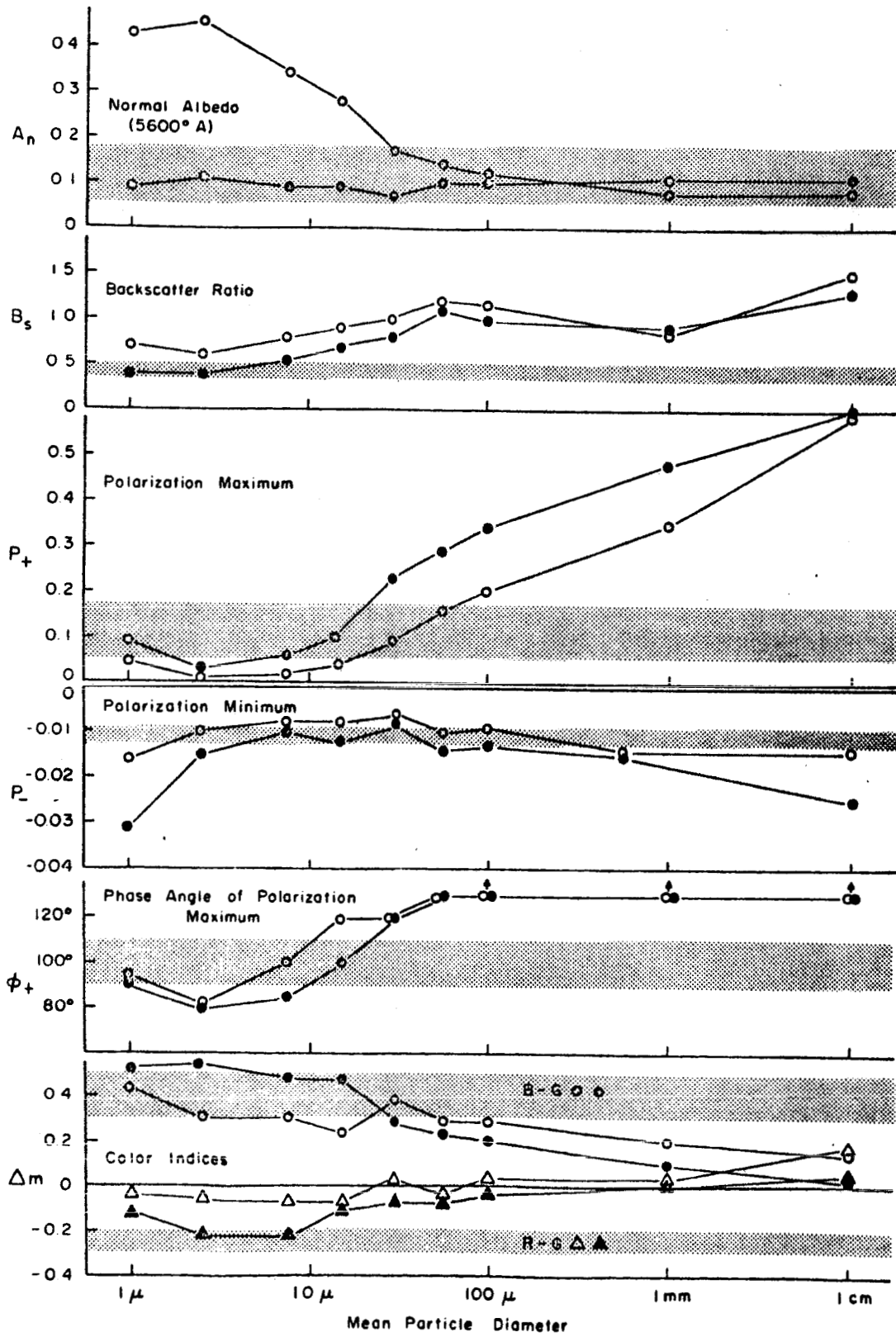


FIGURE 7-13: Photometric properties of olivine-basalt powders vs particle size.

tion of particles composing the lunar soil peaks somewhere between 1 and 10 μ .

Figure 7-14 shows the effect of radiation dose on the photometric properties of olivine basalt powder. All the curves saturate in a time on the order of a hundred thousand years or so on the moon. The effect of gamma ray irradiation is also

shown in this figure; the optical properties of material treated with gamma rays is virtually the same as for the unirradiated material. The effect of helium ion irradiation to a dose of about 88 coulombs/cm² is essentially the same as a three to five times larger dose of hydrogen ion irradiation.

On the basis of these curves, it is reasonable to

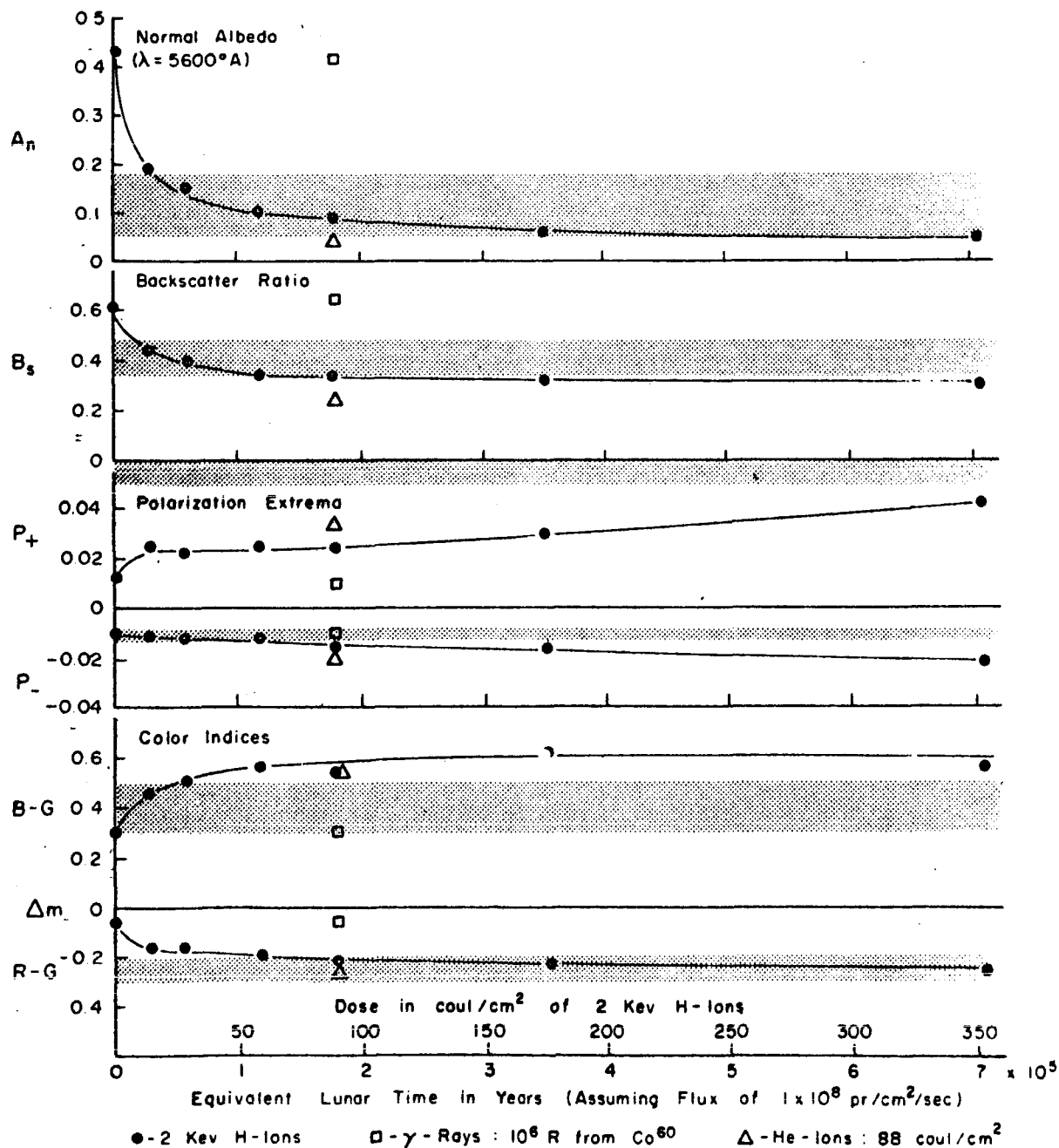


FIGURE 7-14: Photometric properties of 1-5 μ olivine-basalt powders vs irradiation time.

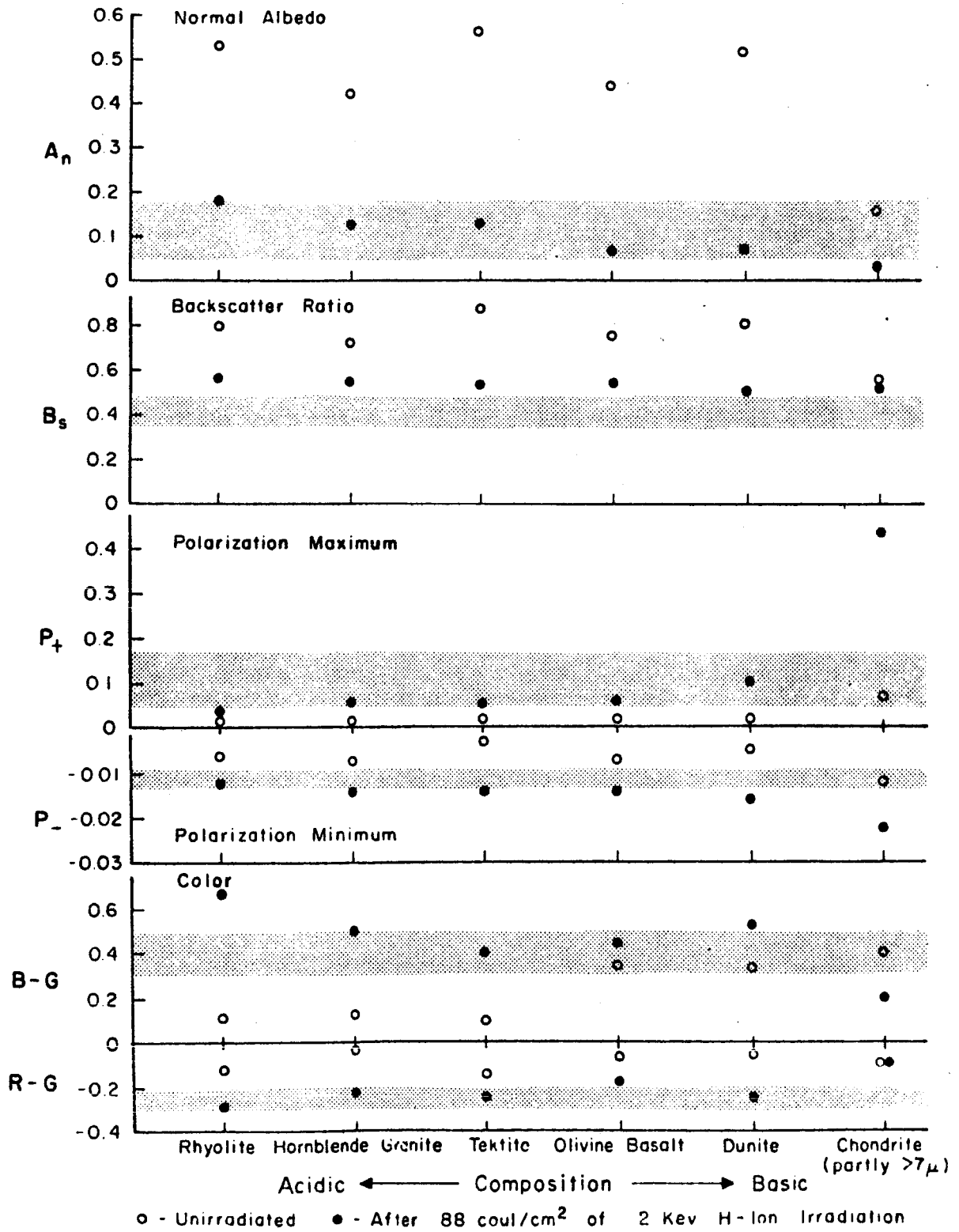


FIGURE 7-15: Photometric properties of igneous rock powders.

state that the average particle on the lunar surface has been exposed for a time on the order of a hundred thousand to a million years. This is much less than any estimates of the ages of most features on the lunar surface.

After prolonged irradiation the albedo of most rock powders actually gets lower than the lunar surface albedo. Hence, it appears that some agent is counteracting this darkening process. Some irradiated rock powder was placed in a vacuum furnace and heated to 450°C and held there for over a day. There was no appreciable change in the photometric properties; these coatings appeared to be quite stable.

A reasonable explanation for the higher lunar albedo is that micrometeorites are continually stirring up the surface and exposing undarkened materials. At all times one sees a mixture of darkened material and undarkened material such that the average particle must have been exposed on the lunar surface for something like a hundred thousand years.

We also investigated the effect of porosity of the surface. We took the same powder and formed surfaces, by pressing, pouring, and sieving the powder, in order to see the effect of compaction on the photometric properties. In the case of both the pressed and the sieved material, the photometric peak is wider than that of the moon, but for different reasons. Only the poured material gave the correctly shaped backscatter peak. The pressed powder does not have a sufficiently complex and open structure to backscatter well. The sieved powder has the requisite complex structure, but even after irradiation the particles are somewhat translucent. In a loose structure, light can shine through the particles and the powder will appear too bright at large phase angles. When a powder is poured, the particles form clumps sufficiently complex to backscatter well, but which will also block some of the transmitted light. Surfaces with the correct optical properties can be made by pouring the powder in a vacuum as well as in air.

Apparently the lunar surface is not porous to the extreme extent that Hugh Van Horn and I suggested previously. The surface does not have an extremely underdense, fairy castle structure, but rather consists of loose clumps of fine particles which are quite complex and capable of backscattering strongly. The porosity is about 80 per cent, instead of being something like 90 per cent,

which would be the case for the fairy castle structure. This is still quite underdense. The powder is very compressive; it has the consistency of baking flour. If there were even a few feet of this material, an astronaut would sink into it up to his knees and would have great difficulty churning his way through. The dust would stick to him and would likely be quite a nuisance in a number of ways, and I imagine that on the moon anything which is a nuisance is dangerous.

Figure 7-15 shows the effect of chemical composition on the photometric characteristics of rock powders. In all cases, the effect of irradiation is to bring the photometric properties close to those of the moon. The backscatter ratio of the irradiated powder shown here is a little bit high. However, in this experiment we were more interested in investigating the effect of composition on the photometric properties than in duplicating those of the moon, so uniformity of the samples was our primary concern. As shown in Figure 7-2, the backscatter ratio, at least for basic rock powders, can be reduced by a proper preparation of the surface.

Most rocks, when ground to a fine particle size, are relatively colorless, so their color indices are quite low. Only after irradiation does the color move toward the lunar values. The general tendency of the effect of irradiation is to redden rock particles. Evidently the dark compounds that coat these particles absorb more heavily in the blue than in the red.

There are a few remarks that can be made about the effect of composition. As one goes from an acidic to a basic material the albedo of the irradiated powder decreases. There is a slight tendency for the backscatter ratio to decrease. The polarization maximum tends to increase, and this is directly connected with the decrease in albedo. The polarization is dependent on two things: (1) the light which is reflected from the surface of the particles, which is positively polarized; and (2) the light which is refracted through the particles, which is negatively polarized and which tends to cancel out some of the positive polarization. As the material is darkened and made more absorbing, some of the refracted, negatively polarized light is cut out and the positive polarization is enhanced. Roughly speaking, irradiated acidic materials are redder than the basic materials, especially their blue-green index. However, there is not much variation in the red-green index. These are rough

trends, but there are departures from these trends.

Now consider the powdered chondrite shown at the extreme right of Figure 7-15. This is a sample of Plainview, a bronzite chondrite. After receiving the same amount of irradiation as the rest of the rocks, its albedo dropped far below that of the lunar surface. The polarization positive maximum was way up to 43 per cent. The negative minimum dropped down to 2.5 per cent. The colors remained much bluer than the moon. There may be some indication here that at least chondritic meteorites do not come from the moon. One might say that perhaps the flux of micrometeorites at the lunar surface which is stirring up the material is bigger than we think it is, so that the average particle is irradiated just very slightly. This would tend to keep most of the optical properties of the chondrite within the range of lunar values except for the red-minus-green index, which would stay too low.

The primary reason that the photometric properties of the chondrite are different from those of igneous rocks is the high metallic iron content of the meteorites. Adding 15 per cent by weight of metallic iron to any rock has the effect of increasing the positive and negative polarizations and of decreasing the color, making the material much bluer.

Finally I would like to see if these studies can give any indication concerning the composition of the highlands and the maria. As you know, there are two theories. One says that the highlands are of different composition than the maria. Figure 7-15 is consistent with the theory of the highlands' being more acidic than the maria.

The other theory, due to Gold, is that the material on the highlands contains a larger admixture of unirradiated material than that in the maria. That is to say, the material exposed on the surface of the maria is older on the average than the material covering the highlands. However, Figure 7-14 shows that all the photometric properties are monotonically changing functions of radiation dose. That is, as one increases the dose, the positive polarization rises, the negative polarization decreases, the color indices all change monotonically.

Thus, if the *only* effect were one of exposure age, then we would expect that the differences in photometric properties of the highlands and the maria would always be in the same direction everywhere on the moon. It is known that this is not always the case. As far as I know, there is no correlation between, for instance, the amount of negative polarization and the albedo, although there is a correlation between positive polarization and albedo. In general, the maria tend to be somewhat bluer than the highlands; this is just the opposite from what would be expected of most rocks, which tend to get redder with increasing dose, rather than the other way around. However, this last argument is not a very strong one because igneous rocks which are rich in ferric oxides are initially red and become bluer under irradiation. Nevertheless, I feel that there are some tentative indications that the differences in the photometric properties of the light and dark areas of the moon are at least partly due to real differences in composition and not just to differences in exposure age.

8.

The Application of Polarized Light for the Study of the Surface of the Moon

A. Dollfus

Observatoire de Paris, Section d'Astrophysique, Meudon (Seine et Oise), France

The curve of polarization of the moon is the plot of the percentage of polarization as a function of the phases of the moon. The polarization is called positive if the largest component is perpendicular to the plane of the sun, the earth, and the moon, and is called negative if this component is parallel to this plane. Figure 8-1 shows the fringe polariza-

meter that we used for those measurements. The accuracy is 10^{-3} or 0.1 per cent in the amount of polarization.

Figure 8-2 is the original curve that Lyot produced more than half a century ago. It shows the maximum of polarization for the evening moon and the morning moon. We immediately see that we

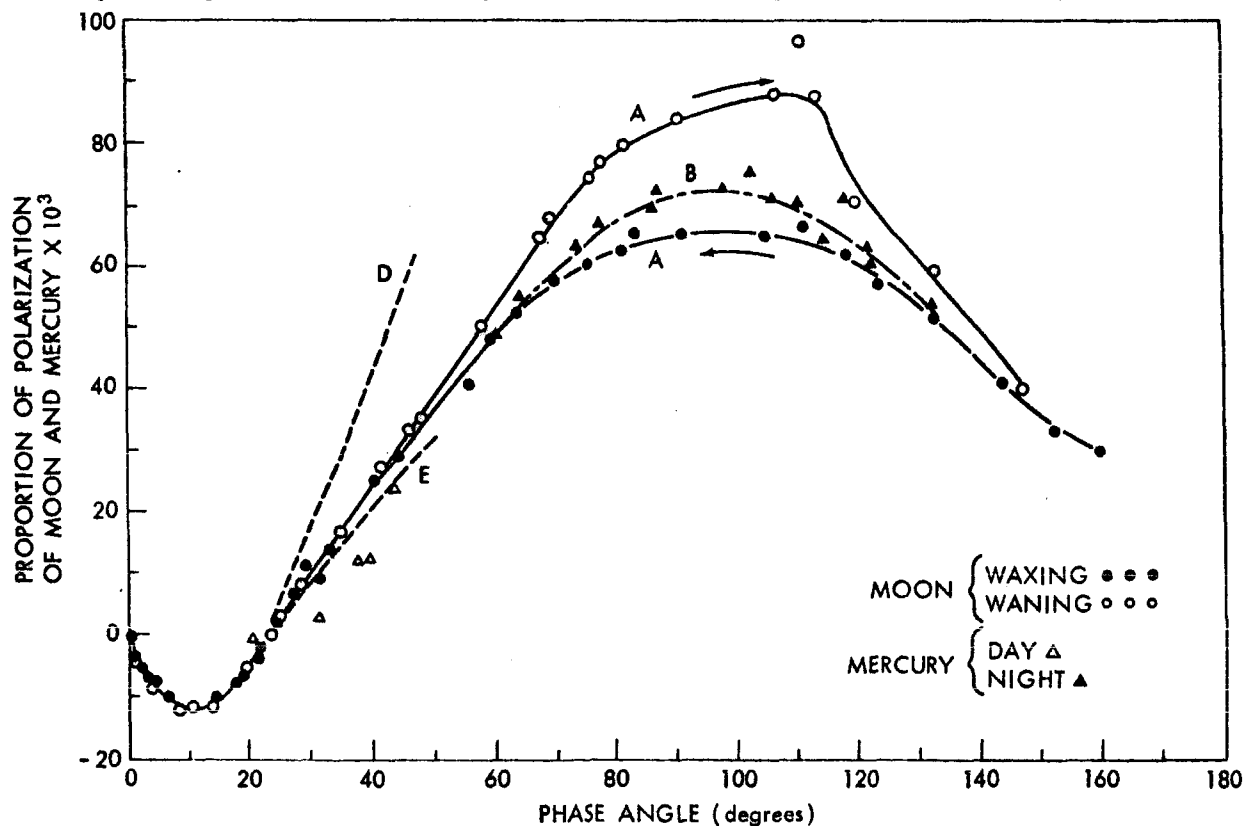


FIGURE 8-1: Polarization of the moon (after Lyot, 1929).

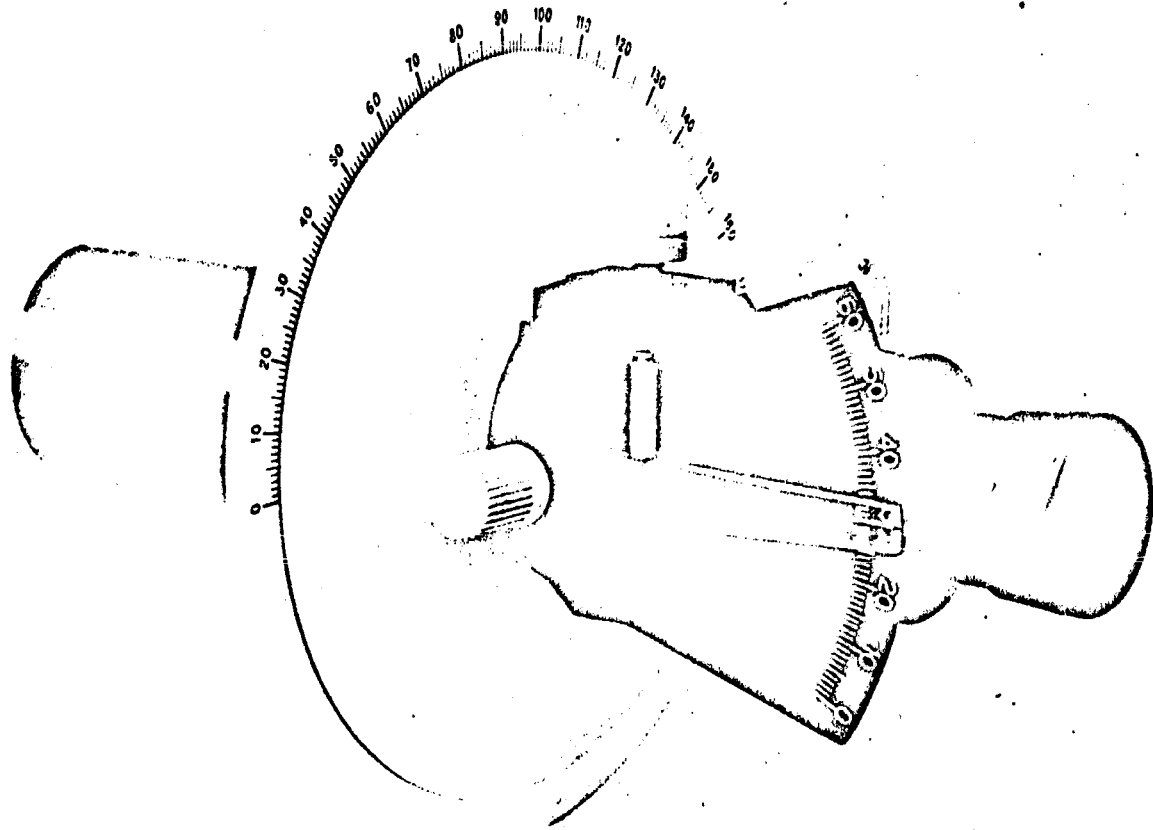


FIGURE 8-2: The fringe polarimeter used to measure the polarization of the moon.

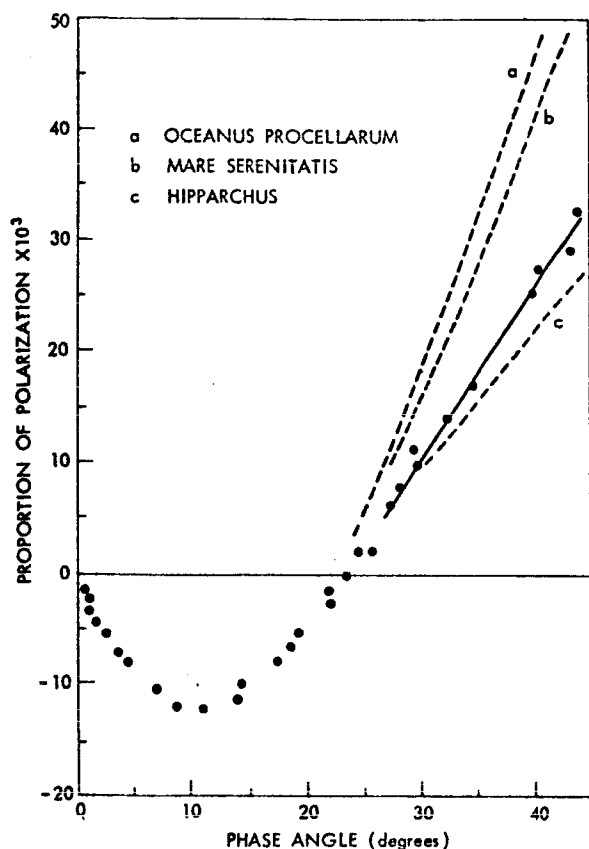


FIGURE 8-3: Measurements on the negative branch of the polarization curve.

can split the problem in two: first, the explanation of the negative branch, and second, the discussion of the maximum of polarization.

Figure 8-3 shows measurements of the negative part of the curve. It is close to the full moon, just before an eclipse, when the phase angle is very small. The dispersion of the measurement is less than 0.1 per cent. Curves are given for the darkest maria, like Mare Procellarum, and for the bright areas. Departures for the near curves occurred for phase angles larger than 20 degrees, but all of these measurements are the same in the negative branch. For measurements made in all spectral ranges from visible light to infrared at 1.05μ , the negative branch remains exactly the same. This branch is not sensitive to the wavelength nor to the albedo of the surface.

At the laboratory we are able to reproduce such a curve and it appears that it is very specific of a special kind of surface; it can be reproduced only

on powders of dark grains of all sizes stuck together, the grains completely absorbing the light in a few wavelengths of thickness.

Figure 8-4 shows laboratory results about the negative branch of the polarization on different kinds of material, in cases of loose deposits and compact deposits of powders. The loose deposits of dark grain materials reproduced exactly this property of the surface of the moon. The compact deposit did not. We measured many other kinds of materials. I published some results in the past in Professor Kopal's book and in Professor Kuiper's book; therefore, I prefer not to discuss it extensively here.

The case is that all the surface of the moon gives the same curve. So we must conclude that the surface of the moon is covered in all the parts by a layer of dust at least a millimeter thick, which is made of small grains and is completely absorbing. I would like to be very positive on this point. It is certain, because fortunately the curve is very specific for powder of dark grains for all the areas of the surface of the moon.

I have another proof of this property: it is depolarization of the light. If a sample is lighted by a completely polarized light, the scattered light is partly depolarized; the residual amount of polarization is a function of the reflecting power of the surface. We measured the depolarization factor of the surface of the moon by measuring the polarization of the ashen light, because the ashen light is the scattering by the moon of the light coming from the earth. The light of the earth at 90 degrees is very highly polarized. Therefore, if we measure the polarization of the ashen light, and if we know the initial polarization of the light of the earth, we can deduce the depolarization factor of the surface of the moon.

Figure 8-5 is a picture that we took at Pic-du-Midi with the coronagraph, which was used for this study of the moon. The occulting disk of the moon has a window with absorbing glasses, showing the edge of the moon, namely Mare Crisium. The ashen light is passing at the edge of the disk. The last mountains at the terminator are seen at the edge of the disk. This plate was taken before the full moon, with a phase angle of about 20 degrees. We are able to detect and measure the ashen light very close to the full moon.

Polarimetric measurements on the ashen light selected with the coronagraph enabled us to give

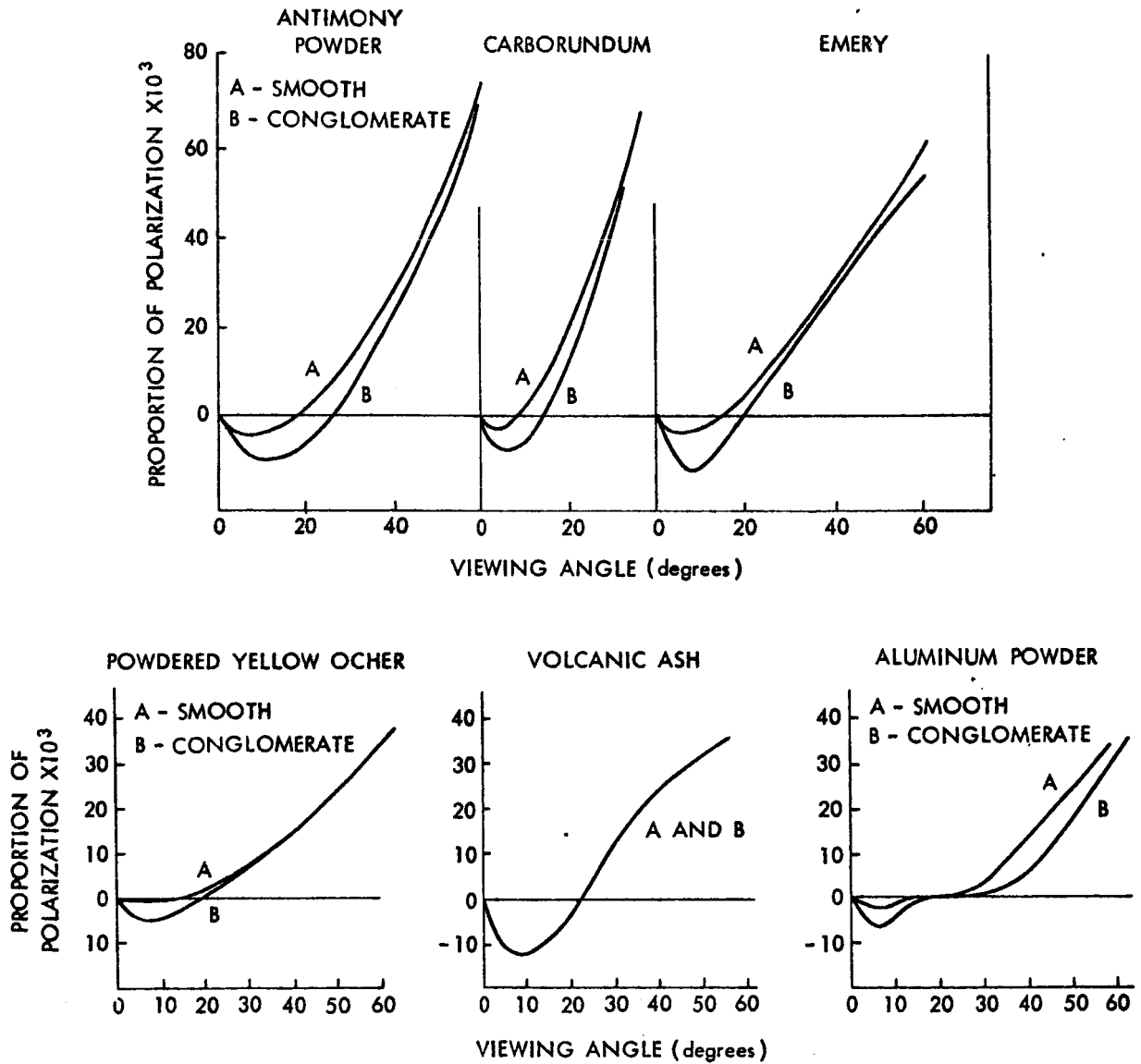


FIGURE 8-4: Laboratory-derived negative-branch polarization curves for various materials.

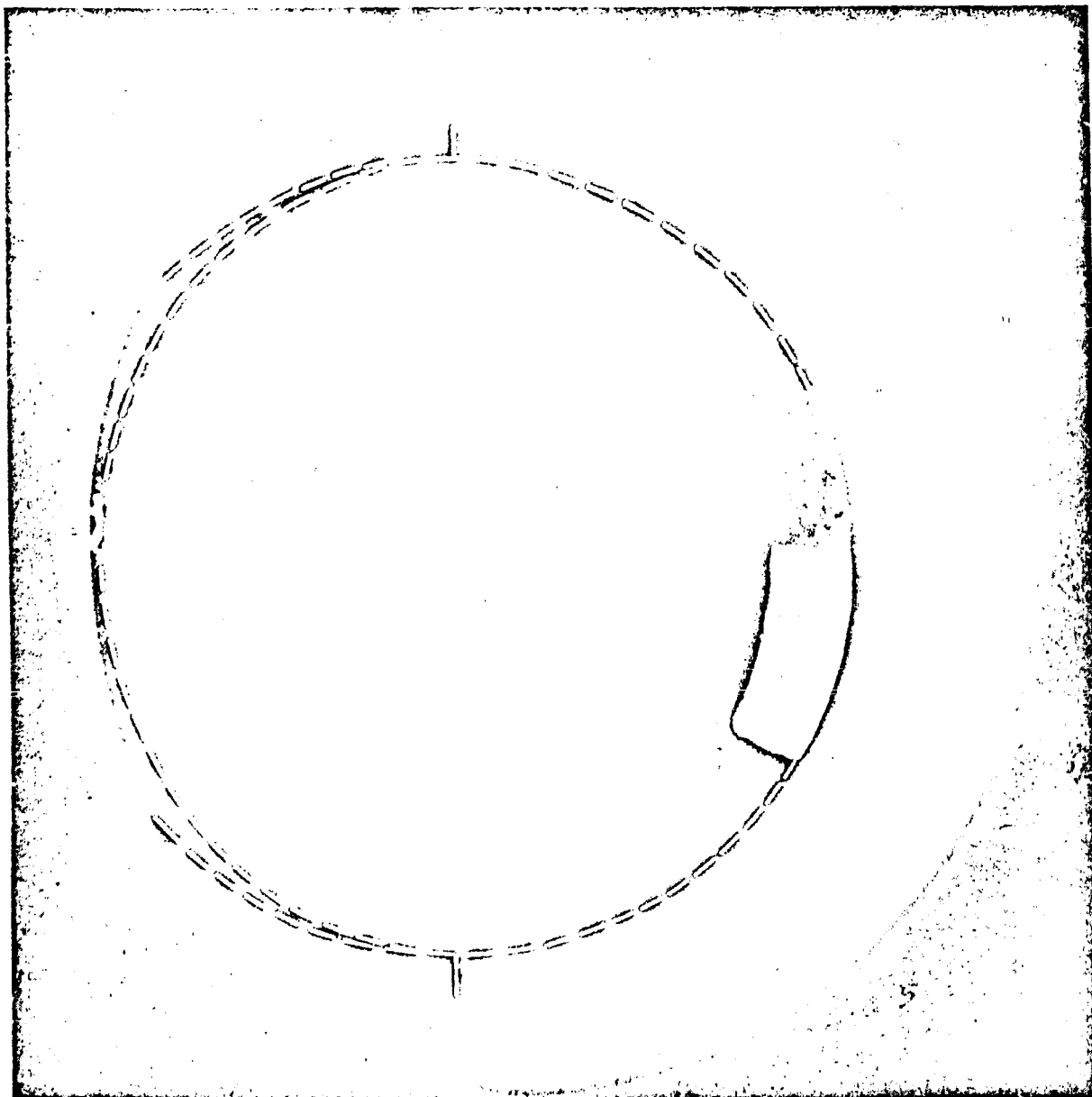


FIGURE 8-5: Coronagraph picture of the moon, creating an artificial lunar eclipse with the ashen light shown at the edge of the occulting disk.

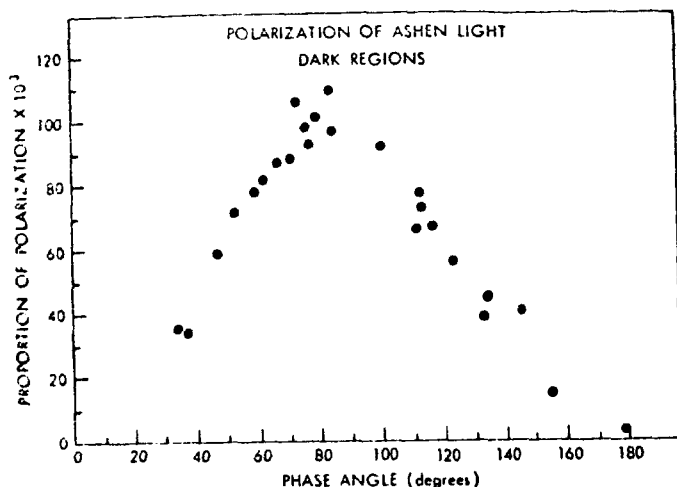


FIGURE 8-6: Polarization of ashen light on the dark regions of the lunar surface.

the complete polarization curve of this ashen light, as seen in Figure 8-6. The plots are the phase angle vs the amount of polarization. If we compute the polarization of the earth we conclude that most of the polarization is due to scattering by the atmosphere of the earth. The maximum polarization is expected to be about 80 degrees. It is exactly what we found. But we have to know the exact amount of polarization given by the earth at an 80-degree phase angle. We did that by measurements from balloons.

Figure 8-7 shows one of the flights we made in France. This particular flight we launched from the Meudon Observatory. On the occasion of such flights using a visual polarimeter we measured the polarization at several heights and were able to extrapolate the polarization as if the earth were seen from the outside.

Figure 8-8 shows some of the results. One of the two curves at the top is a measurement of the surface from the ground. The other is taken at a height of 1 km. With similar measurements we are able to extrapolate to infinity. If we know the amount of polarization of the moon, we are able to deduce the depolarizing factor of the earth.

In Figure 8-9 the open circles are the measurements from the ashen light, of the depolarization factor of the surface of the moon as a function of the albedo of the surface. The dots and crosses are measurements obtained on dark powders made of small grains of completely absorbing material. It fits exactly the measurements; other kinds of materials like bare rocks or powders of transparent grains did not. All other kinds of surfaces are

completely different. Again, the depolarization factor is a very crucial result, characteristic of a powder of very absorbing grains. This powder covers all the surface of the moon.

Figure 8-10 is a microscopic picture of a typical powder that is probably similar to the surface of the moon; the size is 3 mm square. This powder gives exactly the negative range of polarization and the depolarization coefficient of the surface of the moon.

The next problem will be to try to improve these results by studying the maximum of polarization. The variation of maximum polarization may enable us to give additional data about the composition and the nature of these powders. Unfortunately we have not yet completed this work; we are doing the measurements. I would like to report here the current state of the measurements. We tried to extend the polarization to a larger range of wavelengths because the maximum of polarization is wavelength dependent.

We divided the moon in selected areas in which we are taking polarimetric measurements (Figure 8-11). We have two kinds of areas: 14 large ones for the infrared to ultraviolet measurements in all the ranges accessible from earth, and smaller areas for careful studies of variations of polarization on special features. We have several polarimeters for several wavelength ranges. Figure 8-12 shows the telescope itself, with photoelectric polarimeter. It is a Cassegrainian coudé, and the light is reflected by a mirror, introducing a spurious polarization that we have to take into account in the final study of the measurements.

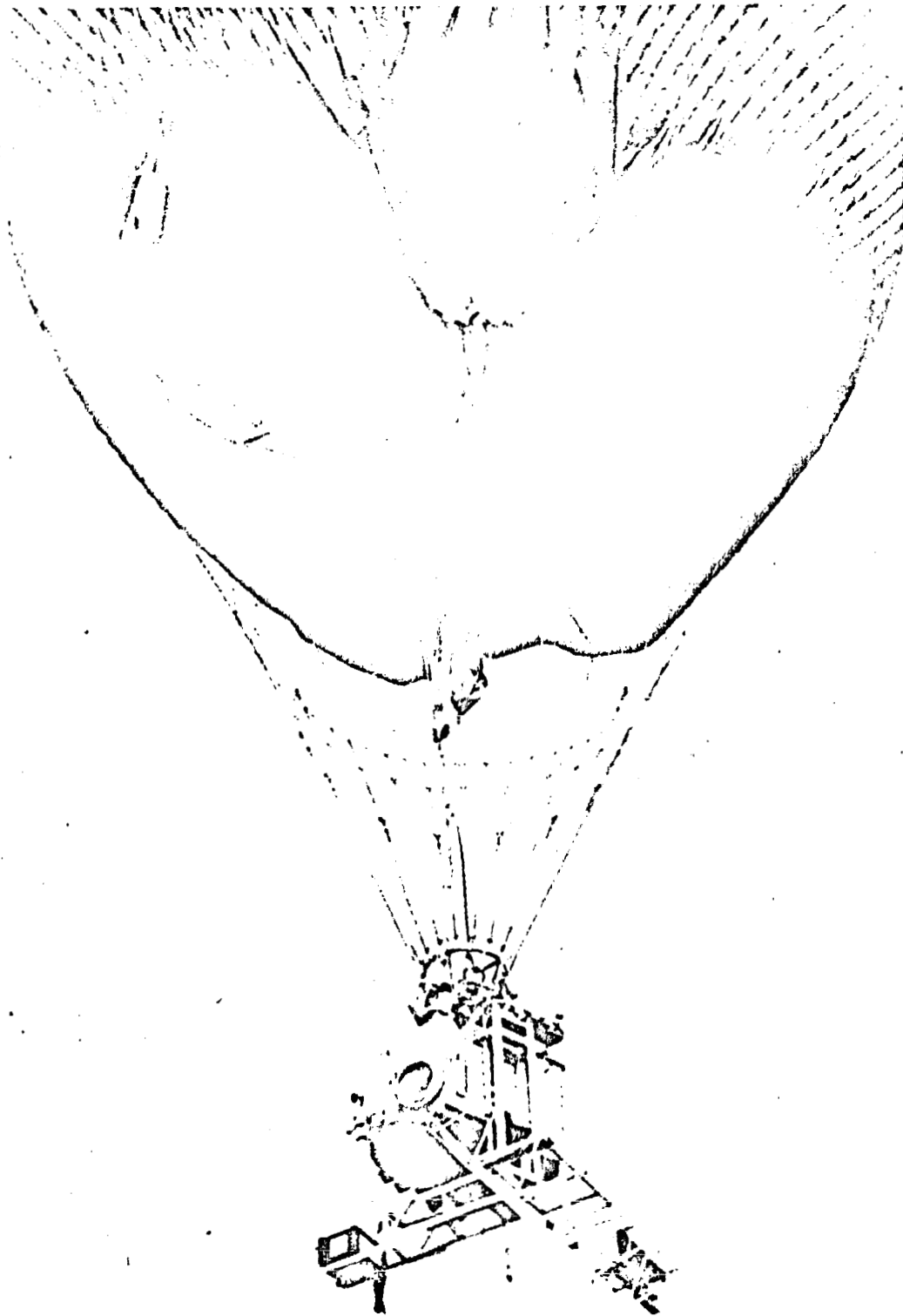


FIGURE 8-7: Flight launched from Meudon Observatory.

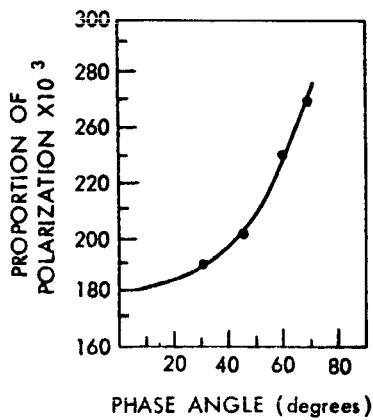
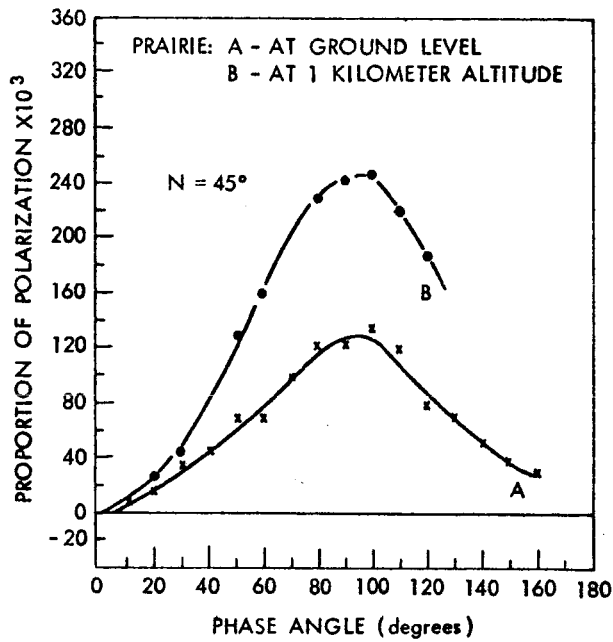


FIGURE 8-8: Polarization measurements of the ground from near the surface of the earth and from a height of 1 km.

Figure 8-13 shows the infrared measurements for special areas, at 0.85μ wavelength. One of the two curves is for one of the darkest surfaces of the moon, Mare Tranquillitatis. An idea of the accuracy of the measurements is given by the scattering of the dots. The other curve is for one of the lightest areas on the surface of the moon, northeast of Mare Crisium; the negative branch is

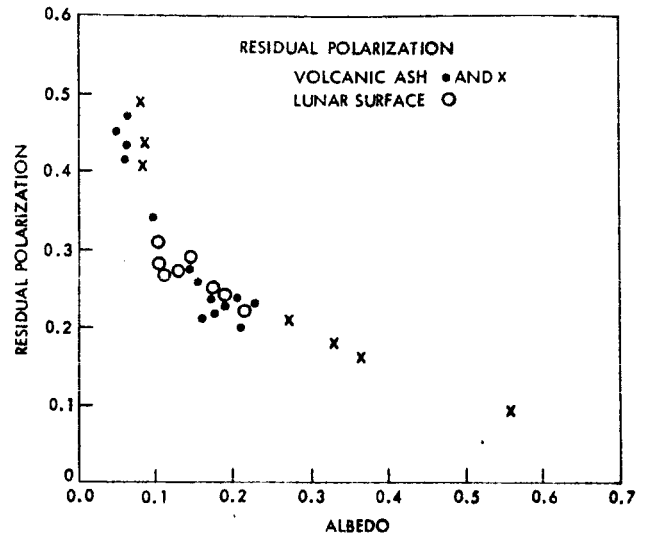


FIGURE 8-9: Measurements of the depolarizing factor of ashen light and dark absorbent powders.

completely independent of the albedo, but the maximum of polarization is strongly dependent on the albedo.

Now going more to the infrared, Figure 8-14 shows the curves for 0.95μ . The polarization is reduced in the two cases. Again the negative branch is still the same. Figure 8-15 is for 1.05μ , and again the scattering of the measurements is good, but the polarization is still reduced. The maximum of polarization is a function of the albedo and of the wavelength.

Now we have enough measurements to disentangle these two factors; Figure 8-16 shows the variation of the maximum of polarization as a function of the brightness or the albedo. For visible light we have a very sharp variation of the maximum of polarization with brightness, and for infrared measurements we have again this variation, but with a lower amount.

Figure 8-17 shows the variation of the maximum of polarization as a function of wavelength. This is for four different areas: Mare Tranquillitatis, one of the darkest areas on the moon; Mare Crisium; and two light continents. The curves show the strong variation of maximum of polarization as a function of wavelength, from 1.1 to 0.6μ .

So we have now about all the quantitative information about the properties of the variations of the maximum of polarization with albedo and wavelength. We can make comparative measure-

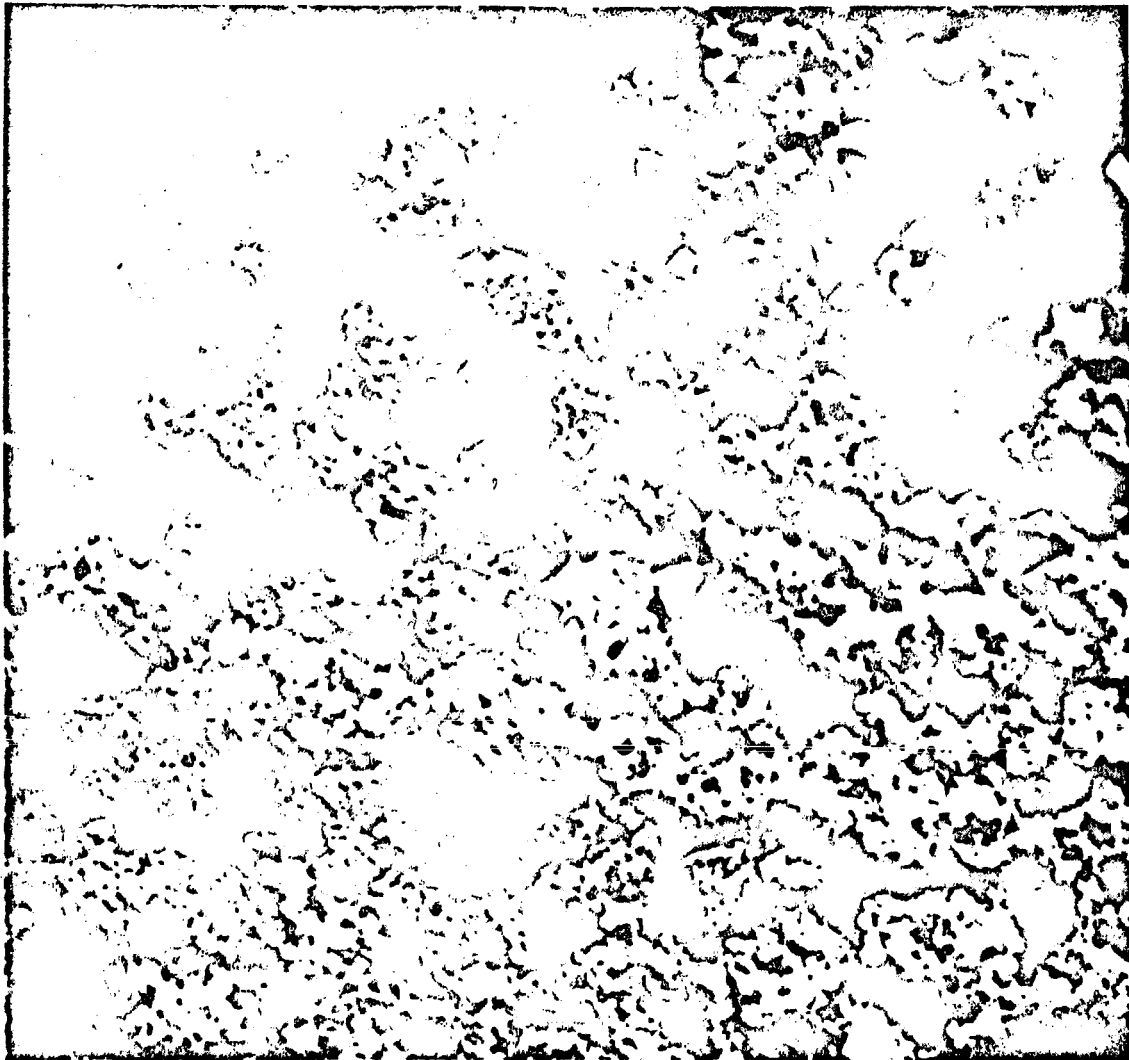


FIGURE 8-10: Picture (3 mm square) of a typical powder viewed through a microscope.

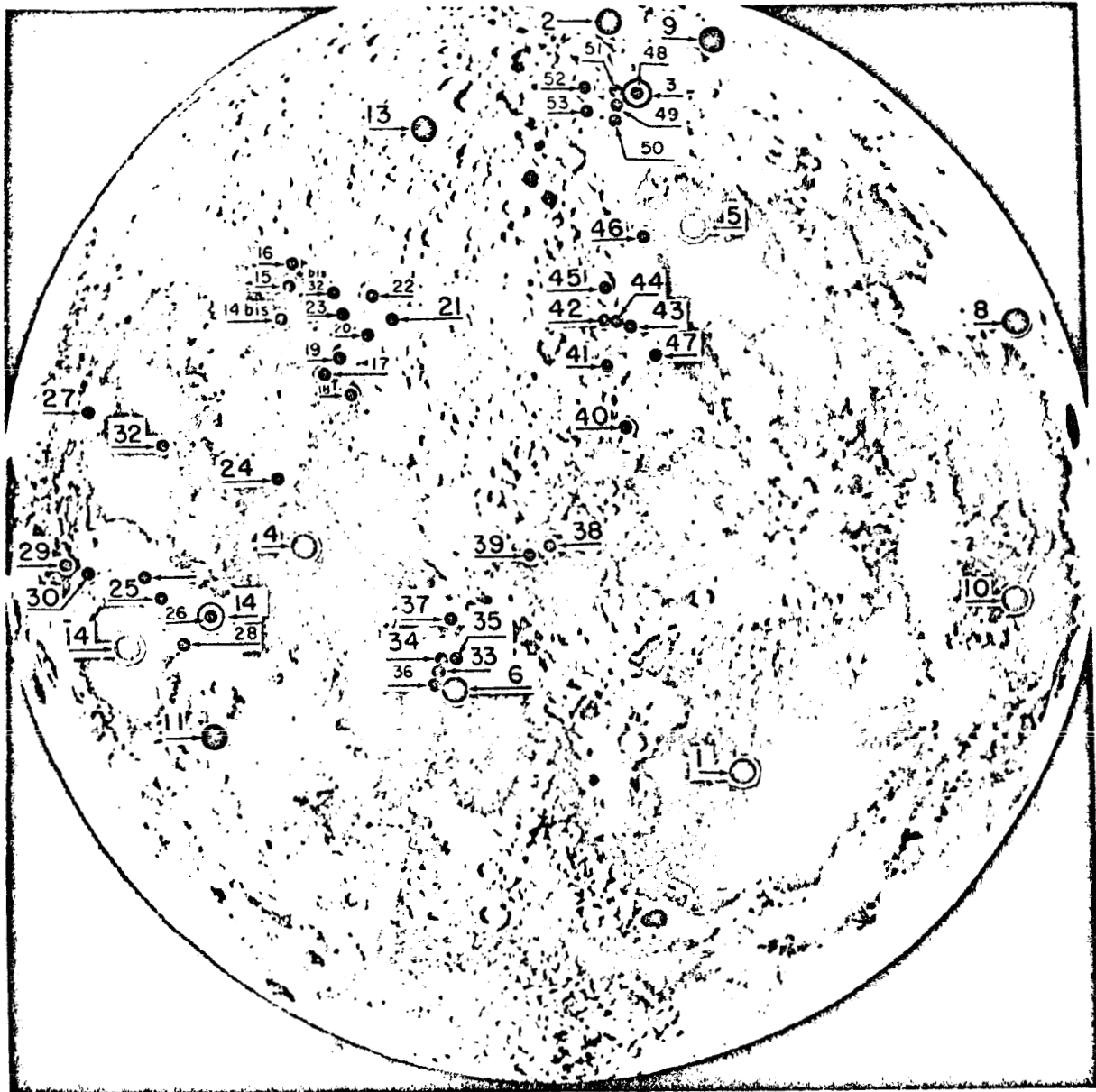


FIGURE 8-11: Selected areas under polarimetric measurement study.



FIGURE 8-12: 40-inch Telescope at Meudon Observatory used for photoelectric measurements of polarization on planets and the moon.

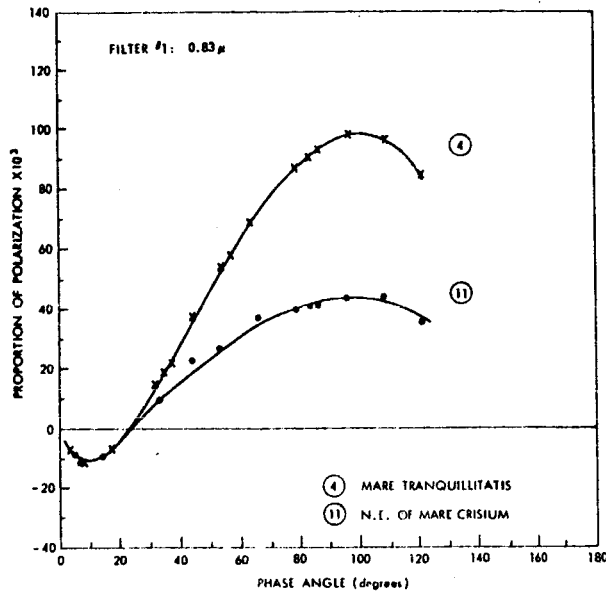


Figure 8-13: Infrared measurement, 0.83μ of wavelength; 4 is Mare Tranquillitatis, 11 is northeast of Mare Crisium.

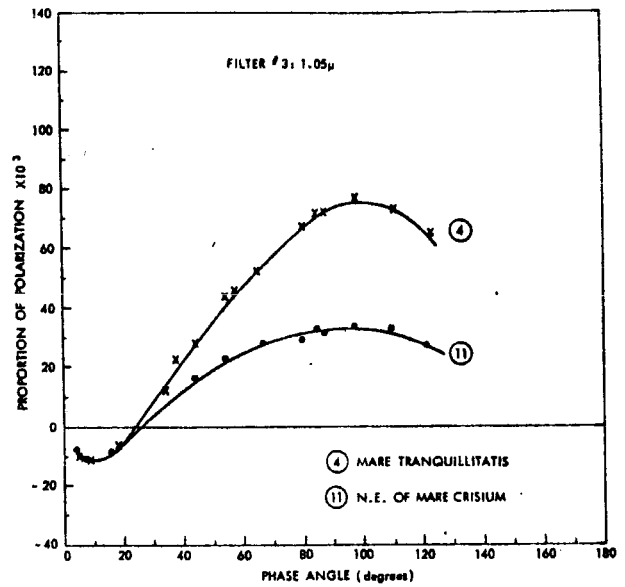


FIGURE 8-15: Infrared measurement, 1.05μ of wavelength; 4 is Mare Tranquillitatis, 11 is northeast of Mare Crisium.

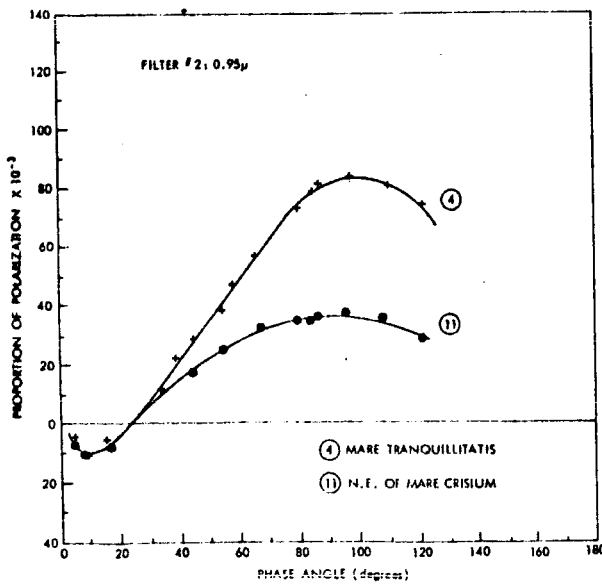


FIGURE 8-14: Infrared Measurement, 0.95μ of wavelength; Mare 4 is Tranquillitatis, 11 is northeast of Mare Crisium.

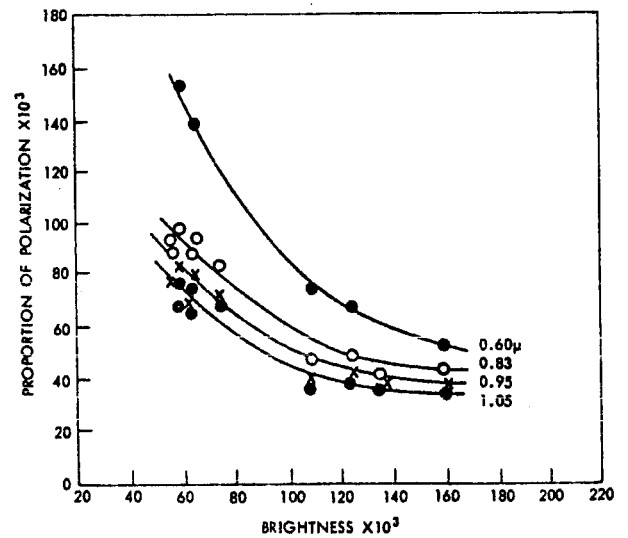


FIGURE 8-16: Variation of the amount of the maximum polarization as a function of brightness.

ments at the laboratory to see if some information can be deduced from these data. We measured at the laboratory with the photoelectric polarimeter and with the visual polarimeter.

Figure 8-18 shows one of the instruments we used for laboratory measurements. The sample is put in the holder, and we can change the angle and azimuth of the light. We can also tilt the direction of observation of the photoelectric polarimeter.

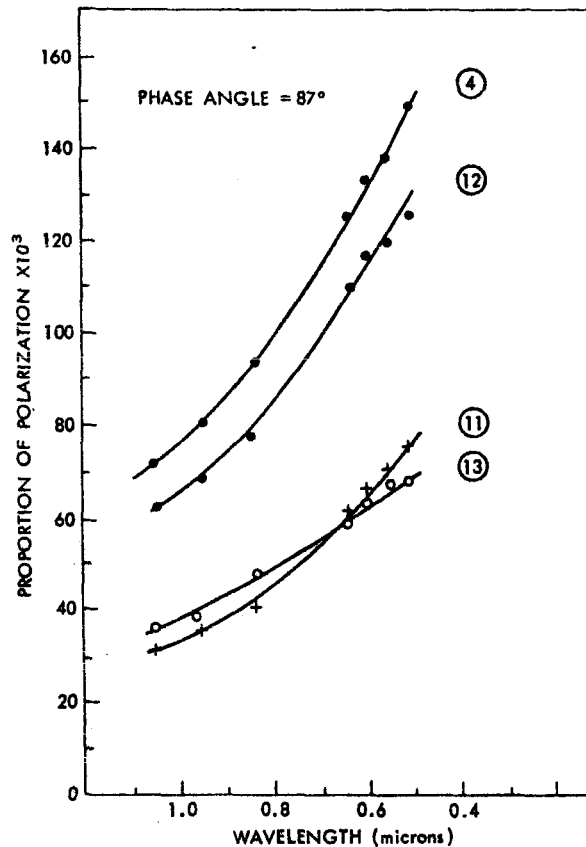
Figure 8-19 shows some characteristic curves with materials selected for obvious theoretical reasons: two kinds of obsidian, the brecciated coating of the Meteor Crater in Arizona, tektites, etc. We measured also several other powders of this kind. It can be seen immediately that all these curves are too flat; they are not able to reproduce the negative branch. This is because these surfaces are not dark enough. I pointed out that we must use powder of grains in loose deposits of very absorbing material; all these surfaces are not dark enough.

Figure 8-20 shows different kinds of achondrite meteorites with enstatite. The negative branch cannot be reproduced because the powders are far too light. The maximum of polarization is completely out of scale.

Figure 8-21 shows the results for the different kinds of chondritic meteorites with enstatite, bronzite, hypersthene. Most of these have not enough negative branch. But one of those is closer to the moon; it is a meteorite very rich in olivine, and the blackness is 0.045. This curve, number 1, is not very far from the moon, but cannot reproduce exactly the surface of the moon. Olivine meteorites give a first indication about the interpretation.

The best fits are given by ash flows of broken lava. If we pulverize lava samples, or if we measure ashes from volcanic areas, we are very close to the surface of the moon, as can be seen in Figure 8-22. Different varieties of Vesuvius and other volcanic ashes are represented. If you accept the last one as being far too light with an albedo of 0.56, and the other having brightness of the same order as in the case of the moon, it can be seen that the negative branch fits the curve of the moon well and the variation of P maximum with albedo is of the same order as indicated on the moon. We are proceeding at the laboratory to make more complete investigations about the ash and lava powders.

However the situation is far more complicated, as Dr. Hapke pointed out, because we must take



- ④ MARE TRANQUILLITATIS
- ⑪ N.E. OF MARE CRISIUM
- ⑫ MARE CRISIUM
- ⑬ ZAGUT

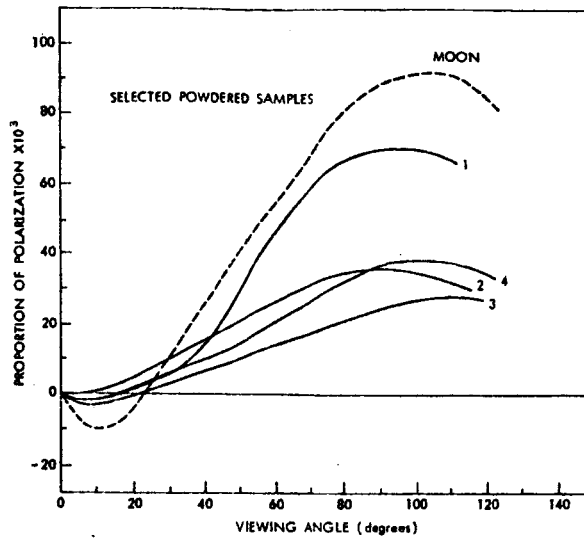
FIGURE 8-17: Variation of the amount of the maximum polarization as a function of wavelength.

into account the effect of the proton-darkening. This proton-darkening confuses the situation because some of the light materials of which we gave curves may fit the curve of the moon after appropriate bombardment by radiation.

In Figure 8-23 is a measurement we made with Dr. J. Geake at Manchester. The sample is an enstatite achondrite; the darkest area was darkened by 16-kv bombardment. Figure 8-24 shows that the properties of the darkened part of this material give a very good reproduction of the negative branch of the polarization. The curve of polariza-

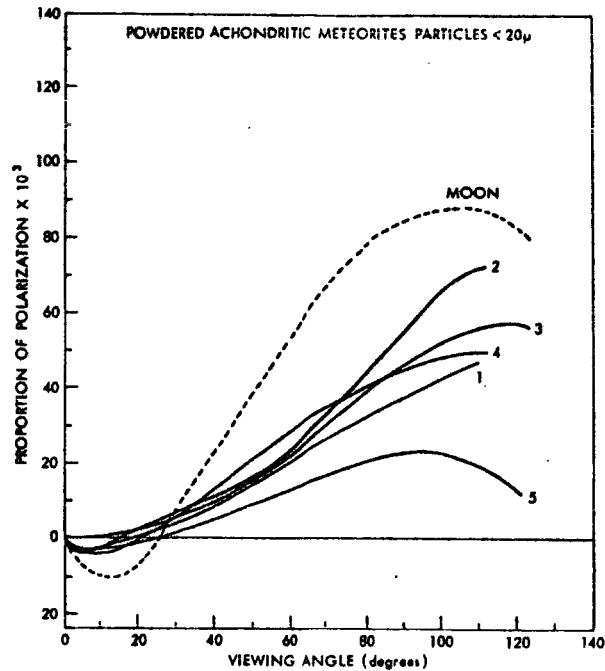


FIGURE 8-18: Laboratory polarization measurement device.



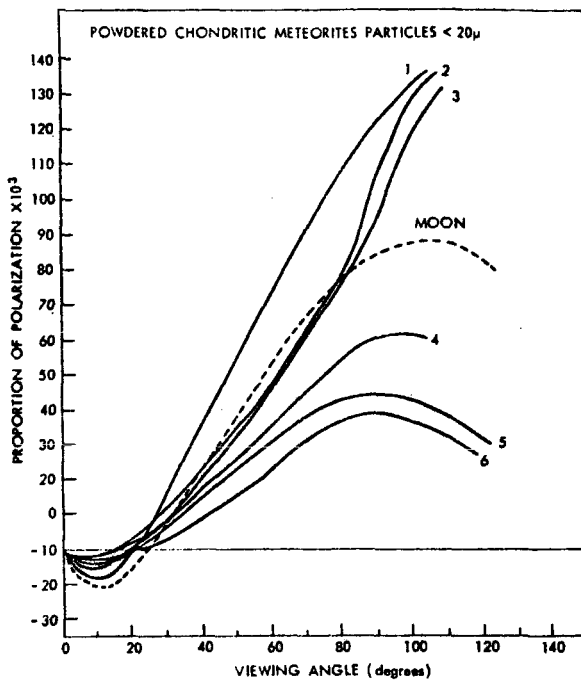
- ① OBSIDIAN, BLACK (ASCENSION ISLAND)
- ② OBSIDIAN, RHYOLITIC (CANTON LAKE, OREGON)
- ③ METEOR CRATER, ARIZONA-INTERIOR BRECCIA
- ④ TEKTITES (DALAT, INDOCHINA)

FIGURE 8-19: Characteristic polarization curves of two kinds of obsidian, the breccia of the Meteor Crater (Arizona), and tektites.



- 1 BISHOPVILLE WITH ENSTATITE $B = 0.35$
- 2 BUSTEE-ALBRITE WITH ENSTATITE $B = 0.30$
- 3 KHOR TEMIKI WITH ENSTATITE (NO IRON) $B = 0.30$
- 4 JUVINAS-EUCRITE RICH IN CADMIUM
- 5 TATAQUINE-DIOGENITE WITH HYPERSTHENE

FIGURE 8-20: Comparison polarization curves of the moon and achondrite meteorites.



- 1 KAROONDA WITH OLIVINE $B = 0.05$
- 2 KHAIRPUR WITH ENSTATITE $B = 0.15$
- 3 DANIELS KUILS WITH ENSTATITE $B = 0.18$
- 4 OCHANSK BRONZITE
- 5 OUBARI WITH HYPERSTHENE
- 6 PUTLISK BRONZITE

FIGURE 8-21: Characteristic polarization curves of different kinds of enstatite, bronzite, and hypersthene chondritic meteorites.

tion of the enstatite achondrite is shown before darkening; it has no negative branch at all. The curve measured after the darkening is identical to the curve of the moon. The reproduced negative branch is unexpectedly good. This seems to give a definite fit of optical properties.

A great number of powders may fit this negative branch, provided they are darkened enough by proton bombardment. Furthermore the variation

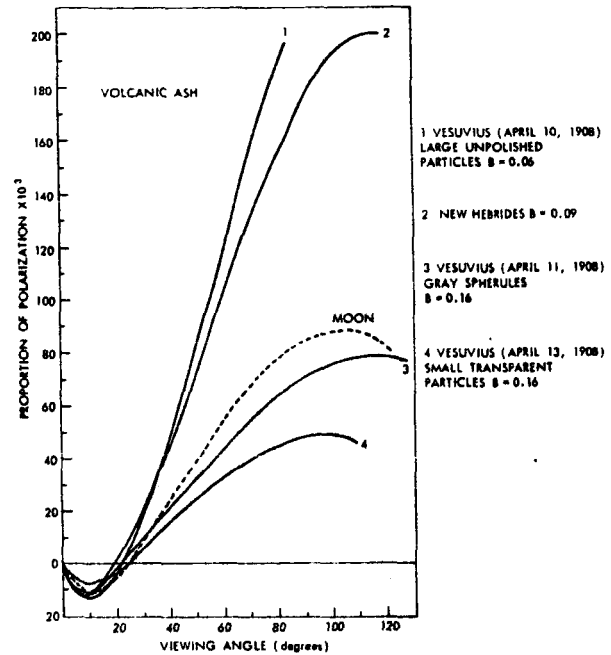


FIGURE 8-22: Characteristic polarization curves of ashes from various volcanic areas.

of maximum of polarization with wavelength is very good. The only point in the sample shown is that the variation of brightness with wavelength is too high in this special kind of sample.

As a conclusion I would like to point out that polarization gave a very certain result, that the surface of the moon is covered in all parts, in all areas, by a coating, a layer of dust of small particles, not compacted, and very absorbing. For the explanation of the nature of the powder, polarization techniques are not so specific because several possibilities occur. The proton bombardment may have something to do with the result. But we follow in two ways now: a careful study of the igneous volcanic rocks, broken into powder, and the effect of darkening by protons.

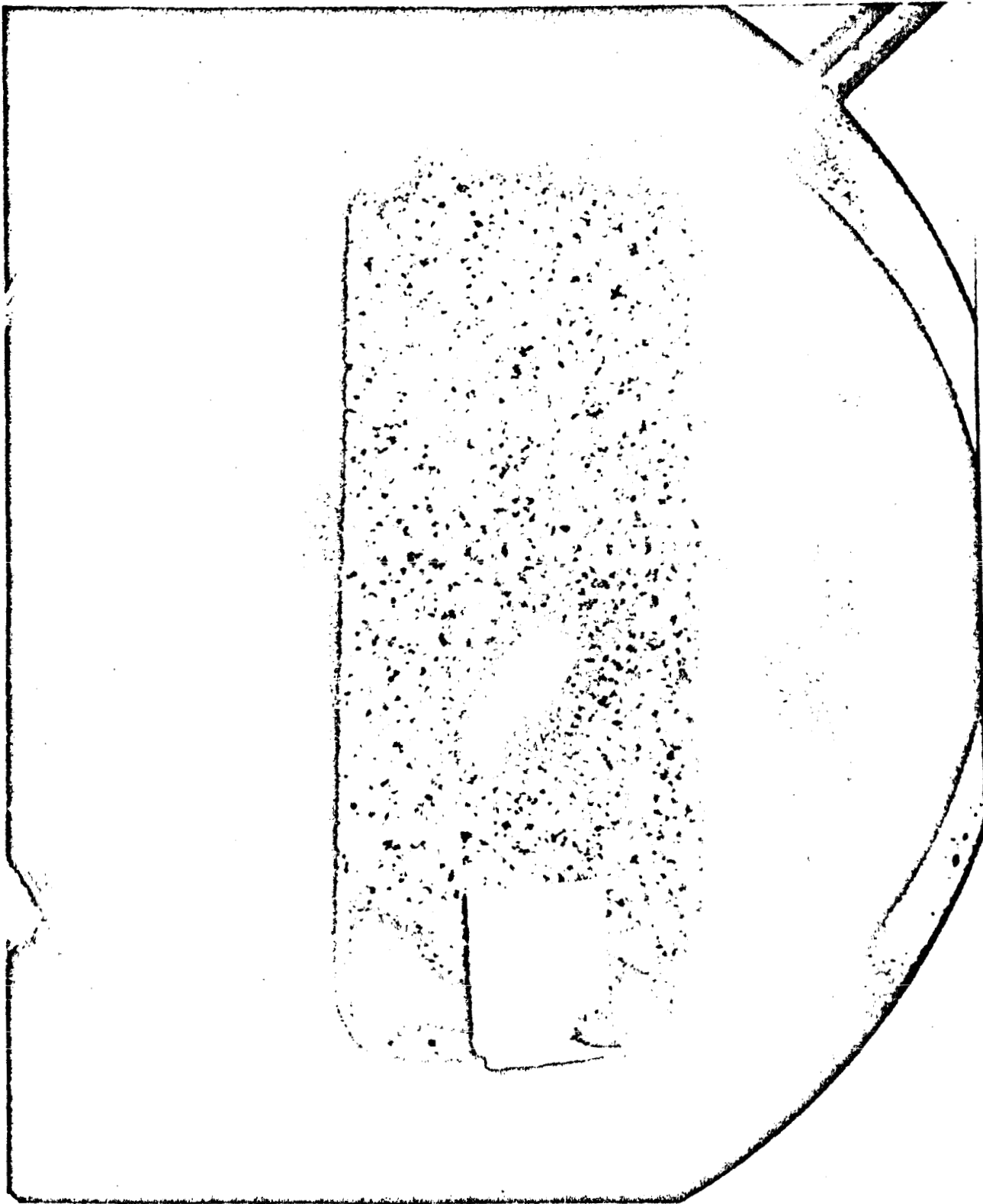


FIGURE 8-23: Sample of an enstatite achondrite, part of which has been darkened by proton bombardment.

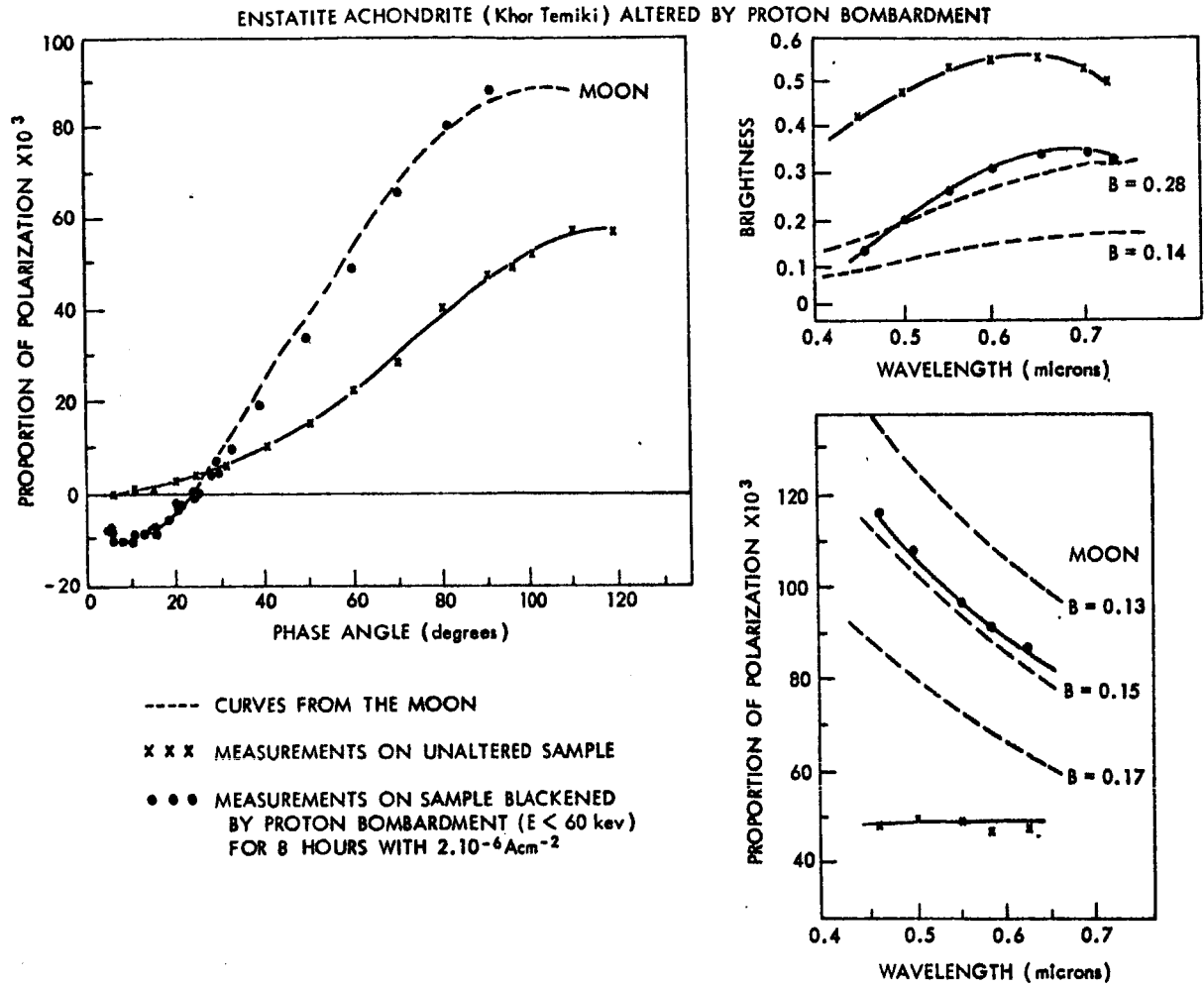


FIGURE 8-24: Characteristic polarization curves of enstatite achondrite before and after being darkened by proton bombardment.

17.

Radio Measurements of the Moon**F. Drake***Cornell University, Ithaca, New York*

I want to discuss briefly some radio measurements of the moon at 3-mm wavelength, which seem to develop points relevant to some of the previous discussions, particularly the infrared measurements of Shorthill, Saari, and Ingrao. The work I want to call to your attention was done principally by Bruce Gary at the Jet Propulsion Laboratory and Joseph Stacey at Aerospace

Corporation, using the 15-foot antenna of Aerospace Corporation which is shown in Figure 17-1.

With this antenna, lunar maps with a resolution of one-tenth of the lunar diameter have been made at a number of epochs in a lunation as shown in Figure 17-2. In making the maps, a sensitive radiometer and digital techniques were used.

The next three figures show maps that are typical examples of the results obtained. The brightness-temperature contours are in degrees Kelvin. Figure 17-3 is nearly at the time of the new moon. The optical appearance of the moon is shown in the upper right-hand portion of these



FIGURE 17-1: The 15-foot antenna of Aerospace Corporation.

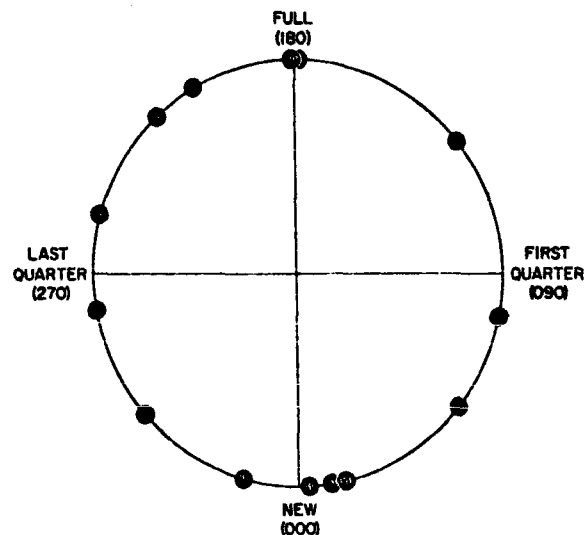


FIGURE 17-2: Lunar phases at which maps of brightness-temperature have been made.

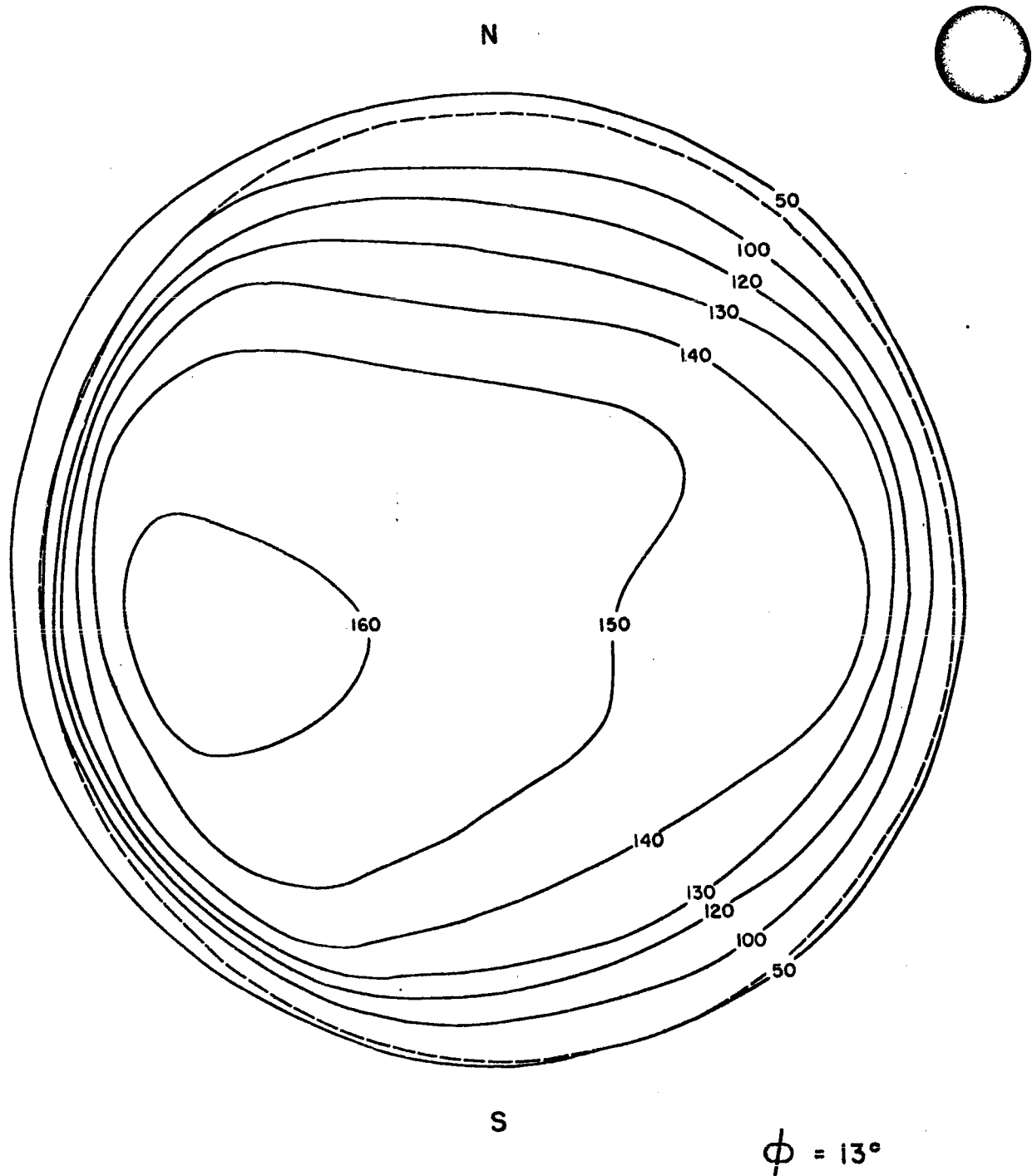
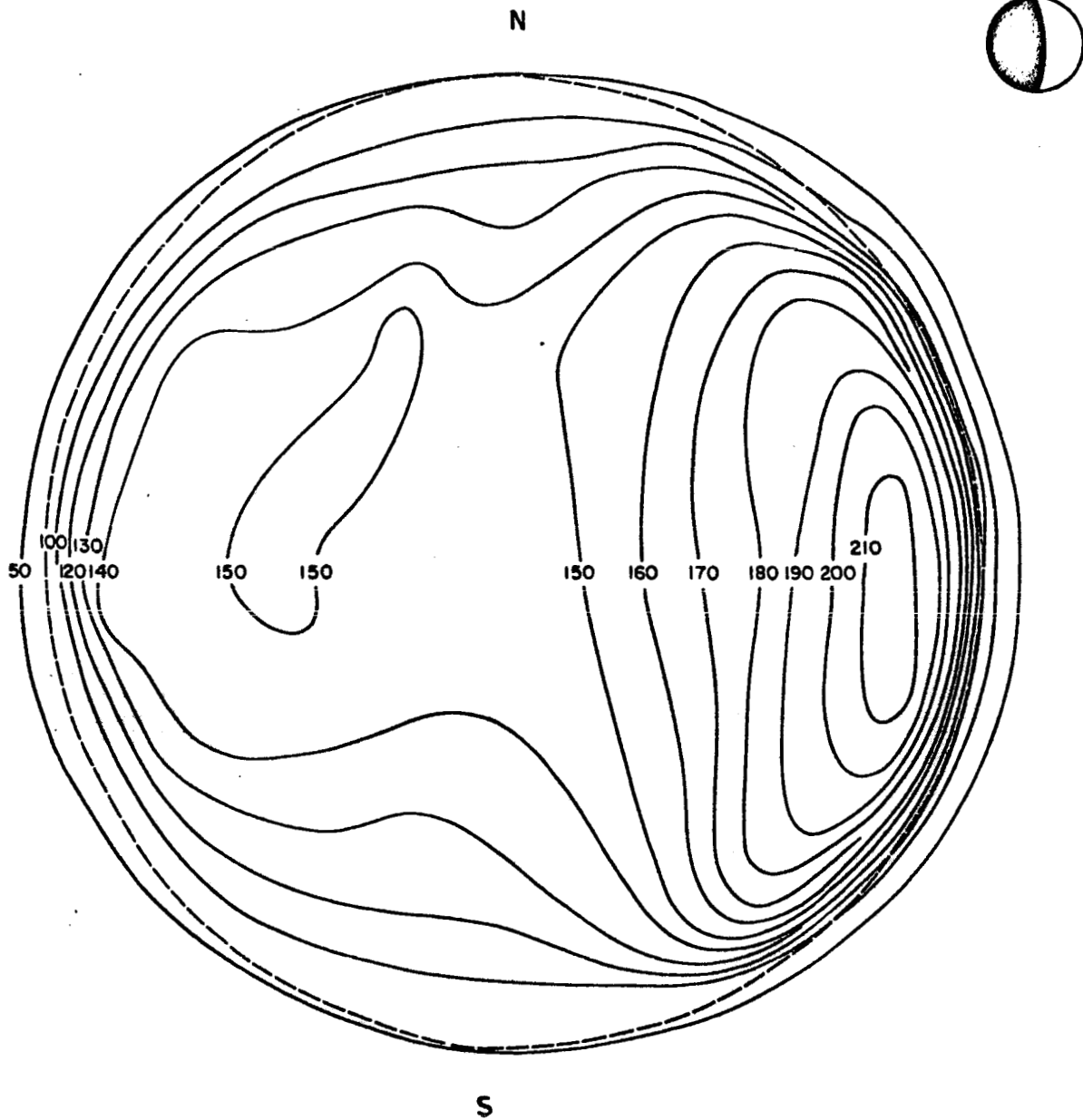


FIGURE 17-3: Map showing the brightness-temperature in degrees Kelvin, at the time of the new moon.



18 MAY 64

$\phi = 78^\circ$

FIGURE 17-4: Map showing the brightness-temperature in degrees Kelvin, at the time of half-moon.

figures. We note that the level from which the radiation is coming is about 3 cm or so below the surface of the moon, very near the surface. The minimum temperature is about 150°K.

Figure 17-4 shows the half-illuminated moon. It can be seen that where the sunlight is illuminating the moon, it has become much warmer. The minimum temperature is still 150°K in the portion of the moon that has been dark longest.

Figure 17-5 shows the situation at full moon. Notice the asymmetrical displacement of the contours, which is the well-known phenomenon of the thermal wave lagging the insolation.

Looking at Figure 17-6 we see that the maximum temperature is about 280°K, which means that even at depths of only a few inches, slightly below the level to which we are observing, the temperature never rises above the freezing point of water.

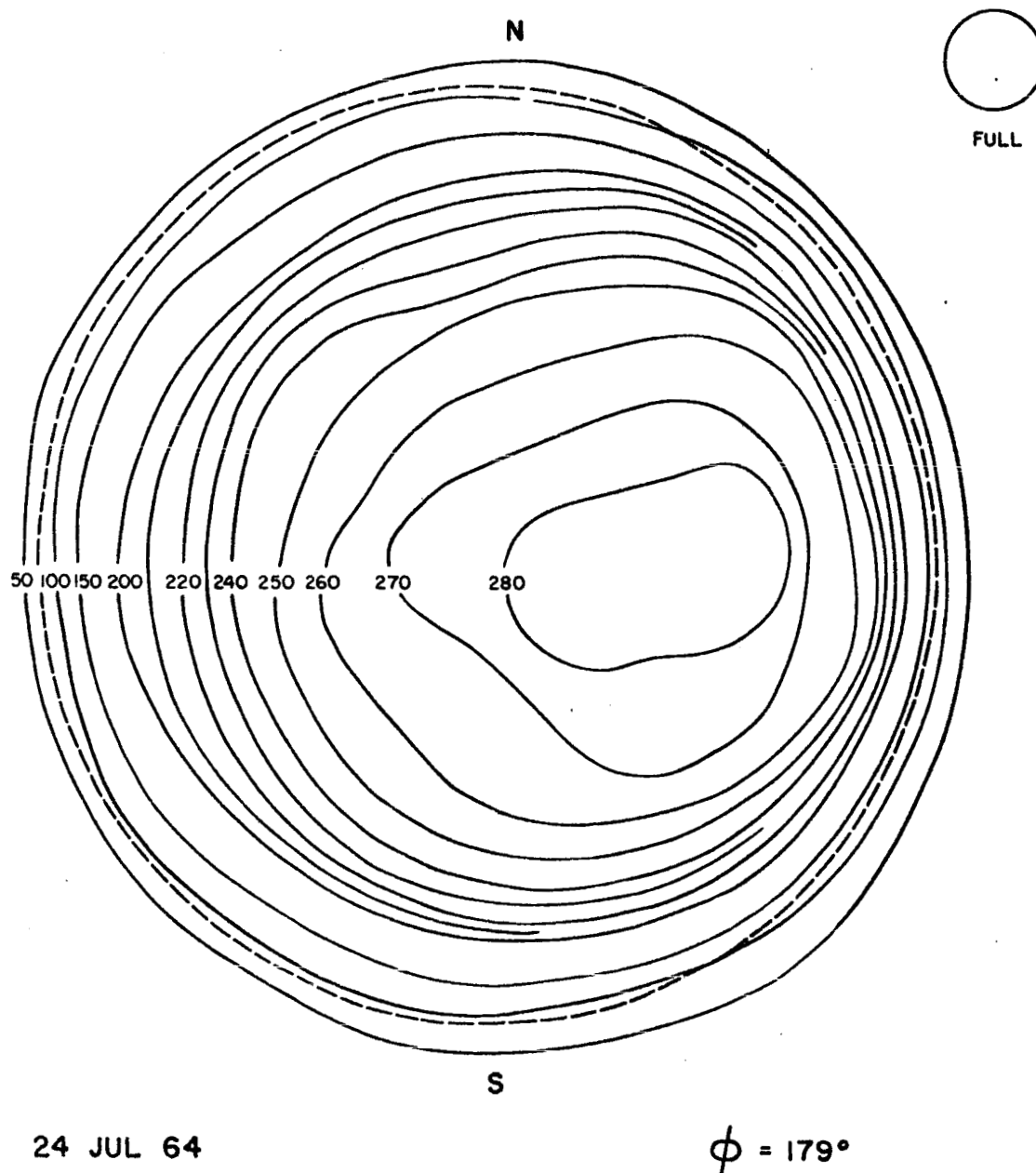


FIGURE 17-5: Map showing the brightness-temperature in degrees Kelvin, at the time of the full moon.

Another important point which is not apparent from these figures is that when we follow a point of constant phase, we observe essentially the same temperature, suggesting that the radioemissivity of the moon at this wavelength is very nearly isotropic. This requires structures everywhere on the surface of the moon that are a fraction of a millimeter in size or larger, which is consistent with remarks made previously by many speakers here.

These data can be used to produce a lunar phase curve, which is shown in Figure 17-6. This curve is for the equatorial region. The mean temperature is 206°K, somewhat less than that observed at longer wavelengths. However, when one takes the errors into account, there is not yet a significant difference in the mean temperature from, say, 21 cm to this wavelength. This is contrary to the conclusions of Troitskiy.

An interesting point in this curve is that the phase lag is about 22 degrees in general, as it should be, indicating we have a substance of very low thermal conductivity. However, there is an abrupt rise in the curve at phase 90 degrees when the sunlight first appears. Also, there is a point of inflection at about 280 degrees phase. This means that the simple theory for the lunar radio emission cannot fit these phase curves. We appear to have principally material of very low thermal con-

ductivity, but to explain the abrupt rise at 90 degrees and the point of inflection, there must be a second component, not in depth, but on the surface. This is, of course, consistent with the irregularities shown by the radar and by the infrared measurements.

Figure 17-7 shows phase curves for many latitudes. These can be used to compare measurements at specific points on the moon with the average lunar behavior to find thermal anomalies in the radioemission.

This part of the reduction is still in process, but Figure 17-8 shows the results one gets when one compares simply the mare ground against the highland ground. We find systematic temperature differences which average out to $3.0 \pm 0.3^\circ\text{K}$.

This 3°K difference is more than can be explained by the albedo difference effect on the solar radiation absorbed. That albedo difference, using the optical albedo, would give a 1.5°K difference. There is another 1.5°K that is unexplained. We think a simple explanation of this is that the infrared emissivity of the mare ground is slightly less, about 4 per cent, than with the highland ground.

Figure 17-9 shows an attempt to go a bit further. Here we have a detailed map of the differences in

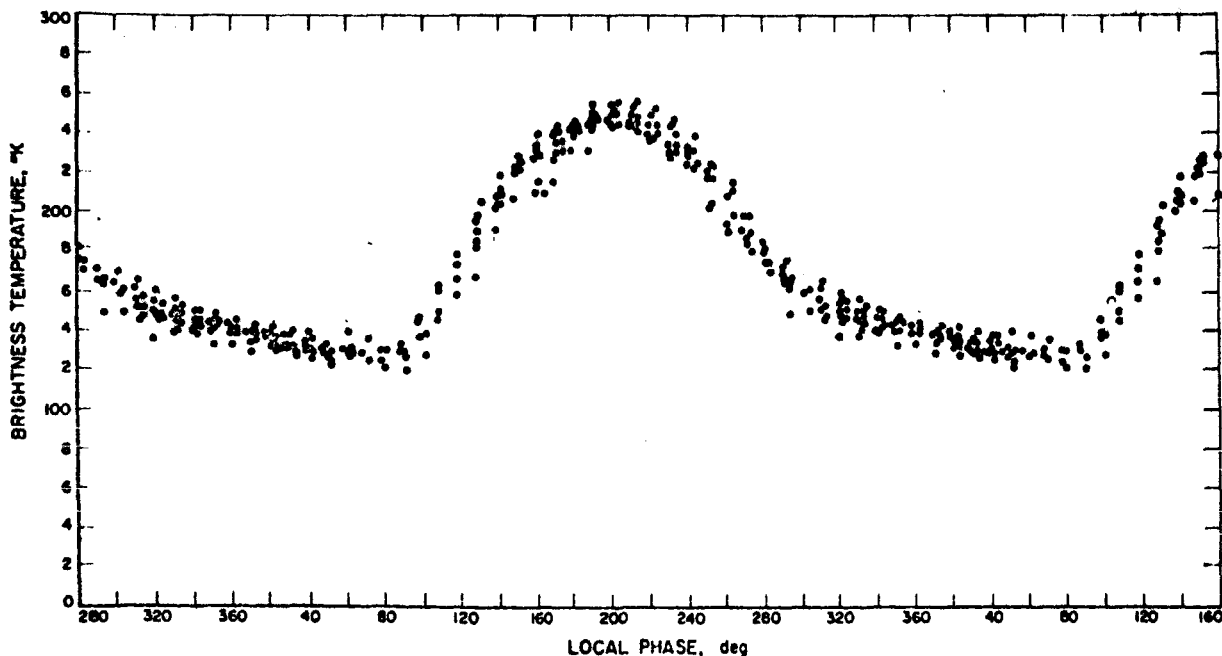


FIGURE 17-6: Lunar phase curve for the equatorial region.

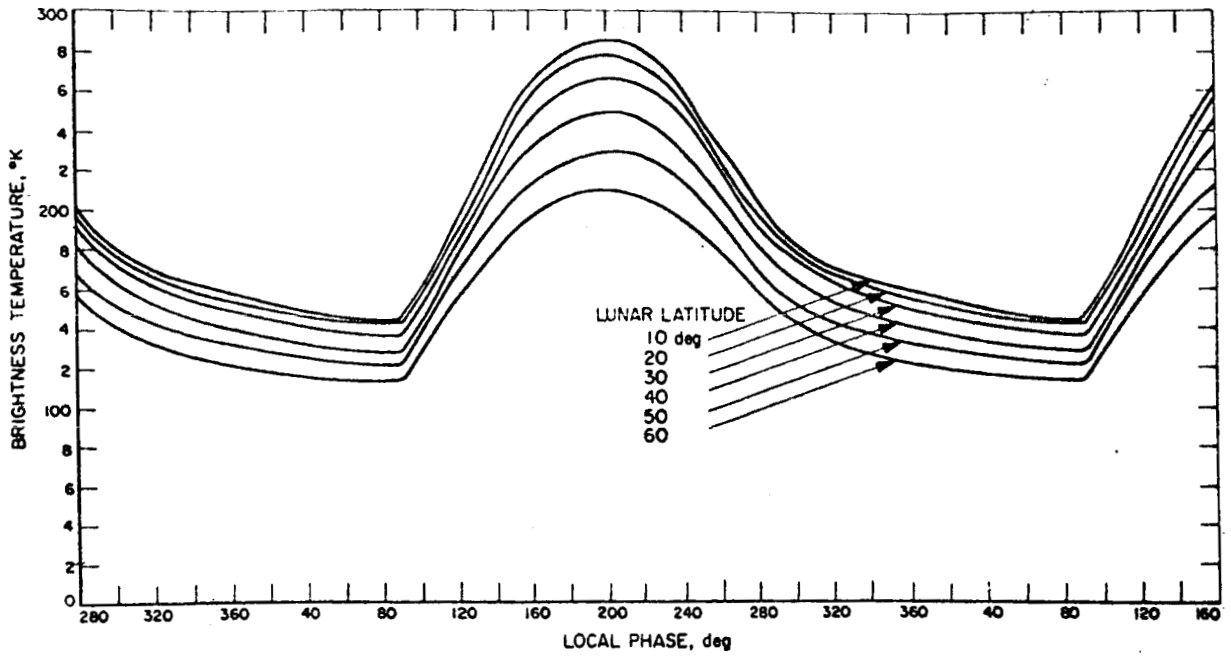


FIGURE 17-7: Lunar phase curve for many latitudes.

temperature from the expected means, superimposed on the map of Shorthill and Saari. The gross structure of these anomalies simply correlates with the arrangement of highland and mare regions indicating that it is simply the albedo difference that is causing most of the observed effect. In addition there is some correlation with the anom-

alies indicated by Shorthill and Saari, for instance, in the Mare Humorum. Our coldest region is where they see the fewest thermal anomalies, also. This correlation is again consistent with a low infrared emissivity, because such emissivity will also explain the thermal anomaly seen in the infrared at the time of a lunar eclipse.

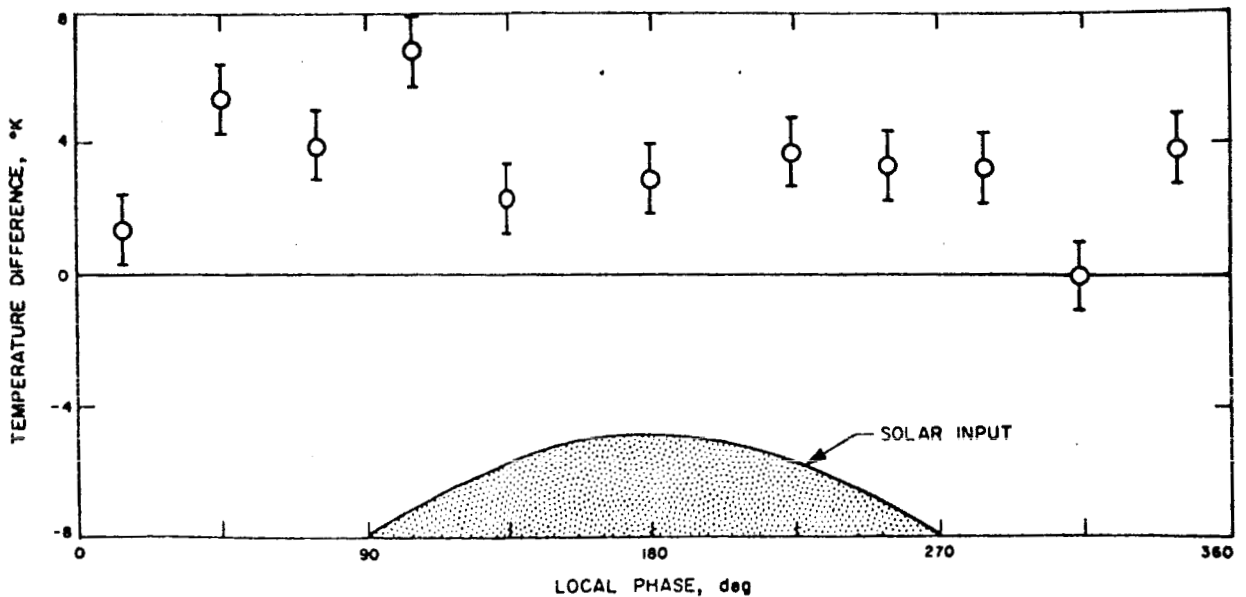


FIGURE 17-8: Comparison of temperature differences between the mare ground and the highland ground.

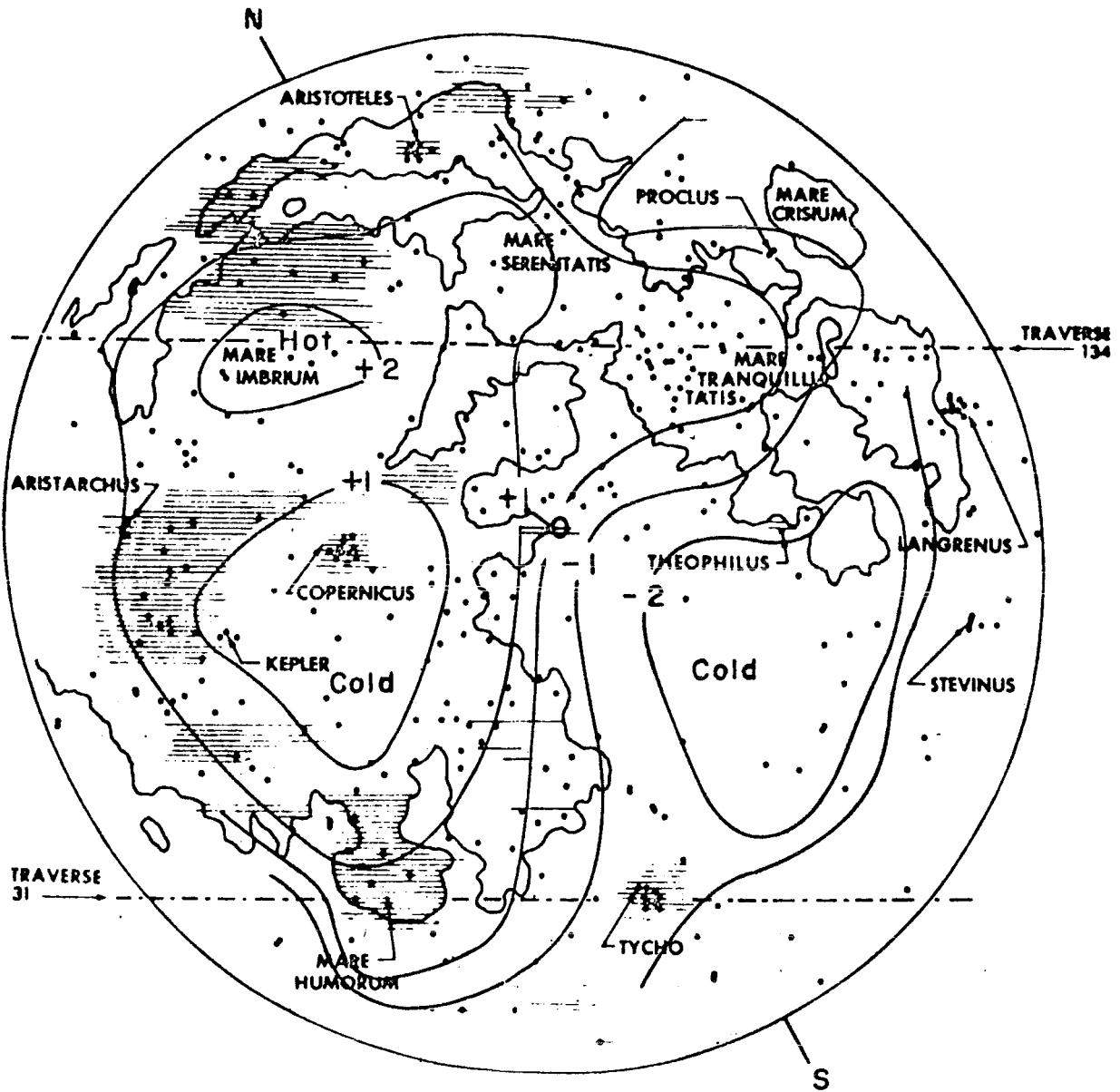


FIGURE 17-9: Detailed map of the differences in temperature from the expected mean superimposed on the map of Shorthill and Saari.

The points I want to stress are the apparent correlation with the infrared anomalies; the fact that we need 1-mm structures all over the surface; the fact that at least a two-component model seems required; and lastly that the phase curve itself supports the old idea that the moon is a very poor thermal conductor in its upper layers.

DISCUSSION

SAGAN: I would like to comment about the problem of relating measured brightness temperatures with temperatures deduced from visual albedoes. We have measured the reflectivities as a function of wavelength of a variety of common materials. There is in almost every case a tendency for the reflectivity to increase markedly longward of about 7,000 angstroms, that is in the near infrared.

There is a perfectly good reason for this—electronic transitions occur in the ultraviolet and visible. The infrared fundamentals occur in the three- to ten- μ region. Around 1 μ we are stuck with the second or third overtone, which is down many orders of magnitude in absorption coefficient.

Therefore, a photon incident on a granular material at 1 μ can make many reflections and re-emerge without having been absorbed, which is not the case in further infrared or shorter wavelengths.

It follows that the infrared reflectivity of the moon should be much larger than it is in the visible, and the integrated or bolometric albedo should be much larger.

I would think that a discrepancy of 1 or 1.5 degrees between the predicted and computed temperatures for the maria and highlands can be attributed to a difference in the infrared part of the reflectivities, or at least a major fraction of it, and we can also probably squeeze something out of the emissivities.

DRAKE: Yes. I am in agreement. Let me clarify what I said. It is simply that there is a difference, evidently in the infrared emissivity, between the highlands and mare, and this we take as evidence

that there are different materials there. By that I am trying to confirm statements made previously by other people.

INGRAO: I would like to make the following remarks: It frightens me that we are discussing models and talking about differences in temperature in absolute measurements of only a few degrees.

I made a very simple calculation that I wanted to discuss yesterday—it is to compute the coefficient of the propagation of errors in the parameter that you use to reduce your data. When you do that, it will frighten you that you are using parameters that are not so reliable to reduce your data. You are assuming emissivities for the reflectance of the middle that you don't find there always.

We worked out two-layer models, and the infrared measurements are very insensitive when the outer layer is bigger than 2.5 mm. So I don't think I am in a position to accept or to give validity to infrared measurements that give a result of dust layer thickness or measurements of the order of 10 or 7 mm, because all of the lines go together. There is a very small difference between the cooling curve for 7 mm, 10 mm, and infinity. The answer will come only from people like Dr. Drake in the radio measurements.

I have a curve that gives, at different times of the eclipse, the variation in temperature with depth. You can detect the difference that Dr. Drake is talking about in models at 3 cm, but in the infrared measurement we cannot do anything to differentiate between some models because the systematic errors are big enough to mask a distinction between models.

I think, as Dr. Drake did, that the selection of models will come from measurements. We can complement with the surface measurements. Moreover, in our paper (Chapter 10) we make an analysis computing the efficiency of propagation of errors, and we bracket the errors that you should expect for high temperatures of this solar point and for low temperatures. To take subsolar temperatures, you will have to find very, very carefully what technique has been used in order to find out if there is any systematic error hidden there.

Vacuum Ultraviolet Scattering Distributions

M. C. Johnson

Measurements of reflectance and the profile of scattered intensity from rough and smooth surfaces are reported for incident radiation of 1216 Å. The profiles show the intensity of scattered uv in the plane of incidence at various incident angles. Black appearing surfaces are found to have reflectances higher than expected.

Introduction

Quite frequently experiments involving the detection of intermediate energy particles, such as soft x rays or low energy charged particles, are plagued with background noise caused by vacuum uv photons. In view of this, it was surprising to find that literature describing methods for minimizing reflections of vacuum uv radiation is quite sparse. Most of the work reported in this area has involved methods of increasing the reflectance of surfaces in this spectral region and measurements of the reflectance of polished and evaporated surfaces.¹⁻⁷

We here describe work which was recently done in our laboratory to measure the total reflectance of various surfaces which have been treated or coated to reduce their vacuum uv reflectivity. The question to be answered was, "How much does a roughened or coated surface reduce and redistribute reflected vacuum uv radiation?"

Three general types of surfaces were investigated. The first type included smooth metallic surfaces evaporated onto glass slides and highly polished (3- μ finish) samples of bulk metals. The slides were prepared to obtain data which could be compared with published data on similar surfaces—the comparison showed our results were in close agreement with reported values. The second type included mechanically or chemically roughened surfaces, such as those obtained by sand-blasting or by anodization. While the manner of reflection in the latter two cases is different, the resulting radiation distribution is similar. The third type included very black absorber surfaces, such as soot, gold black, and carbon crystals, which have a large fraction of their reflecting microspheres inclined at large angles to the average surface plane.

The apparatus devised to measure the reflectances of these surfaces is illustrated in Fig. 1. Monochromatic

uv radiation was provided by an 0.5-m Soya-Namioka monochromator and an open-window capillary discharge. The radiation emerging from the slit passed through a 1.3-mm diam stop and into the experimental chamber, which was pumped independently of the monochromator. The beam size at the sample at normal incidence was 1.5 mm in diameter.

A Channeltron multiplier with an 8-mm cone shaped input was used as a detector (Fig. 2). This detector, which is described elsewhere,^{8,9} has several unique features which permit this type of measurement to be made. It can be operated at very high gains in a saturated mode and has low noise so that every event at the aperture which produces a photoelectron(s) is counted. Noise counts average about one per one hundred seconds. Therefore, at 1216 Å, as few as ten to twenty photons per second produce a significant output signal. Additionally, all of the input events produce output pulses of nearly the same magnitude when the detector is operated in the saturated mode. At vacuum uv wavelengths, the quantum efficiency of the surface of the cone is roughly the same as tungsten, ranging from 10% to 20% at 500 Å to 1000 Å and then dropping sharply to less than 0.001% at 1850 Å.

The high sensitivity and low noise characteristics of the Channeltron multiplier are very important in this type of measurement, since the intensity of the reflected radiation intercepted by the cone is extremely low. These characteristics and the small size of the detector (it occupies less than a cubic inch) permit the intensity distribution of the scattered radiation to be measured quite accurately. Generally, this type of measurement is undertaken with a very large aperture type detector,^{10,11} which is inherently less suited for accurately measuring the distribution of the reflected intensity.

The detector was mounted on a rod (Fig. 1) such that it could be rotated about the sample in the plane of incidence. Another cone Channeltron multiplier was mounted on the same fixture at 45° to the plane of incidence. The sample was then positioned at the desired angle with respect to the beam and the detectors were

The author is with Bendix Research Laboratories, 20800—10.1/2 Mile Road, Southfield, Michigan 48076.

Received 2 November 1967.

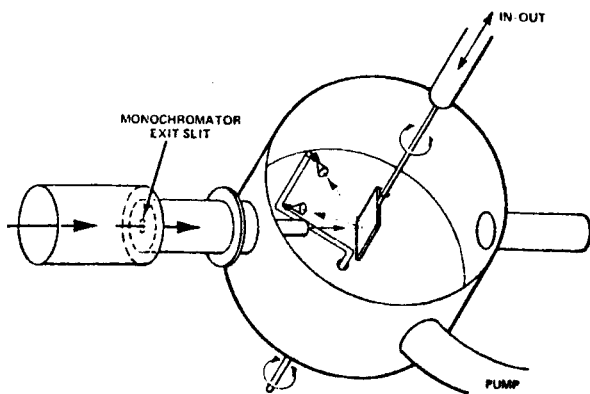


Fig. 1. Reflectance measurement goniometer chamber.

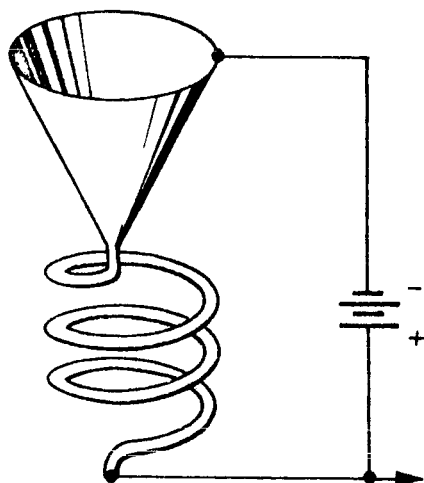


Fig. 2. Cone-helix Channeltron multiplier.

rotated above the sample counting the flux in selected 0.0227-sr solid angles.

The sample holder was mounted on a rod which could be withdrawn from the beam. The detector was then rotated into the direct beam for incident intensity measurements. The Channeltron multiplier aperture was large enough to capture the entire incident beam.

Figure 3 shows the results obtained at a wavelength of 1216 Å and an incident intensity of about 10^7 photons/sec. The results show that, as one might expect, the size of the specular peak is inversely related to the apparent blackness of the surface to visible light. Furthermore, the very black surfaces which were formulated in our laboratory scatter a significant fraction of the light in all directions. The evaporated metallic blacks were applied to aluminum substrates in 0.05–0.1 torr of argon using an amount of material equivalent to that required for a vacuum deposition thickness of 1000 Å. The black epoxies were made by sifting 400 mesh carbon crystals onto the surface of commercial epoxies such as Varian Associates Torr Seal (black epoxies 1 and 3) and Hysol PC 15 (black epoxy 2). The carbon was pressed into the curing epoxies until a black appearing surface formed.

In order to determine the total reflectance of these surfaces, an assumption had to be made regarding the

intensity distribution out of the plane of incidence. Consequently, it was intuitively assumed that the curves shown in these figures can be considered as the central cross section of a cylindrically symmetrical intensity distribution.¹² That is, it was assumed that the two (or more) angles (in Fig. 3) at which a given scatter intensity occurs define the diameter of a circle of con-

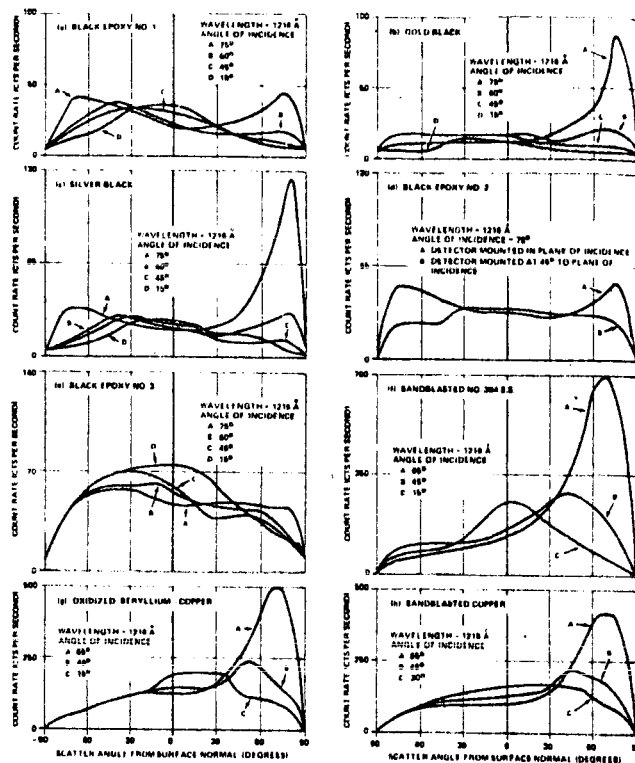


Fig. 3. Reflected intensity distributions of various materials

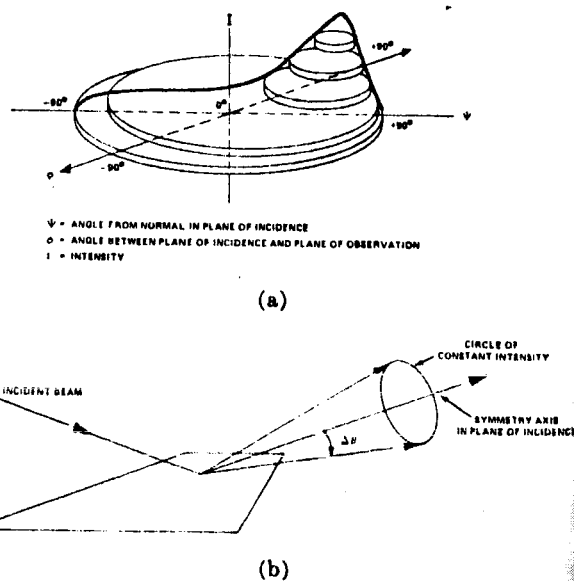


Fig. 4. Symmetry assumption used to calculate total reflected intensity: (a) constant intensity cylinders used to integrate total reflected intensity; (b) illustration of symmetry assumption.

Table I. Diffuse Reflectors

Surface	Angle-of-Incidence	Hemispherical Reflectance
1. Gold-Black	15°	0.765%
	45°	0.871%
	60°	1.633%
	75°	2.34 %
2. Nickel-Black	45°	11.1 %
3. Sintered Conducting Glass	15°	11.1 %
	30°	10.0 %
	45°	12.4 %
	65°	12.9 %
4. Silver-Black	15°	1.77 %
	45°	1.95 %
	60°	2.58 %
	75°	3.1 %
5. Black Epoxy No. 1	15°	2.22 %
	45°	2.42 %
	60°	3.02 %
	75°	3.69 %
6. Black Epoxy No. 2	15°	5.52 %
7. Black Epoxy No. 3	15°	4.64 %
	45°	5.33 %
	75°	6.77 %

Table II. Intermediate Reflectors

Surface	Angle-of-Incidence	Hemispherical Reflectance
1. Sandblasted No. 304 Stainless Steel	15°	15.2%
	45°	23.3%
	65°	25.1%
2. Sandblasted Oxygen Free Copper	30°	18.0%
	45°	18.4%
	65°	20.6%
3. Oxidized Beryllium Copper	30°	10.7%
	45°	11.3%
	65°	19.7%
4. Sandblasted Beryllium Copper	15°	10.0%

stant intensity out of the plane of incidence, as illustrated in Fig. 4. This assumption is supported by measurements of intensity 45° out of the plane of incidence, as indicated in Fig. 3(d). Based on this assumption, a computer program was written which calculated the total reflected intensity from the data. The results are listed in Tables I, II, and III.

Comments

There are a number of interesting features about these data. It is somewhat surprising that the very black appearing surfaces are only about a factor of ten more absorbing in the vacuum uv than surfaces which are highly reflecting in visible light. This means that the reflectivity of these black appearing surfaces does not decrease as rapidly with decreasing wavelength as does the reflectivity of shiny appearing surfaces. Also, easily prepared black epoxies are very nearly as absorbing as gold black which is difficult to apply and has undesirable mechanical properties. Finally, sandblasting, anodization, etc. have very little effect on the total reflectance at these wavelengths, although these processes do scatter the reflected radiation.

Much can be done to reduce unwanted vacuum uv reflections by intelligently employing various combinations of specular reflectors and black surfaces. Specular

Table III. Specular Reflectors

Surface	Angle-of-Incidence	Hemispherical Reflectance
1. Commercial Black Anodized Aluminum	15°	12.5%
	30°	13.6%
	45°	14.1%
	65°	45.5%
2. Aquadag	15°	18.7%
	30°	19.8%
	45°	20.7%
	65°	47.0%
3. Evaporated Bismuth	75°	80.0%
4. Bulk Polished Nickel	15°	10.4%
	30°	10.6%
	45°	11.9%
	65°	24.5%
5. Bulk Polished No. 304 Stainless Steel	15°	10.4%
	30°	10.7%
	45°	13.0%
	65°	24.0%
6. Bulk Polished Beryllium-Copper	15°	9.9%
	45°	12.1%
	65°	26.4%
7. Bulk Polished Oxygen Free Copper	15°	12.1%
	30°	12.6%
	45°	15.3%
	65°	34.8%
8. Bulk Polished Aluminum	15°	8.1%
	30°	9.6%
	45°	13.7%
	65°	31.0%
9. Evaporated Copper	15°	7.65%
	30°	7.65%
	45°	9.50%
	65°	22.00%
10. Evaporated Aluminum	15°	28.4%
	30°	29.3%
	45°	34.4%
	65°	52.7%
11. Evaporated Tellurium	75°	53.0%
	15°	10.0%

reflectors may be used to direct the radiation in a harmless direction, and black surfaces may be used to prevent high intensities from being scattered in any one direction.

The author would like to acknowledge the help of J. S. Miller who made up the surfaces and made these measurements.

References

1. P. Berning, G. Hass, and R. Madden, *J. Opt. Soc. Amer.* **50**, 586 (1960).
2. R. Madden, L. Canfield, and G. Hass, *J. Opt. Soc. Amer.* **53**, 620 (1963).
3. W. Walker, O. Rustgi, and G. Weissler, *J. Opt. Soc. Amer.* **49**, 471 (1959).
4. L. LeBlanc, J. Farrel, and D. Juenker, *J. Opt. Soc. Amer.* **54**, 956 (1964).
5. M. Watanabe, R. Kato, and Y. Nakai, *J. Phys. Soc. Japan* **21**, 191 (1966).
6. G. Sabine, *Phys. Rev.* **55**, 1064 (1939).
7. L. Canfield and G. Hass, *J. Opt. Soc. Amer.* **55**, 61 (1965).
8. G. Goodrich and W. Wiley, *Rev. Sci. Instrum.* **33**, 761 (1962).
9. K. Schmidt, *IEEE Trans. Nucl. Sci.* **NS-13**, 100 (1966).
10. "Symposium on Thermal Radiation of Solids," *NASA SP-55*, p. 259 (1965).
11. D. Look, Jr., *J. Opt. Soc. Amer.* **55**, 1628 (1965).
12. R. Johnston, L. Canfield, and R. Madden, *Appl. Opt.* **6**, 719 (1967).

APPENDIX G

Proceedings of the Apollo 11 Lunar Science Conference, Vol. 3, pp. 1993 to 2000.

Directional spectral and total reflectance of lunar material

R. C. BIRKEBAK and C. J. CREMERS
University of Kentucky, Lexington, Kentucky
and

J. P. DAWSON
Scientific Specialties Corporation, Houston, Texas

(Received 2 February 1970; accepted in revised form 2 March 1970)

Abstract—The directional reflectance was measured for lunar fines and chips from three different lunar rocks. The spectral reflectance of the fines varied from approximately 7.0 per cent at 0.6μ to 15 per cent at 2.0μ . The total reflectance for white light at near normal incidence is approximately 10 per cent. The reflectance increased by approximately 40 per cent when the angle of illumination was increased from 20° to 60° .

INTRODUCTION

THE ENERGY balance of the lunar surface requires the knowledge of the absorptance as a function of the angle of illumination over the spectral range of solar energy. Presented in this paper is the directional reflectance as a function of wavelength from 0.5 to $2.0 \mu\text{m}$, and for white light for angles of illumination of 20 , 30 , 45 and 60 degrees. The directional absorptance is readily obtained from our reflectance results by subtracting the directional reflectance from unity. These measurements are not only useful for lunar energy balance calculations but also to the lunar spacecraft and instrumentation designers to aid them in estimating the overall heat transfer to their systems. Further, these data are useful in that they confirm remote sensing results.

In order to determine the reflectance characteristics of lunar fines and rock chips, a vacuum integrating sphere system was developed which operated at pressure levels down to 10^{-7} torr.

MEASUREMENT TECHNIQUES

The standard integrating sphere reflectometer is familiar to many investigators; however, the modified sphere system used in our measurements is not in this category. We, therefore, present a discussion on the modes of operation of our integrating sphere reflectometer.

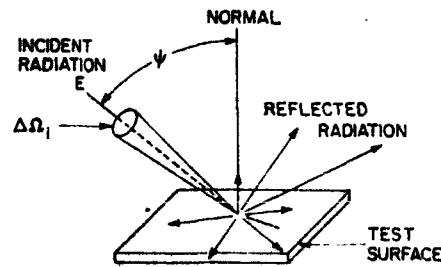
The directional reflectance was obtained with a sample, center-mounted in a 20 cm dia. integrating sphere reflectometer. The sphere coating was magnesium oxide. The sphere system is constructed with the sample held in a horizontal position, a necessity for powders, while by rotation of the sphere and external optics, angles of illumination or viewing up to approximately 75° are obtained.

Since the theory of the integrating sphere is well known, it will be only briefly reviewed. Radiation directed on a test sample within the integrating sphere is reflected onto the sphere wall. If the wall is coated with a highly reflective and diffuse material, then any radiation hitting the wall is reflected diffusely throughout the sphere. The total radiation incident on a given area will be a summation of intensities from

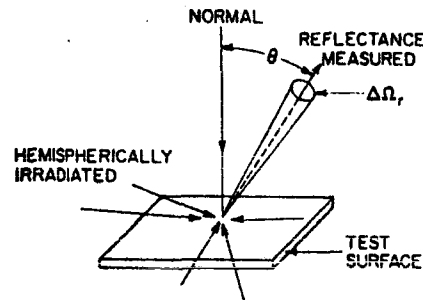
the multiple reflections. A detector mounted at the sphere wall measures the intensity of the radiation striking a given area within the sphere. Two optical modes are commonly used for the center-mounted sample integrating sphere reflectometer.

Directional hemispherical reflectance

Let the incident radiation be contained in a solid angle, $\Delta\Omega_i$, oriented at a specific angle ψ relative to the surface normal, Fig. 1a, and let reflected radiation be collected



a. DIRECTIONAL-HEMISPHERICAL TECHNIQUE



b. HEMISPHERICAL-DIRECTIONAL TECHNIQUE

Fig. 1. Reflectance definition and coordinates.

over the entire hemispherical space above the surface. We then define the directional hemispherical reflectance as

$$\rho(\psi) = \frac{de_{r,h}}{de_i} \quad (1)$$

where $de_{r,h}$ is the reflected radiant energy that is collected over the entire hemispherical space and de_i is the radiant energy contained in the incident beam. In general, the magnitude of $de_{r,h}$ will depend upon the angle of illumination ψ of the incoming beam. This is called the direct mode of operation for the integrating sphere.

Hemispherical-directional reflectance

Let the surface under study be illuminated hemispherically with diffuse radiation, $e_{i,h}$, while the reflected intensity, $I_r(\theta)$, is collected in a small solid angle $\Delta\Omega_r$, Fig. 1b.

The hemispherical-directional reflectance is defined as

$$\rho(\theta) = I_r(\theta) / [e_{i,h} / \pi]. \quad (2)$$

With the use of reciprocity, the reflectances in equations (1) and (2) can be shown to be identical if the solid angles are the same, $\Delta\Omega_i = \Delta\Omega_r$.

$$\rho(\psi) = \rho(\theta) \quad \text{for} \quad \theta = \psi. \quad (3)$$

The measurement of $\rho(\theta)$ with the integrating sphere is called the reciprocal mode.

Our integrating sphere was operated in the reciprocal mode, that is, the sample was illuminated by diffuse light from the sphere walls. The ratio of intensity when

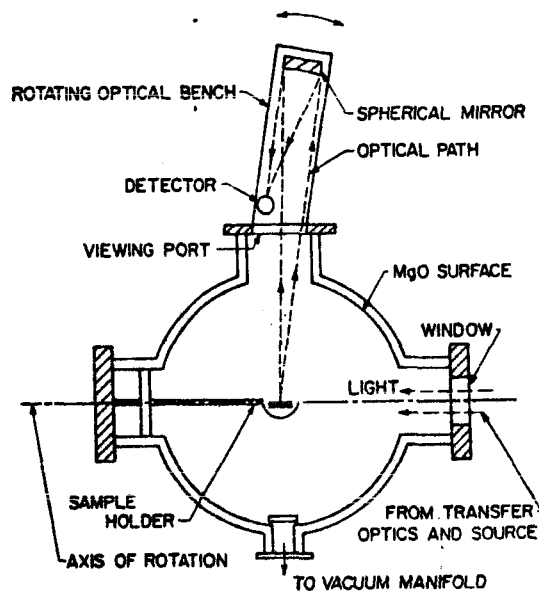


Fig. 2. Schematic of integrating sphere reflectometer.

the center mounted sample was viewed to the intensity when the wall was viewed is the directional reflectance $\rho(\theta)$, (equation (2)). As represented in equation (3) this measurement is equivalent to illuminating the sample at an angle of incidence ψ equal to the angle of viewing θ .

APPARATUS

A sketch of the apparatus used in this research is shown in Fig. 2. The integrating sphere was constructed of stainless steel hemispheres, 20 cm in dia., flanged and joined by a copper gasket seal. The interior of the sphere was smoked with MgO until a uniform coating of 2 mm thickness was obtained. Ports were provided on the sphere for the test sample, detector optics, light source, and vacuum pump.

The sample holder was a stainless steel cup, 3.8 cm in dia., which could be located along the diametral plane of the sphere and always held in a horizontal position.

The viewing optics were arranged so that the sample or sphere wall could be viewed by rotating the optical bench, Fig. 2. The spectral results were obtained with a Perkin-Elmer 112 U

spectrometer having a tungsten-iodine source and a lead-sulfide detector. The total or white light measurements were made with a 1000 W tungsten-iodine lamp (DXW) with a reflector. The detector was a Kipp-Zonen CA-1 thermopile. Details of the design and construction are presented in a technical report, BIRKEBAK *et al.* (1969).

PROCEDURE

Prior to installation of the lunar samples, the sphere system had been pumped down to approximately 10^{-6} torr and held there for several weeks. Those parts of the apparatus which would become contaminated by handling were cleaned with a methanol and benzene solution prior to loading of the lunar samples. The lunar sample was loaded under atmospheric conditions and then immediately installed in the sphere and evacuated to pressures below 10^{-5} torr. Also, all rock chips and one sample of fines were tested in an atmosphere of dry nitrogen. Prior to loading of the lunar fines the sample holder was cleaned with a methanol-benzene solution. The rock chips were held in place with double backed tape.

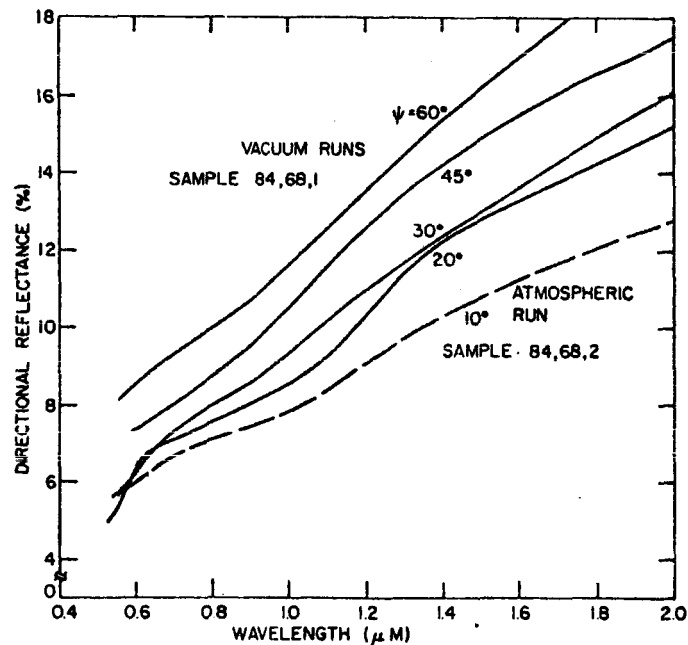


Fig. 3. Directional reflectance of lunar fines sample 10084-68.

RESULTS

Measurements were made on Apollo 11 lunar samples numbers 10057-29 (type A); 10047-23 (type B); 10048-21 (type C) and 10084-68 (type D).

The directional reflectance of the lunar fines, 10084-68, measured for angles, $\psi = \theta$, of 10° , 20° , 30° , 45° and 60° are presented in Fig. 3. The curves are a smooth fit through data points taken at $0.02 \mu\text{m}$ interval to $1.0 \mu\text{m}$ and $0.05 \mu\text{m}$ to $2.0 \mu\text{m}$. Sample 10084-68-1 was mounted in the sphere and the system evacuated to pressures below 10^{-5} torr. There are no apparent absorption bands in the data over the spectral range studied. ADAMS and JONES (1970) shows a very slight band at $0.95 \mu\text{m}$ on

sample 10084-66 and his results correspond closely to the remote sensing results of McCORD *et al.* (1969). We are at the present time increasing our resolution in order to study the 0.95 μm region of the spectrum. ADAMS and JONES (1970) points out, the band is <5 per cent change in the reflectance in this region. The vacuum reflectance measurements are in general accord with McCORD *et al.* (1969) over the rest of the range of spectrum compared.

The effect of angle of illumination on the reflectance is present in Table 1. The

Table 1. Normalized directional reflectance
reflectance (ψ)/reflectance ($\psi = 20^\circ$)

Wavelength (μm)	Sample 10084-68 Angle of illumination ψ			
	20°	30°	45°	60°
0.55	1.0	1.09	1.54	1.58
0.6	1.0	0.97	1.45	1.38
0.7	1.0	1.06	1.13	1.44
0.8	1.0	1.02	1.17	1.33
1.0	1.0	1.09	1.22	1.34
1.2	1.0	1.08	1.25	1.34
1.4	1.0	1.02	1.16	1.24
1.6	1.0	1.03	1.19	1.30
1.8	1.0	1.05	1.15	1.29
2.1	1.0	1.03	1.19	1.31
white light*	1.0	1.07	1.18	1.41

* Source, 1000 W DXW tungsten-iodine lamp.

results are presented as the ratio of reflectance $\rho(\psi)$ to the reflectance at $\rho(20^\circ)$. The reflectance is seen to increase as the angle of illumination increases and this is in accord with electromagnetic theory. There appears to be a slight wavelength effect present in this data, that is, for shorter wavelength the reflectance at large ψ is greater than that at the longer wavelengths. However, further studies are in process to obtain additional data to clarify this trend. Listed in the table are results obtained with a 1000 watt tungsten-iodine lamp [DXW]. The results are similar to the shorter wavelength data.

Sample 10084-68-2 was run at atmospheric pressure 2 months after No. 1 sample and No. 2 had been resealed and stored in the original shipping container for these 2 months. The vacuum measurements are higher than those obtained at one atmosphere for identical ψ 's. For the sake of clarity of presentation of results in Fig. 3, the atmospheric results for ψ other than 10° have not been presented. The difference could possibly be caused by the surface roughness or texture, contamination, and/or material packing. HAPKE *et al.* (1970) discuss the effects of packing on reflectance and state that the looser the packing the lower the reflectance. These measurements point out the need for a study using a vacuum packaged sample under controlled conditions.

Total directional reflectances were obtained for the powder under vacuum and dry nitrogen atmospheres. The vacuum results are higher for these measurements than for the atmospheric pressure results as in the case of spectral measurements. The results are given in Table 2. The near normal total reflectance is approximately 10 per cent.

Table 2. Total directional reflectance of Apollo 11 material*

Angle of viewing ψ	No. 10084-68-1		Sample		
	Vacuum run	Atmospheric run	10057-29-1	10047-68-2	10048-21-1
10°	0.102	0.098	0.137	0.118	0.162
20°	0.101	0.096	0.163	0.126	0.166
30°	0.117	0.103	0.145	0.124	0.168
45°	0.115	0.113	0.135	0.128	0.175
60°	0.148	0.135	0.129	0.129	0.183

* Source, 1000 W DXW tungsten-iodine lamp.

Sample 10047-23-2 a basaltic type, shows a reflectance spectrum most similar to the lunar powder as shown in Fig. 4. There are no major absorption bands in the spectrum but possibly a minor one around $1 \mu\text{m}$. The reflectances at other angles of illumination also indicated a band at $1 \mu\text{m}$. This rock chip as well as the others were run under atmospheric conditions. Photographs of all rock chips were taken for documentation and the area used for study on each sample has been recorded.

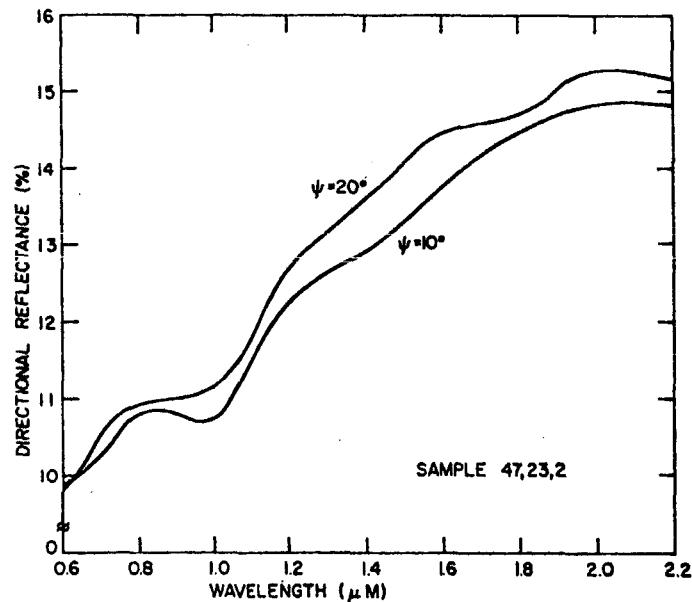


Fig. 4. Directional reflectance of sample 10047-23-2.

It should be noted here that the measurement of the reflectance on the rock chips as a function of angle is somewhat questionable because of the irregular shape and condition of the surface. However, for those rock chips where it was reasonable to make these measurements, they were obtained.

The remaining rock chip measurements in Fig. 5 and 6 show very pronounced

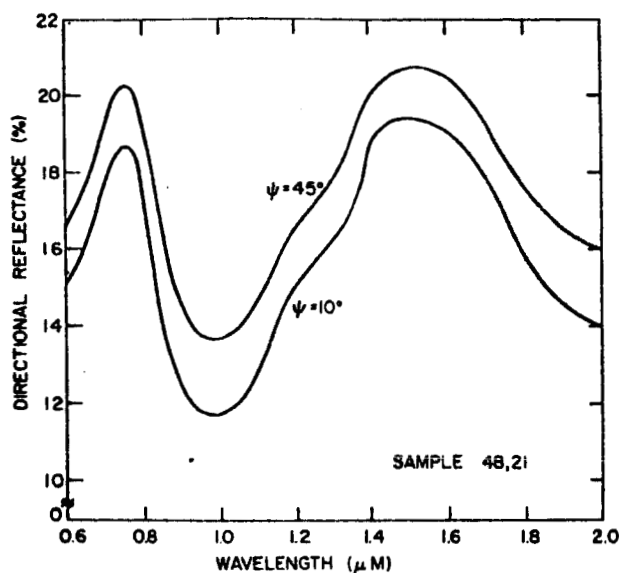


Fig. 5. Directional reflectance of sample 10048-21.

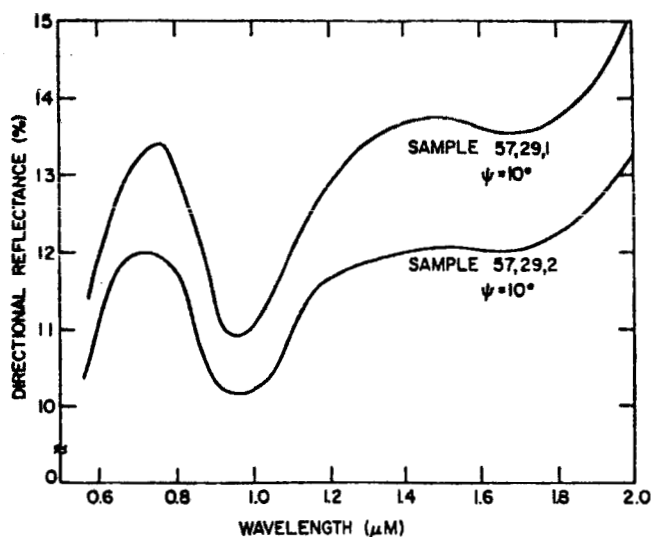


Fig. 6. Directional reflectance of sample 10057-29.

absorption bands. Sample 10048-21-1, Fig. 5, a breccia type, has a minimum reflectance between 0.95 and 1.0 μm and an apparent band centered beyond 2.0 μm . The reflectance spectrum of sample 10057-29-1, Fig. 6, a crystalline type of material with a cinder-like appearance, has a strong band at 0.95 μm but does not have any other strong bands. However, the data suggest a weak band around 1.7 μm . A second sample 10057-29-2 was also tested. Its reflectance over the wavelength range

was between 10 and 20 per cent below that of 10057-29-1. These measurements again show the strong band at $0.95 \mu\text{m}$ but a much weaker one, if any, at $1.7 \mu\text{m}$. The difference in reflectance is most likely due to the greater density of surface holes and craters of sample 10057-29-2.

CONCLUSION

The results for the lunar fines confirm in general the measurements made by remote sensing. The directional reflectances of the fines must be studied further with emphasis placed on packing and surface texture effects. The measurements made on rock chips are not useful, at the present time, in energy balance calculations. However, they are useful in mineralogical studies.

Acknowledgments—We thank C. NEVILLE, JR., C. ALLEN, E. YATES, E. HOOVER and W. BUCHHOLTZ for their assistance and support with the design and construction of the equipment. We also want to thank MARK BIRKEBAK and TODD BIRKEBAK for their assistance in data reduction. Support by NASA grants NAS 9-8098 and NGR 18-001026 is gratefully acknowledged.

REFERENCES

- ADAMS J. B. and JONES R. L. (1970) Spectral reflectivity of lunar samples from Apollo 11. *Science* **167**, 737-739.
- BIRKEBAK R. C. and CREMERS C. J. (1969) Preparation for lunar material thermophysical property measurements, TR-1. High Temperature and Thermal Radiation Laboratory, University of Kentucky, Lexington, Kentucky.
- HAPKE B. W., COHEN A. J., CASSIDY W. A. and WELLS E. N. (1970) Solar radiation effects in lunar samples. *Science* **167**, 745-747.
- MCCORD T. B., JOHNSON T. V. and KIEFFER H. H. (1969) Difference between proposed Apollo sites 2. Visible and infrared reflectivity evidence. *J. Geophys. Res.* **74**, 4385-4388.

APPENDIX H

Proceedings of the Apollo 11 Lunar Science Conference, Vol. 3, pp. 2013 to 2023.

Spectral reflectance and albedo of Apollo 11 lunar samples: Effects of irradiation and vitrification and comparison with telescopic observations

J. E. CONEL and D. B. NASH
Jet Propulsion Laboratory, Pasadena, California 91103

(Received 2 February 1970; accepted in revised form 4 March 1970)

Abstract—Spectral reflectance (0.23–2.5 μm) and albedo (0.4–0.7 μm) measurements were made on fresh powders of rock 10020 before and after both proton irradiation and vitrification. Doses of 2 keV protons, equivalent to 20,000 yr exposure to the solar wind, reduced the albedo from 20 to 18 per cent, while artificial vitrification reduced it to 8 per cent. Vitrification is thus a possible lunar darkening mechanism.

The crystalline and glassy materials studied show important differences in spectral reflectivity. Rock powder of 10020 is characterized by prominent absorption features near 1.0 μm and 2.2 μm , and relatively strong reflection in the blue, all attributed to pyroxene. Synthetic glass, on the other hand, has broad absorption bands at 1.02 μm and 1.8 μm and strong reflection near 0.7 μm . Weak structure near 0.95 μm in the spectrum of lunar fines arises mostly from pyroxene.

Lunar rocks and fines and synthetic lunar glass are used to interpret qualitatively color differences for some bright and dark areas of the Moon's surface obtained by McCORD and others. Reflectance ratios in the visible spectrum are interpreted to indicate that bright craters are covered in part by crystalline rock or crushed debris derived therefrom, and dark areas by material similar to Tranquillitatis fines.

INTRODUCTION

SPECTRAL reflectance (0.23–2.5 μm) and albedo (0.4–0.7 μm) measurements have been made on samples of crushed lunar material,* as a measure of changes in optical properties resulting from proton irradiation experiments and from artificial vitrification. Reflectance changes produced by such experiments have been summarized by NASH *et al.* (1970). Here we expand on those results and present some applications to available telescopic data for the moon.

Darkening of lunar surface material by solar-wind bombardment was suggested by HAPKE (1965, 1966) and WEHNER *et al.* (1965) as a result of their experimental work on silicates. NASH (1967) showed that darkening of silicates can result experimentally from carbon and metal contamination and high sample temperature in the presence of a hydrogen atmosphere. COHEN and HAPKE (1968) later suggested that solar u.v. radiation, electrons and protons may increase rather than decrease the albedo of lunar surface debris. The reflectance measurements reported here show that freshly crushed crystalline material (Type A, 10020) darkens slightly as a result of the proton irradiation experiment. However, contamination is suspected and we cannot attribute the sample darkening observed exclusively to the proton irradiation itself.

Type D fines (< 1 mm size fraction) contain up to 50 per cent glass (WOOD *et al.*,

* The samples used in this study are described by NASH and GREER (1970).

1970). Like holocrystalline rock, crushed synthetic glass darkens slightly with proton irradiation. Vitrification reddened the material fused, and has reduced the albedo by more than a factor of one-half. Thus, glass may contribute to the low reflectance of the Tranquillity fines, and to the slightly red color of the material.

Using the synthetic glass of 10020 as a reference in some differential reflection experiments, reflectance ratios have been produced that qualitatively resemble those obtained by McCORD (1969) and McCORD and JOHNSON (1969) for some dark and bright areas of lunar surface. The implications of this experiment are: (1) McCORD's standard area (Mare Serenitatis 2) may have reflectance properties similar to the laboratory-prepared glass in the visible, (2) dark lunar areas reflect in the visible like Tranquillity fines and (3) that some bright craters have reflectance properties resembling those of crystalline rock 10020 and 10058.

EXPERIMENTAL METHODS

Hemispherical spectral reflectance measurements were made with a DK-2A ratio-recording spectroradiometer. The standard instrument was modified to accept horizontal, uncovered samples of granulated or solid material by installing 45° flat front-surfaced aluminized mirrors in special housings at the exit ports of the integrating sphere. The integrating sphere, housings and reference surfaces were coated with fresh-smoked MgO.

The comparative reflectance data are given in such a way that reported sample reflectance $R_s(\lambda)$ at wavelength λ is approximately

$$R_s(\lambda) = R_i(\lambda) \cdot R_{\text{MgO}}(\lambda),$$

where $R_i(\lambda)$ is "true" sample reflectance and $R_{\text{MgO}}(\lambda)$ the reflectance of MgO.

From repeated spectral measurements the signal-noise ratio is estimated to be approximately 500 throughout the visible and i.r. regions, and 100 in the ultraviolet region. An error analysis based on the method of data reduction shows the accuracy of any spectrum to be approximately 0.5 per cent relative to MgO in the region 0.36–2.4 μm , and 2 per cent between 0.23–0.36 μm .

Samples were handled and prepared in dry N_2 . This procedure was not followed after experiments showed no detectable effects on any of our measurements from exposure of the samples to air. Reflectance measurements, however, were routinely made with the instrument flushed with dry N_2 .

The albedo, meaning here the bi-directional integral reflectance (0.4–0.7 μm) measured with vertical illumination and phase angle of 15°, was determined with a goniophotometer using a xenon lamp. All such bi-directional measurements were made in air relative to fresh-smoked MgO.

The irradiation apparatus and experimental procedures used have been described in detail elsewhere (NASH, 1966, 1967). However, in the present work, design of the proton source was optimized for the luminescence investigation (NASH and GREER, 1970) by the addition of ion beam apertures to reduce background light from the ion source. This modification increased the likelihood of sample contamination by aluminum metal sputtered from the walls of the apertures.

Long term irradiation experiments were conducted with fresh fine-grained crystalline rock (10020) and with artificial glass prepared from this material, both crushed to particle sizes $< 50 \mu\text{m}$. Much of the Type D fines (10084) consists of glass, a component that presumably formed in part from crystalline parent material judging from glass lined pits and glass spatters on crystalline rocks. To determine the effects of irradiation on the reflectance and albedo of fresh glass a representative sample of 10020 was fused in platinum in a high purity dry nitrogen atmosphere.

Powdered crystalline and glass samples were lightly packed in sample cups and subjected to 2 keV proton irradiations at fluxes in the range $3 \cdot 10 \times 10^{12}$ protons $\text{cm}^{-2} \text{sec}^{-1}$ for doses of 4- and 2×10^{19} protons cm^{-2} (equivalent respectively to approximately 2×10^4 and 10^4 years exposure to the solar wind).

RESULTS

Reflectance spectra of these materials before and after irradiation are shown in Figs. 1 and 2. In general the reflectance of unirradiated rocks, fines and glass increase with increasing wavelength. The reflectance of crystalline material has a prominent minimum close to $1.0 \mu\text{m}$ and other more subtle structures near $1.3 \mu\text{m}$, $1.7 \mu\text{m}$ and $2.2 \mu\text{m}$. In glass there are broad minimums at $1.02 \mu\text{m}$ and near $1.8 \mu\text{m}$. By comparison, the spectrum of lunar fines (10084) shows a single shallow minimum close to $0.95 \mu\text{m}$.

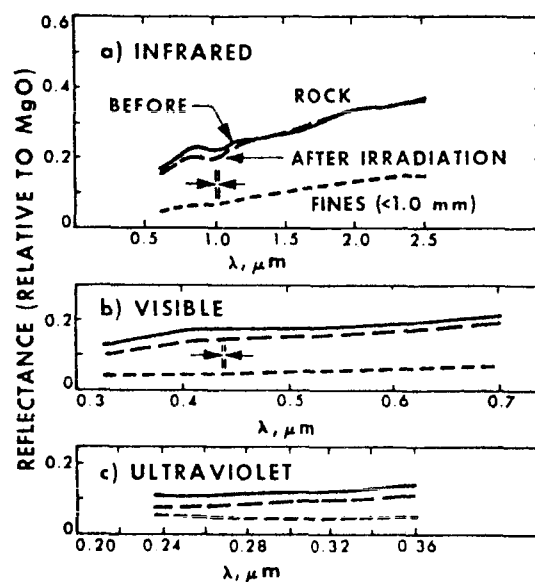


Fig. 1. Hemispherical reflectance spectra of fine grained crystalline rock 10020 (crushed to $< 50 \mu\text{m}$) before and after 2 keV proton irradiation simulating $\sim 2 \times 10^4$ yr (4×10^{18} protons cm^{-2}) solar wind bombardment. Spectra of natural lunar fines (10084) shown for comparison. Infrared curves show typical line key for other spectra. Approximate resolution is denoted by arrowtips within vertical bars.

In the visible, the spectrum of 10020 has relatively high reflectance in the blue compared to synthetic glass, in which there is pronounced enhancement in red reflectance. Comparing Figs. 1 and 2, the lunar fines (Type D) give a spectrum similar to artificial glass, but with greatly reduced spectral contrasts.

In the u.v. the spectrum of 10020 shows two subtle structures near 0.25 and $0.32 \mu\text{m}$. The reflectance of soil has a subtle minimum near $0.30 \mu\text{m}$. The spectrum of glass is essentially featureless. All of the indicated structures, however, are close to the limits of detectability.

In all spectral regions, the reflectance of both irradiated and unirradiated glass is less than that of the original crystalline sample by as much as a factor of one-third.

The experimental proton irradiations have reduced the spectral reflectance of both crystalline material and synthetic glass in the infrared below about $1.5 \mu\text{m}$, and uniformly in the visible; indicated changes in the u.v. reflectance of glass are within experimental uncertainty.

The small displacements in band position seen in spectra of irradiated material can be attributed to distortion of band shape from sloping spectral background, and not necessarily from changes in mineral or glass structure.

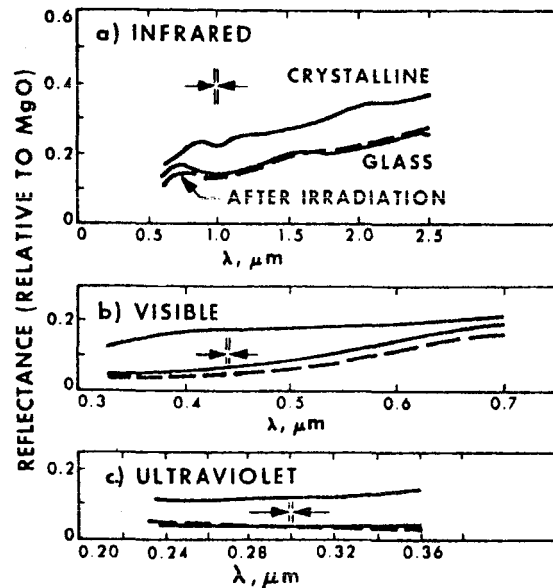


Fig. 2. Hemispherical reflectance spectra of crystalline material (10020), its glass equivalent crushed to $< 50 \mu\text{m}$, and glass after irradiation. The 2 keV proton dose is equivalent to $\sim 10^4$ yr (2×10^{19} protons cm^{-2}) exposure to the solar wind. Infrared curves show typical line key for other spectra. Approximate resolution is denoted by arrowtips within vertical bars.

The irradiation has reduced the albedo of the crystalline material from 20 to 17 per cent, and that of the glass from 8 to 5 per cent; vitrification alone changes the albedo from 20 to 8 per cent for the sample studied.

The cause of experimental proton irradiation darkening is not fully understood, but contamination by aluminum is suspected to play a role. The situation for previous experiments is discussed by NASH (1967). The contaminant films involved are estimated from thin-film measurement to be on the order of several hundred angstroms or more in thickness. Films of this dimension are not readily amenable to compositional analysis by techniques available to us, and the nature of the contaminants is uncertain. Based on the present experiments we are thus cautious in asserting that proton irradiation produces significant lunar darkening, or from study of scanning electron photomicrographs, detectable changes in microscopic surface structure.

Alternatively, vitrification may be an important darkening process. Except in the u.v., neither the experimental irradiation dose nor artificial vitrification alone has produced material with the reflectance properties of lunar fines.

Table 1. Albedo of selected lunar materials

Sample	Albedo*
Fines, <1.0 mm, gravity packed	0.061
Fines, <150 μm , gravity packed	0.069
Fines, 150–1000 μm fraction ground to <50 μm	0.075
Solid rock surface (10020, exterior bottom)	0.125
Powdered rock (10020, ground to <50 μm , gravity pack)	0.197
Powdered rock (10058, ground to <50 μm , gravity pack)	0.200

* Normal incidence illumination, 15° phase angle.

In addition to the albedo measurements of irradiated material, we have determined the albedo of some other unirradiated lunar samples available to us. The results are given in Table 1. In particular, we note the increase in albedo arising from pulverization of holocrystalline rock to values like those measured for some lunar rays (VAN DIGGELEN, 1969). These data support pulverization as one commonly accepted mechanism of lunar ray production.

Hand picked separates of plagioclase and calcium-rich clinopyroxene, each containing 15–20 per cent of the other, were prepared from our sample of 10058.

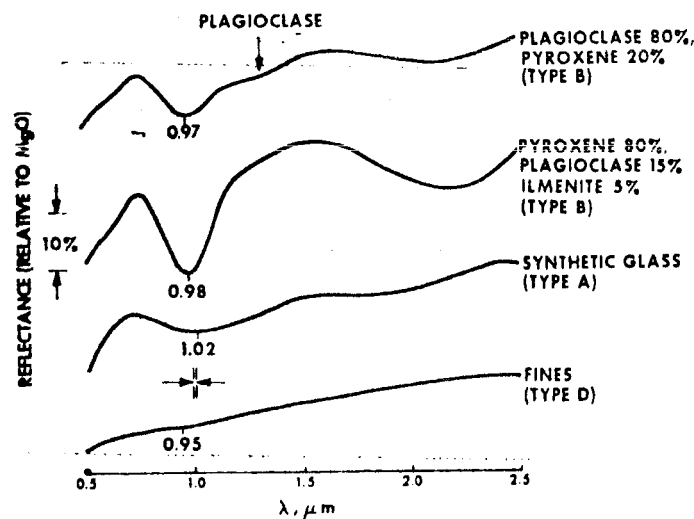


Fig. 3. Hemispherical reflectance spectra of partial separates of plagioclase and pyroxene from rock 10058 (Type B), and synthetic glass of 10020 (Type A) compared to spectrum of lunar fines 10084 (Type D).

The rock contains no olivine. [The mineralogy of 10058 is discussed by AGRELL *et al.* (1970) and HARGRAVES *et al.* (1970).] Using the spectra of these separates (Fig. 3) and glass, we can deduce the origin of some bands in the spectra of 10020, 10058 and 10084. The curve for the plagioclase-rich separate is dominated by the presence of pyroxene, but comparison of the two spectra suggests the 1.3 μm band in this spectrum

and in the spectrum of rock 10020 (Fig. 4) arises from plagioclase. Strong bands near $1.0 \mu\text{m}$ and $2.2 \mu\text{m}$ in rock 10020 are attributed mainly pyroxene. However, this rock contains 3–5% modal olivine (HAGGARTY *et al.*, 1970) which may contribute to the $1.0 \mu\text{m}$ structure. The weak inflection in our spectrum of rock 10020 near $1.7 \mu\text{m}$ is not apparent in the spectra of either plagioclase or pyroxene mineral separates (Fig. 3), and the structure does not appear in the spectrum of rock 10058 (Fig. 4). An important difference in the mineralogy of these two rocks is the absence of olivine in 10058. However, such structure is not typical of the olivines (ADAMS, 1968), nor was a

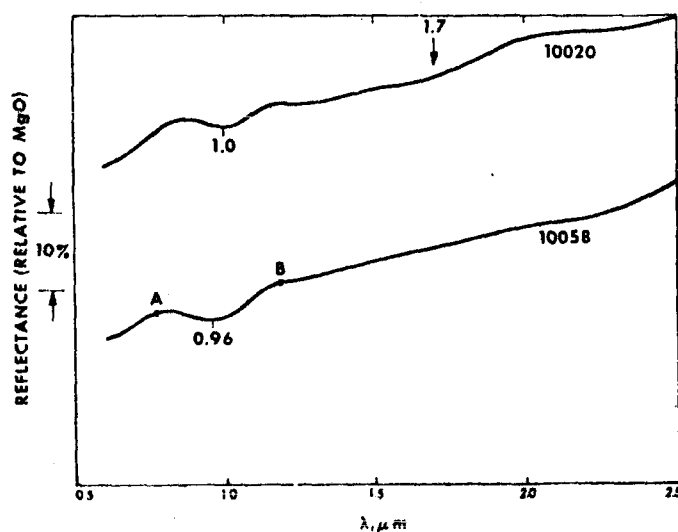


Fig. 4. Comparison of the infrared reflectance of 10058 and 10020 showing the absence of $1.7 \mu\text{m}$ structure in spectrum of 10058. A line through points A and B is background assumed for correcting apparent position of $0.96 \mu\text{m}$ band to "true" position at $0.98 \mu\text{m}$.

band at this wavelength reported by HAGGARTY *et al.* (1970) in their microscopic measurements of the absorption spectra of olivine in 10020. The rock is reported to be holocrystalline (LSPET, 1969) so that the structure cannot be attributed to glass. The origin of this feature is uncertain.

The spectrum of synthetic glass is dominated by two broad bands at $1.02 \mu\text{m}$ and $1.8 \mu\text{m}$ (Fig. 3), which is characteristic of results we have obtained with other synthetic rock glasses. By analogy with crystalline silicates (WHITE and KEESTER, 1966; BANCROFT and BURNS, 1967) and silicate melts (BURNS and FYFE, 1967) we attribute these bands to electronic transitions within Fe^{+2} ions in octahedral and tetrahedral sites in the glass structure; the breadth of the bands may arise from large variations in metal–oxygen distances in glassy vs. crystalline structures. No absorption bands are observed that are attributed to d -orbital transitions in Fe^{+3} ions.

In macroscopic appearance large fragments of the artificially fused material are black, vitreous and opaque. Powdered glass is dark brown. Microscopically individual glass fragments are transparent and yellow to red-brown in color. Analysis of iron in the sample using Mössbauer techniques shows that the ratio $\text{Fe}^{+3}/\text{total Fe} < 0.04$. There is no detectible Fe_2O_3 .

The mechanism of coloration of artificial glass 10020 and similar natural lunar glasses is an interesting question. Orange, red and brown lunar glasses are characterized by relatively high ferrous iron and titanium contents (DUKE *et al.*, 1970; KEIL *et al.*, 1970). ROSS *et al.* (1970) have reported high titanium and aluminum contents in lunar pyroxene associated with intense reddish brown color, with the valence of titanium apparently +4. It is difficult to see how $d-d$ transitions in Ti^{+3} alone or in combination with similar transitions in Fe^{+2} can account for strong blue absorption in the glasses. Alternatively, a charge transfer (ligand-metal) transition involving ionic forms of iron and titanium is an attractive possibility. Charge transfer bands are strong, and are known to occur in the near u.v. part of the spectrum (COTTON and WILKINSON, 1966), and thus can produce absorption in the blue.

From study of the mineral separate spectra, we conclude that the shoulder spanning the visible spectrum of 10020 between 0.39–0.5 μm (also in 10058) is due principally to pyroxene. However, because of the small amount of material available, and because of the impurity of the separates, some contribution to this structure from plagioclase is possible. ADAMS and JONES (1970) show a shallow absorption band in the spectrum of 10020 at 0.5 μm , which appears indistinctly in our spectrum; they attribute the band to titanium in the pyroxene.

Most absorption bands in the reflection spectra thus far presented are broad shallow structures which are distorted by contributions from other minerals present in the assemblages involved, and by sloping spectral background. The effect of mineralogy (in this instance plagioclase) is demonstrated by the apparent displacement to a shorter wavelength of the 2.2 μm band of pyroxene (Fig. 3). Corrections for spectral background require assumptions of undistorted band shape and knowledge of the undistorted background. For example, assuming symmetrical band shape and taking the background to be represented by a line connecting A–B in Fig. 4 for 10058, the true position for that structure is found to be 0.98 μm in agreement with the band position determined for pyroxene. A similar correction applied to 10020 yields a corrected band position of 1.02 μm , which from the absorption measurements on single olivine crystals in 10020 by HAGGARTY *et al.* (1970) implies some contribution to the band from olivine if the pyroxenes in 10020 and 10058 are comparable. It is not possible to analyze accurately the poorly defined band near 0.95 μm in the fines in a similar fashion; the corrected band position is determined to lie between 0.95 and 1.06 μm .

Comparison of all spectra in Fig. 3 with that of fine material (10084) suggests that the structure at 0.95 μm , the true position of which is at some longer wavelength, may arise from pyroxene and possibly glass. (Determining the contribution of glass, in the absence of olivine, hinges on accurate knowledge of band position and shape.) Other structures near 2 μm expected from these components are not present in our spectra of the fines. The contribution of olivine cannot be determined from these spectra.

COMPARISONS WITH TELESCOPIC RESULTS

MCCORD (1969), MCCORD *et al.* (1969), MCCORD and JOHNSON (1969), and JOHNSON and SODERBLOM (1970) have presented relative spectral reflectance curves between 0.4 and 1.1 μm for many areas on the lunar surface. While a great variety of curve shapes have been obtained, certain structures tend to recur in many of the results. These include maxima (or minima) near 1.0 μm , a minimum (or maximum) in the red between 0.60–0.80 μm and a maximum in the blue near 0.46 μm . The spectral reflectivity differences measured with respect to the standard area, Mare Serenitatis 2, are usually small (<5 per cent). Using our lunar samples and synthetic glass discussed previously we can make a suggestive (but necessarily qualitative)

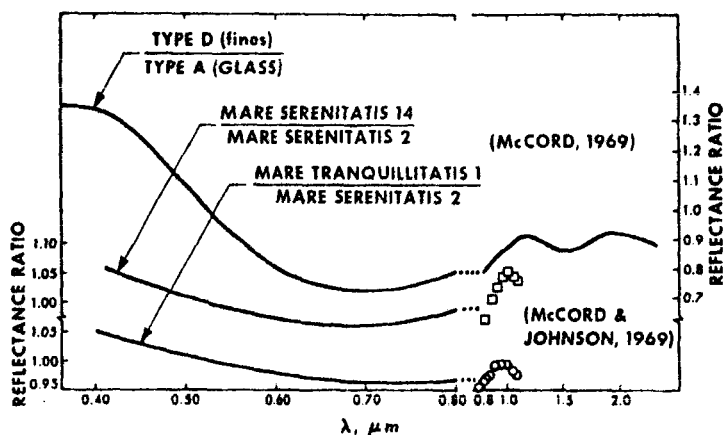


Fig. 5. Ratio of reflectance of fines 10084 (Type D, ~ 1 mm size fraction) to synthetic glass 10020 (Type A) simulating reflectance of dark lunar regions Mare Serenitatis 14 and Mare Tranquillitatis 1 relative to standard area Mare Serenitatis 2. Telescopic data from MCCORD (1969) and MCCORD and JOHNSON (1969). Ordinate scale on right refers to laboratory curve.

interpretation of some of these results. Accurate comparisons are not possible since, among other things, we are comparing laboratory hemispherical with telescopic bidirection reflectance measurements. In addition, this interpretation may not be unique.

Experimentally we have modeled the telescopic observations by using synthetically fused lunar rock (10020) as the reference material, and the lunar fines (10084) and crushed microgabbro (10058) to represent selected dark and bright lunar regions, respectively. Glass was chosen as the reference since it alone of the materials examined has a reflectance maximum near 0.7 μm , and thus will produce features near this wavelength in reflectance ratios. The reflectance ratios obtained, normalized to unity at 0.52 μm , are shown in Figs. 5 and 6.

The present interpretation then is that minima in the lunar curves at 0.7 μm arise from comparing a maximum in red reflectance in the reference area with a featureless spectrum (or one that varies relatively little with wavelength) of the source

area. The precise location of the red minimum in any instance will depend in detail on the shapes of both curves. The appearance of a maximum in the blue in bright regions depends upon the existence of a blue shoulder (or maximum) in the spectrum of crystalline material, presumably resulting from pyroxene, the precise location and shape of this feature again depending on the detailed shapes of both curves. Comparison of reflectance ratios with data of McCORD and JOHNSON (1969) beyond $0.8 \mu\text{m}$ (Fig. 5) suggests that the $1.0 \mu\text{m}$ structure seen in their data occurs in the reference area, but for the most part is not attributable to glass of the type we have made from rock 10020.

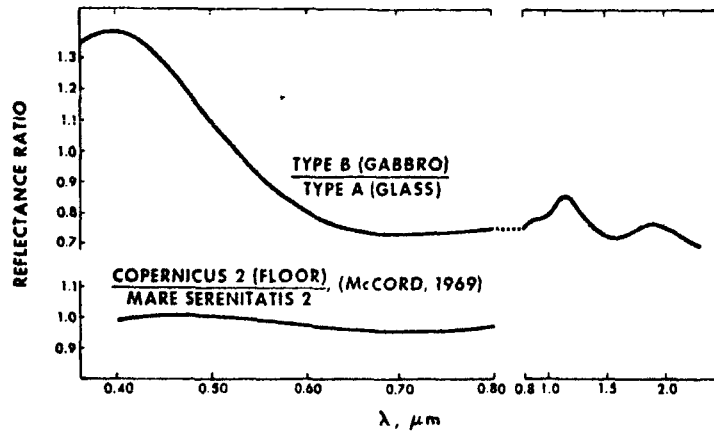


Fig. 6. Ratio of reflectance of crushed rock 10058 ($<50 \mu\text{m}$) to synthetic glass 10020 (Type A), simulating the reflectance of the bright crater Copernicus (floor) relative to standard area Mare Serenitatis 2. Telescopic data from McCORD (1969).

The contrasts in our reflectance ratios are much greater than those observed telescopically. This implies that actual reflectance contrasts on the moon are lower than our laboratory samples, perhaps because dark fines or other absorbing materials are mixed in varying amounts with crystalline rock debris on the moon's surface.

SUMMARY AND CONCLUSIONS

Spectral hemispherical reflectance measurements of Tranquillity samples and synthetic glass prepared from such samples before and after experimental proton irradiation equivalent to approximately 20,000 yr exposure to the solar wind, show that these materials darken somewhat as a result of such irradiation. The precise mechanism of darkening is not understood. Vitrification reduces the spectral reflectance in all spectral regions, and reduces the albedo to within a few per cent of average Tranquillity fines. Important absorption features in the visible and infrared spectra are attributed primarily to pyroxene. The spectral reflectance of glass in the infrared is distinct, and may contribute measurably to a subtle minimum observed near $0.95 \mu\text{m}$ in lunar fines; otherwise this structure is attributed principally to pyroxene.

Synthetic glass of rock 10020 was used as a reference material to model results of lunar telescopic observations. On our interpretation, McCORD's reference area (Serenitatis 2) shows a maximum in red reflectance (possibly due to glass), a minimum near $1.0 \mu\text{m}$, and is relatively featureless elsewhere. Some dark lunar areas resemble Tranquillity fines, and some bright areas crushed microgabbro (10058). The maxima and minima in reflectance ratios are only indirectly indicative of mineralogy.

Acknowledgments—We thank Dr. RAY GREER, WARREN RACHWITZ, CHARLES FISHER and PATRICIA CONKLIN of the Jet Propulsion Laboratory for their assistance. Mr. MIKE BENT and Dr. ROBERT VAUGHAN of the California Institute of Technology very kindly performed the Mössbauer analysis of glass and other samples for us. This paper presents the results of one phase of research carried out at the Jet Propulsion Laboratory, California Institute of Technology, under contract NAS 7-100, sponsored by the National Aeronautics and Space Administration.

REFERENCES

- ADAMS J. B. (1968) Lunar and martian surfaces: petrologic significance of absorption bands in the near-infrared. *Science* **159**, 1453-1455.
- ADAMS J. B. and JONES R. L. (1970) Spectral reflectivity of lunar samples. *Science* **167**, 737-739.
- AGRELL S. O., SCOON J. H., MUIR I. D., LONG J. V. P., MCCONNELL J. D. C. and PECKETT A. (1970) Mineralogy and petrology of some lunar samples. *Science* **167**, 583-586.
- BANCROFT G. M. and BURNS R. G. (1967) Interpretation of the electronic spectra of iron in the pyroxenes. *Amer. Mineral.* **52**, 1278-1287.
- BURNS R. G. and FYFE W. S. (1967) Crystal field theory and the geochemistry of transition elements. In *Researches in Geochemistry*, (editor P. H. Ableson), Vol. 2, pp. 259-285. John Wiley.
- COHEN A. J. and HAPKE B. W. (1968) Radiation bleaching of thin lunar surface layer. *Science* **161**, 1237-1238.
- COTTON F. A. and WILKINSON G. (1966) *Advanced Inorganic Chemistry*, 2nd edition. Interscience.
- DUKE M. B., WOO C. C., BIRD M. L., SELLERS G. A. and FINKELMAN R. B. (1970) Lunar soil: size distribution and mineralogical constituents. *Science* **167**, 648-650.
- HAGHERTY S. E., BOYD F. R., BELL P. M., FINGER L. W. and BRYAN W. B. (1970) Iron-titanium oxides and olivine from 10020 and 10071. *Science* **167**, 613-615.
- HAPKE B. (1965) Effect of simulated solar wind on the photometric properties of rock powders. *Ann. N. Y. Acad. Sci.* **123**, 711-721.
- HAPKE B. (1966) Optical properties of the moon's surface. In *The Nature of the Lunar Surface*, (editors W. N. Ness, O. H. Menzel and J. A. O'Keefe), pp. 141-154. Johns Hopkins Press.
- HARGRAVES R. G., HOLLISTER L. S. and OTALORA G. (1970) Compositional zoning and its significance in pyroxenes from three coarse-grained lunar samples. *Science* **167**, 631-633.
- JOHNSON T. V. and SODERBLUM L. A. (1969) The relative reflectivity ($0.4-1.1 \mu$) at the lunar landing site Apollo 7. *J. Geophys. Res.* Submitted for publication.
- KEIL K., PRINZ M. and BUNCH T. E. (1970) Mineral chemistry of lunar samples. *Science* **167**, 597-599.
- LSPET (1969) Lunar sample information catalogue—Apollo 11. LRL, NASA Manned Spacecraft Center, Houston, Texas.
- MCCORD T. B. (1969) Color differences on the lunar surface. *J. Geophys. Res.* **74**, 3131-3142.
- MCCORD T. B. and JOHNSON T. V. (1969) Relative spectral reflectivity $0.4-1 \mu$ of selected areas of the lunar surface. *J. Geophys. Res.* **74**, 4395-4401.
- MCCORD T. B., JOHNSON T. V. and KEIFFER H. H. (1969) Differences between proposed Apollo sites. 2. Visible and infrared reflectivity evidence. *J. Geophys. Res.* **74**, 4385-4388.
- NASH D. B. (1966) Proton-excited luminescence of silicates: experimental results and lunar implications. *J. Geophys. Res.* **71**, 2517-2534.
- NASH D. B. (1967) Proton-irradiation darkening of rock powders: contamination and temperature effects, and applications to solar-wind darkening of the moon. *J. Geophys. Res.* **72**, 3089-3104.

- NASH D. B., CONEL J. E. and GREER R. T. (1970) Luminescence and reflectance of Tranquillity samples: effects of irradiation and vitrification. *Science* 167, 721-724.
- NASH D. B. and GREER R. T. (1970) Luminescence of Apollo 11 lunar samples and implications for solar excited lunar luminescence. *Geochim. Cosmochim. Acta*, Supplement I.
- ROSS M., BENICE A. E., DWORNIK E. J., CLARK J. R. and PAPIKE J. J. (1970) Lunar clinopyroxenes: chemical composition, structural state and texture. *Science* 167, 628-630.
- VAN DIGGELEN J. (1969) A photometric investigation of the lunar crater rays. *Moon* 1, 67-84.
- WEHNER G. K., ROSENBERG D. L. and KENKNIGHT C. E. (1965) Investigation of spattering effects on the moon's surface. Ninth Quart. Status Report, 2845, Applied Science Division, Litton Systems, Inc., Minneapolis, Minn.
- WHITE W. B. and KEESTER K. L. (1966) Optical absorption spectra of iron in the rock-forming silicates. *Amer. Mineral.* 51, 774-791.
- WOOD J. A., MARVIN U. B., POWELL B. N. and DICKEY J. S., JR. (1970) Mineralogy and petrology of the Apollo 11 lunar sample. *Smithson. Astrophys. Observ. Spec. Rep.* 307.

APPENDIX I

Proceedings of the Apollo 11 Lunar Science Conference, Vol. 3, pp. 2149 to 2154.

Optical and high-frequency electrical properties of the lunar sample*

T. GOLD, M. J. CAMPBELL and B. T. O'LEARY
Center for Radiophysics and Space Research, Cornell University, Ithaca, New York 14850

(Received 12 February 1970; accepted 12 February 1970)

Abstract—Reflectivity and polarization laws for the powder sample and its spectrum are close to the mean for the lunar maria. Solid samples show a marked absorption feature at $0.92 \mu\text{m}$. The low albedo appears to be due to a surface coating on dust grains rather than to volume absorption. The high-frequency electrical properties resemble those of a fine powder made from typical dense terrestrial rocks and are consistent with previous estimates from ground-based radar observations. The differential mass spectrum is almost constant from $100\text{-}\mu\text{m}$ particles down to $0.1\text{-}\mu\text{m}$ particles; most particles are smaller than $0.3 \mu\text{m}$. Their shapes disclose a variety of processes of generation.

LUNAR dust and rock chip samples have been analyzed in the lunar laboratory of the Cornell Center for Radiophysics and Space Research; our concern has been with the optical and electrical properties of the sample and their relation to those known for the lunar surface as a whole, and with the questions surrounding the origin of the lunar dust. Four salient points have emerged.

(1) The optical scattering law and polarization properties of a surface of lunar dust generally correspond closely to these properties as observed for the moon as a whole. The rock chip sample shows a strong absorption feature at $0.92 \mu\text{m}$ which is not prominent in the lunar scattered light. It is probable, therefore, that most of the lunar surface is covered with a material similar to the powder that was investigated.

(2) The dielectric constant is within the range that had been estimated for the moon as a whole by radar methods.

(3) The particle size distribution indicates that the differential mass spectrum as a function of radius is almost constant from $100 \mu\text{m}$ down to 1000 \AA . The shapes of the particles indicate a variety of sources. Some have the sharp edges that are characteristic of fracture; others are rounded, indicating processes of melting or condensation. Some cannot readily be attributed to either of these mechanisms.

(4) The darkness of the lunar dust is mainly due to dark surface deposits on the grains, probably metallic, rather than to absorptivity of the bulk material.

The optical scattering law as a function of phase angle and the optical polarization law were measured with the same instrument that had been used for measuring many sample powders in the past and in the same manner (HAPKE, 1968). The lunar powder proved to resemble, both in appearance and in the measured optical properties, the lunar maria as observed from the earth and the terrestrial powders previously proposed (HAPKE, 1968) as being most closely representative of the moon. These powders also proved to be similar under optical microscope examination. The particle

* This article was reprinted from *Science* (Vol. 167, pp. 707-709, 1970) without further refereeing and with only minor revisions by the authors.

size was similar, the great majority of the particles being less than $10\ \mu\text{m}$ in dia. The adhesion of the small particles to each other indeed created the "dendritic growth" appearance under the microscope that has been given the name "fairy castles". It appears that the large part of the pronounced lunar opposition effect—that is, the brightness surge toward zero phase—can be attributed to the shadows cast by this lacy surface structure.

Figures 1 and 2 summarize the optical properties of the Apollo 11 samples. Each data point represents the mean of several observations of different portions of a sample, and the measurements repeated very well. In Fig. 1 the photometric phase

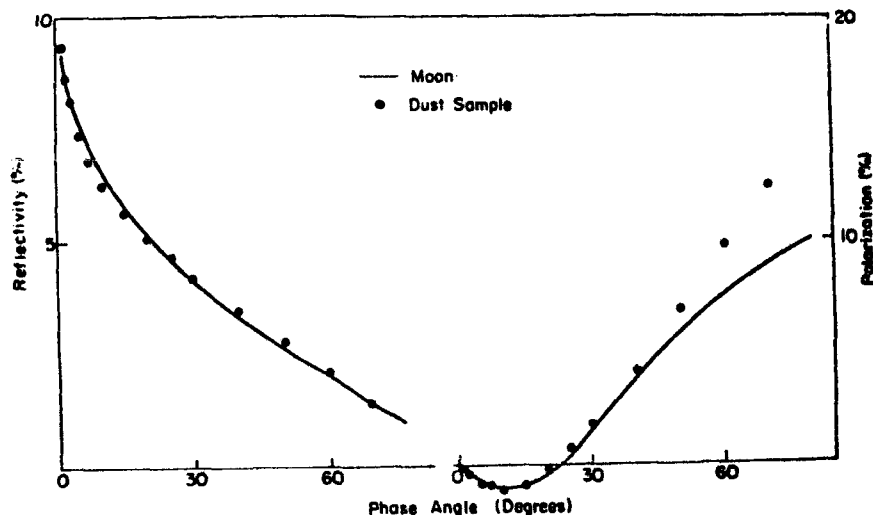


Fig. 1. The dependence of reflectivity and polarization on phase angle at wavelength of $5600\ \text{\AA}$ and at normal viewing. [Curve for the moon from HAPKE (1968), with arbitrary normalization of reflectivities.]

function of the lunar dust sample is generally steeper than the mean lunar case (HAPKE, 1968) for phase angles less than 15° , but the difference is very small. The curve for polarization plotted against phase angle (Fig. 1) also demonstrates the similarity of the dust sample to the moon as a whole, but, again, there are minor differences; the crossover from negative to positive polarization occurs at a lower phase angle, and polarization in the positive branch is greater.

The normal albedo of the dust sample at $5600\ \text{\AA}$ was measured as 10.2 ± 0.2 per cent. This value is in close accord with the value 9.96 per cent for the Apollo 11 site, as derived from Apollo 10 orbital photography (WILDEY and POHN, 1969). Moreover, in the hemispherical reflectance measurements performed on a Cary 14 spectrometer, the albedo values of the dust sample in the visible and near-infrared were similar to lunar maria values obtained from earth-based observations. Both spectra are featureless, climbing steadily in albedo from ~ 0.3 to $1.5\ \mu\text{m}$ (Fig. 2). Lunar rock chip samples were also measured on the spectrophotometer, and a strong absorption band, not present in the powder sample, appeared at $0.92\ \mu\text{m}$. A weak band in this region had previously been suggested, from earth-based observations of the moon (WATTSON

and DANIELSON, 1965; TULL, 1966). Further details of the optical properties of the Apollo 11 samples will be presented in the near future (O'LEARY and BRIGGS, 1970).

Rock powders in the size range of a few microns tend to be very light in color. Most rocks have too low an opacity to absorb much of a light ray, which is generally scattered out of the surface after having traversed only a few microns of material. Trying to account for the very low albedo of the lunar surface has been a long-standing problem, in view of the indication, from the optical scattering and polarization properties, of very small particle size, since even the darkest rocks tend to be quite light when powdered. We have previously, in this laboratory, undertaken sputtering experiments with kilovolt protons and with α -particles on powdered rock surfaces, which have indicated darkening. It has been suggested that this darkening was due

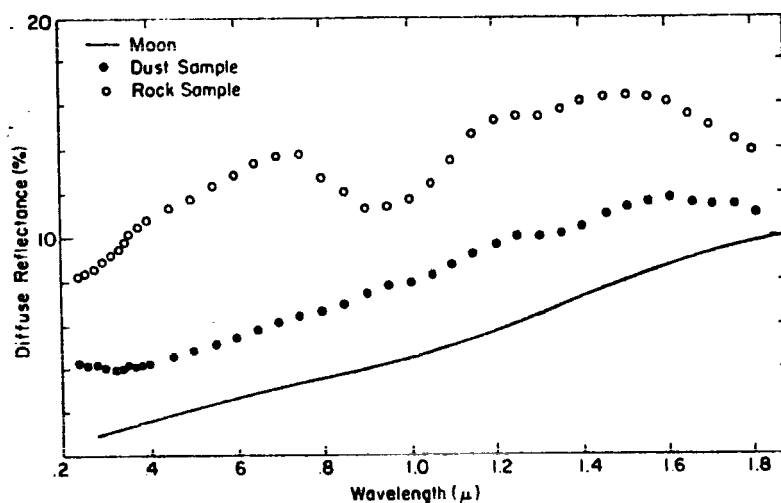


Fig. 2. The spectral reflectance of Apollo 11 lunar samples. [Curve for the moon from WATTSON and DANIELSON (1965).]

to the deposition of reduced metals, perhaps chiefly iron, on the surface as a result of the dissociation by the sputtering process, the partial escape of the oxygen, and the slowness of surface recombination limited by diffusion.

Metallic surface coatings of as little as 30 Å can provide much opacity but would make only an insignificant contribution to the bulk chemical composition. We have seen strong evidence for such coatings, but we have not yet been able to analyze them adequately. Whether they are indeed the result of sputtering or of other metal evaporation (vacuum plating) processes, or whether perhaps they are just the reduction by the hydrogen of the metallic surface layers produced by solar wind, is not yet clear. However, we have had the following indications of the presence of metallic layers.

We observed under the microscope that some larger particles in the size range 50–200 μm that could be found in the lunar soil sample had a metallic appearance, sometimes over only a certain part of their surface. Some particles could be clearly seen as translucent glass in which a well-defined area appeared metallic. One sphere, for example, looked like a honey-colored glass from one side but like a steel ball from

the other. When treated with the common acids (hydrochloric and nitric) that attack metals, the metallic appearance was generally reduced but not completely removed. Hydrofluoric acid generally tended to remove the metallic appearance entirely, even before a visible erosion of the particle had taken place.

For most of the material an optical examination is not feasible because the particles are too small. Nevertheless, when the same acids were applied to a microscopic sample of fine powder it quickly turned very much lighter, almost white. It seems likely, therefore, that in the finer material a metallic surface coating is also normally present, and responsible for the low albedo.

The measurement of a particle size distribution for such small grains is not an easy matter. The cohesion of the grains prevents analysis of the smaller sizes by sieving, as

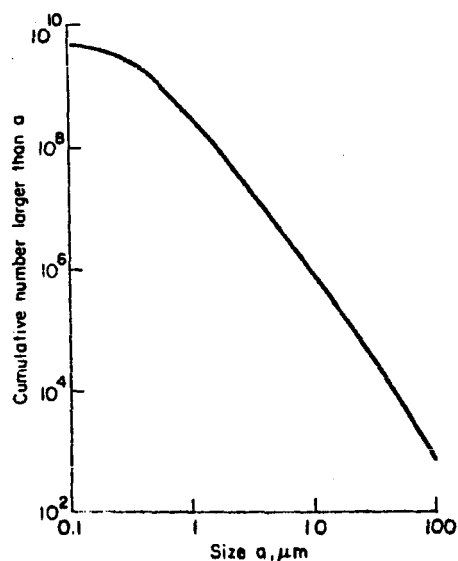


Fig. 3. The cumulative particle size distribution for the bulk sample.

was pointed out by the preliminary investigators (LSPET, 1969). We have used three techniques: (i) making microscope slides of the powder mixed into a transparent varnish and smeared out into a thin layer, which permits us to count the particles with an oil emersion microscope down to sizes of about $2 \mu\text{m}$; (ii) constructing a water sedimentation column in which the descent of particles as small as $1 \mu\text{m}$ can be photographically registered; (iii) determining the size distribution of the smallest particles from the scanning electron micrographs referred to below. The three methods give consistent results (Fig. 3).

The detailed shapes of particles can be seen to a resolution of 300 \AA in numerous scanning electron microscope pictures that were taken to see whether the origin of the material was revealed by the particle shapes.

Our studies indicate that various different effects have been active in producing the fine material. Some particles are spherical and rounded, suggesting condensation from a vapor or freezing of a liquid in free fall. Others are sharp-edged and angular,

undoubtedly the result of fracture. They lack, in general, any obvious indication of a crystalline structure, as neither cleavage planes nor preferred angles are seen. It would appear that most of the fractured material is amorphous, or, if any of it is crystalline, that the size of the crystals is below the limit of resolution.

The spherical or compact round particles seen are less frequent but may form a continuous sequence from the 100- μm range down to very small sizes. The great majority of particles in the 10- to 1- μm size range have, however, more intricate shapes that are not readily understood. There are many rounded surfaces, and yet the particle as a whole is not compact. Elongated objects with rounded ends, surfaces where the sense of the curvature often changes, rough spots occurring in smooth surfaces, and various other features argue against any single explanation—liquid droplets, condensation, or fracturing. Additional processes such as erosion by sputtering, partial melting, and partial evaporation must be considered, and scanning electron microscope study of these mechanisms is needed before all the responsible processes can be identified.

Measurements were made by means of the technique used for determining the electrical properties of terrestrial rock powders (CAMPBELL and ULRICH, 1969). The dielectric constant (ϵ') and loss tangent of lunar dust at several stages of compaction

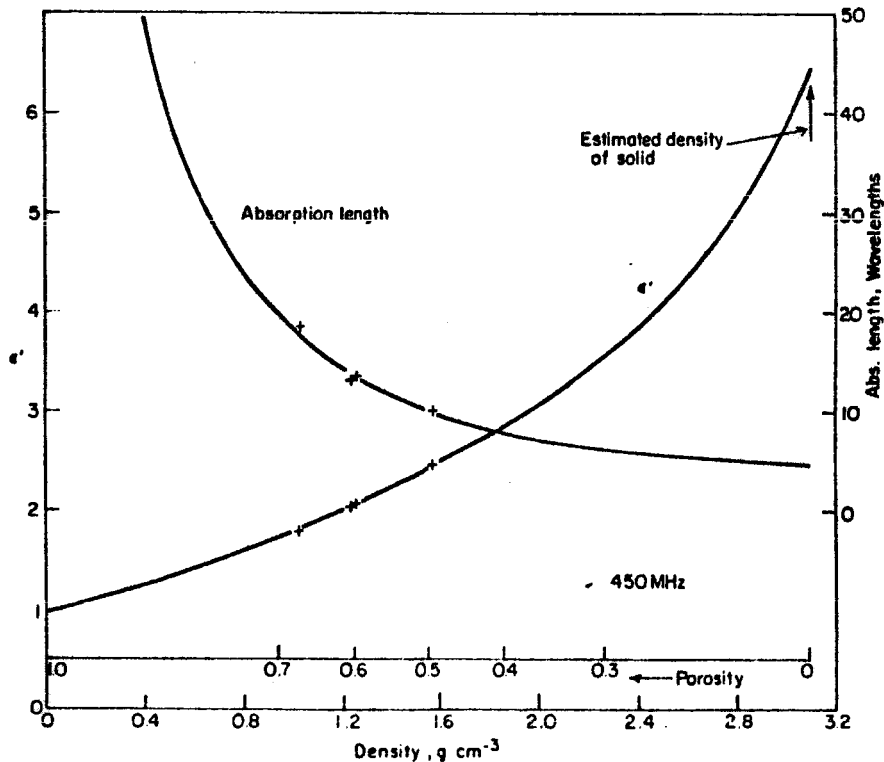


Fig. 4. The dielectric constant and absorption length of the bulk sample at 450 MHz as a function of the powder density. The solid curves are the Rayleigh formula (CAMPBELL and ULRICH, 1969). The estimated density of solid is from LUNAR SAMPLER PRELIMINARY EXAMINATION TEAM (1969).

were measured at 450 MHz. The measurement in each case included a measurement of the density of the sample, and the porosity was calculated from the quoted specific gravity of the rock of which the powder is composed (LSPET, 1969). The dielectric constant and the absorption length (Fig. 4) are consistent with the values deduced from ground-based radar (EVANS and PETTINGILL, 1963) and radiometric observations, respectively. As with terrestrial rock powders, the dielectric constant and loss tangent as a function of porosity follow the Rayleigh mixing formula and, by extrapolation, suggest a dielectric constant for the solid rock of the same composition as the lunar dust which is near the average for dense terrestrial rocks (about 7). The dielectric constant is about 3 for the dust at a typical porosity of 0.4. The absorption length at the same porosity, in this sample, is about 10 wavelengths.

Acknowledgments—This work was done under NASA contract NAS9-8018. We are grateful to Corning Glass Works for the assistance given with the electron micrography. We thank PAUL SHAPSHAK, F. BRIGGS, and J. WINTERS.

REFERENCES

- CAMPBELL M. J. and ULRICHS J. (1969). Electrical properties of rocks and their significance for lunar radar observations. *J. Geophys. Res.* **74**, 5867-5881.
- EVANS J. V. and PETTINGILL G. H. (1963). The scattering behaviour of the Moon at wavelengths of 3.6, 68, and 784 centimeters *J. Geophys. Res.* **68**, 423-447.
- HAPKE B. (1968). Lunar surface: Composition inferred from optical properties. *Science* **159**, 76-79.
- LSPET (LUNAR SAMPLE PRELIMINARY EXAMINATION TEAM) (1969) Preliminary examination of lunar samples from Apollo 11. *Science* **165**, 1211-1227.
- O'LEARY B. and BRIGGS F. (1970) Optical properties of Apollo 11 Moon samples. To appear in *J. Geophys. Res.*
- TULL R. G. (1966) The reflectivity spectrum of Mars in the near-infrared. *Icarus* **5**, 505-514.
- WATSON R. B. and DANIELSON R. E. (1965). The infrared spectrum of the moon. *Astrophys. J.* **142**, 16-22.
- WILDEY R. L. and POHN H. A. (1969). The normal albedo of the Apollo 11 landing site and intrinsic dispersion in the lunar Heiligenschein. *Astrophys. J.* **158**, L129-130.

APPENDIX J

Proceedings of the Apollo 11 Lunar Science Conference, Vol. 3, pp. 2155 to 2161.

Luminescence studies of Apollo 11 lunar samples

NORMAN N. GREENMAN and H. GERALD GROSS

Space Sciences Department, McDonnell Douglas Astronautics Company—Western Division
Santa Monica, California 90406

(Received 10 February 1970; accepted in revised form 2 March 1970)

Abstract—Luminescence measurements with ultraviolet excitation were made of four Apollo 11 lunar rocks, two terrestrial rocks (granite and gabbro), and one terrestrial mineral (willemite) by comparing the spectral curves with the curve of a barium sulfate standard. Upper limits of the efficiency in the 4000–6000 Å band with 3000 Å excitation were between 5×10^{-6} and 2×10^{-5} for the lunar samples, 2×10^{-3} for gabbro, 6×10^{-3} for granite, and 2×10^{-2} for willemite. If these are typical values for other ultraviolet excitation wavelengths, the Apollo 11 site appears to contribute little to the reported lunar luminescence. Preliminary results with excitation by the hydrogen glow discharge spectrum from the far ultraviolet through the visible, which included the Lyman-alpha line at 1216 Å, indicated that possible luminescence in the ultraviolet was produced both as strong lines and as groups of lines.

INTRODUCTION

THE PROGRAM of luminescence studies that we are conducting on the Apollo 11 lunar samples, some of the first results of which are given in this paper, has three objectives: (1) to understand how the luminescence behavior reflects the origin, history, and environment of the lunar lithologic materials, (2) to discover luminescence characteristics of the lunar rocks that might aid in geologic mapping and other lunar exploration activities, and (3) to evaluate the reports of luminescence on the moon based on earth-based astronomical observations. This last objective arose out of a proposal by LINK (1946) that, according to his interpretation of eclipse data, the light of the moon contains a luminescence component in addition to the reflected solar component. Later observations seemed to confirm this idea—in particular, those made by KOZYREV (1956), DUROIS (1959), GRAINGER (1963), and SPINRAD (1964) using the Fraunhofer line-depth technique.

In order to achieve these objectives, the luminescence spectra and efficiencies are being measured and the results compared with those of similar measurements of terrestrial rocks and minerals. The excitation sources used are those of importance in the space environment—u.v. (1216 and 2000–4000 Å), X-rays (0.4–8 Å), protons (2–150 keV), and electrons (2–150 keV). The luminescence spectra are measured from 1216 Å, or from the exciting wavelength if it is longer than 1216 Å, to 6000 Å.

The first results of this program, which are given in this paper, involve measurements with excitation by 3000 Å and by far u.v., including the hydrogen Lyman-alpha at 1216 Å. The objective of the measurements with 3000 Å excitation was to determine the luminescence spectra and efficiencies; that for the measurements with far u.v. excitation was to obtain qualitative spectral information on the luminescence, especially that in the u.v. wavelengths.

EXPERIMENTAL PROCEDURE

For the experiments with middle and near ultraviolet excitation, a Hanovia 2500 W high pressure xenon-mercury lamp was used as a source. The light first passed through a Gaertner quartz prism monochromator with a Corning 7-54 filter at the exit slit; the latter was to prevent wavelengths in the source longer than 4000 Å from entering the sample chamber as a result of scattering in the monochromator. The light from the sample then passed through a Jarrell-Ash 0.25 m grating spectrometer and finally to an EMI 9558QB photomultiplier tube. The photometer output was measured by a Keithley 417 picoammeter and recorded by a Moseley 2D-2 X-Y recorder. For some runs, a Corning 3-74 filter was placed between the sample and the entrance slit of the Jarrell-Ash. This filter was to cut out second orders and scattering of wavelengths shorter than 4000 Å. A wavelength band of about 200 Å full width at half maximum, centered at about 3000 Å, was used for excitation. The band from 2000-6000 Å was recorded, but luminescence could be determined only over the band from about 3500 to about 5500 Å for runs without the 3-74 filter because of the intensity of the first and second order peaks of the excitation wavelength; the luminescence could be determined only over the band from about 4000-6000 Å for runs with the 3-74 filter because of the cutoff at 4000 Å.

The experiments with far u.v. irradiation, including hydrogen Lyman-alpha (1216 Å) at an intensity approximating that from the Sun at the top of the earth's atmosphere, were made with the full spectrum of emission from the hydrogen glow in a capillary-flow direct current discharge lamp (Hunter version). A magnesium fluoride window was placed between the source and the sample to prevent hydrogen gas from entering the sample chamber. The light from the sample was recorded in a way similar to that for the middle and near u.v. measurements except that the Jarrell-Ash spectrometer was flushed with nitrogen to allow the passage of the far ultraviolet, and an EMR 541-F-08 solar blind photomultiplier, with a principal range of sensitivity from 1050-3500 Å, was used in a photon-counting mode with a Solid State Radiations Laboratories Series 1100 photon counter. In this mode, the signals were of the order of 10^3 counts per second, and the dark count was about seven counts per second.

The samples were mounted on a 12-position turntable inside a vacuum chamber. Six samples from four lunar rocks were included as follows:

Coarse-grained igneous: 10044-38 (exterior) and 10044-53 (interior)
 Fine-grained igneous: 10022-55 (surface) and 10057-45 (interior)
 Breccia: 10048-36 (interior) and 10048-37 (bottom).

The exposed surface area ranged from a little less than one to a little less than two square centimeters. Terrestrial comparison samples consisted of granite from the El Capitan formation, Mariposa County, California; gabbro from near San Marcos, San Diego County, California; and willemite from Franklin Furnace, New Jersey, the latter a highly luminescent mineral. The compositions of the two rocks, determined from thin-section study, are:

Granite: 10% quartz, 5% K-feldspar, 60% plagioclase (An_{30}), and 25% biotite.

Gabbro: 13% K-feldspar, 63% plagioclase (An_{48}), 15% biotite, 3% hornblende (mostly as alteration product of augite), and 6% augite

As the feldspars and quartz show much higher luminescence efficiencies than the ferromagnesian minerals (GREENMAN and MILTON, 1968; NASH, 1966), the gabbro is somewhat similar to the lunar rocks in luminescent mineral content, but important differences exist, chiefly in that the lunar rocks contain no K-feldspar, have more calcic plagioclase, and have more abundant nonluminescent components—ferromagnesians, ilmenite—relative to the feldspar (LSPET, 1969). The remaining three turntable positions were occupied by a barium sulfate surface to serve as a reflectance standard, a thermopile for absolute energy calibration, and an aluminized mirror for comparing source and sample spectra in the far ultraviolet measurements.

DATA ANALYSIS AND RESULTS

Irradiation at 3000 Å

Figure 1 shows the spectrum of willemite, which has a relatively high efficiency, about 2×10^{-2} ; the luminescence, which peaks at about 5200 Å, is clearly seen above a low background and separated from the second order peak of the 3000 Å exciting line. The luminescence efficiencies of the other eight samples proved to be too low to give so distinct a spectrum. As a result, the sensitivity of the detector had to be increased by at least an order of magnitude to obtain a usable signal. This served

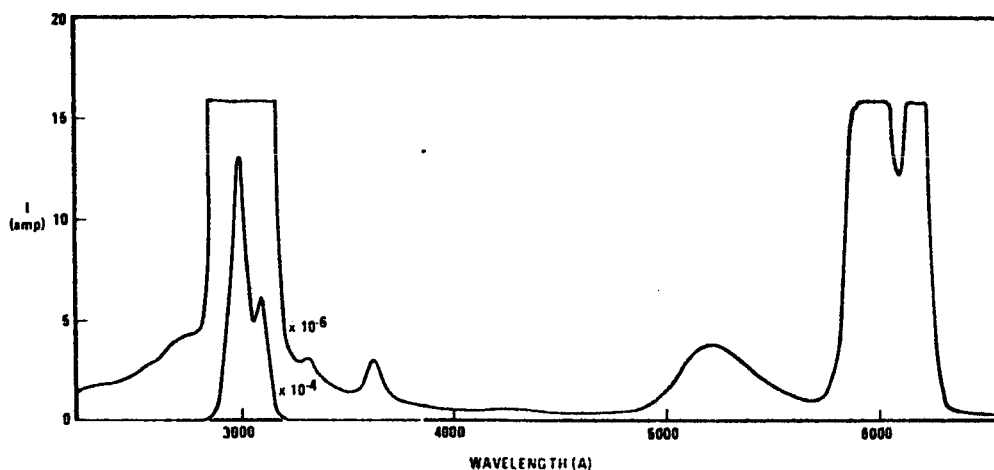


Fig. 1. Luminescence of willemite. Luminescent band with peak at about 5200 Å stands out clearly. Peaks at 3000 and 6000 Å are the first and second order, respectively, of the exciting line. Small peaks at about 3300 and 3600 Å are stray light background from the monochromator; they originate from strong lines in the source.

to amplify scattered light, small amounts of light at visible wavelengths passing through the 7-54 filter, and other effects, so that the signal was background-limited. Therefore, to extract the luminescence signal, a technique of comparing the sample curve with that of the barium sulfate standard was used.

The barium sulfate has a reflectance of very nearly 100 per cent over the wavelength band recorded (2000-6000 Å) and is not known to have any significant luminescence in this band. Its curve, therefore, represents the spectrum of the light impinging on the sample. As a first order correction, it was assumed that a sample with no luminescence would yield a curve that would be in constant proportion to the barium sulfate curve. This assumption is justified by the almost constant ratios of sample and standard curves (Figs. 2 and 3) and by the almost constant reflectance values of the lunar material (ADAMS and JONES, 1970; GEAKE *et al.*, 1970; NASH *et al.*, 1970) and of the granite and gabbro (our unpublished data) over the wavelength band investigated. The sample and standard ratios were calculated and the minimum values (consistent with the published reflectance values) were taken to represent zero luminescence. The wavelengths at which the ratio exceeded the minimum were then considered to be those at which luminescence could have occurred; the currents

Therefore, the background in the curves without the filter must be almost entirely light of wavelengths less than 4000 Å scattered within the system. The maximum luminescence efficiencies were, as a result, calculated from the curves taken with the filter. In the case of the five lunar samples for which such curves were not taken, the apparent efficiency values from the curves without filter were reduced by a factor of 20, the ratio of without-filter and with-filter efficiencies for 10044-53 and gabbro. This seems justified on the basis of the general similarity in both intensity and spectral character of all the lunar samples and of the lunar samples with the gabbro. Table 1 shows the

Table 1. Luminescence efficiencies (4000-6000 Å band) and spectral features (3500-6000 Å band) of lunar and terrestrial rocks and minerals with 3000 Å irradiation

Sample	Efficiency upper limit	Peak wavelengths (Å) in order of decreasing intensity	
		Without 3-74 filter	With 3-74 filter
Lunar:			
10044-38	10^{-8}	5400, 3700, 4000-4200, 5000	
10044-53	10^{-8}	5400, 3700, 4000-4400, 5000	5500, 4300, 5000, 4800
10022-55	10^{-8}	3600, 5300, 3800, 4200, 5000	
10057-45	2×10^{-8}	5400, 3600, 4000-4200, 5000, 4400	
10048-36	5×10^{-8}	3600, 5400 (?), 4000, 4400, 5000 (?)	
10048-37	5×10^{-8}	3700, 5400, 4000, 4400, 5000	
Terrestrial:			
Granite	6×10^{-8}	5400, 4000, 5000, 4700, 3600	4300, 5800 - 6300*
Gabbro	2×10^{-8}	5400, 4000, 4800, 5000, 3600	5600-6300*, 4200-4400
Willemite	2×10^{-8}	5300	5300

* Extrapolated upper limit.

maximum efficiencies over the 4000-6000 Å band of all the samples, together with the wavelength regions of possible luminescence in both the without-filter and with-filter curves. These are total luminescence efficiencies; that is, the ratio of energy in the luminescent band to energy in the 3000 Å line about 200 Å wide incident upon the sample. As residual background effects could still be present in the data, the tabulated luminescence efficiencies are to be considered as upper limits for the conditions of this set of measurements.

Irradiation including the far ultraviolet

To analyze the data from the measurements with far u.v. irradiation, the sample curves were compared with those from the barium sulfate and aluminum mirror surfaces. The results indicate that luminescence was possibly produced in the samples

Table 2. Wavelengths of possible emission (1050–4500 Å) observed with hydrogen glow discharge irradiation (1120 Å and longer)

Sample	Lines (Å)	Groups of lines (Å)
Lunar:		
10044-38	2840, 3260	2600–3700
10044-53	1140, 1180, 1240, 1440, 1800, 2120, 2430, 2545, 2570, 3420, 3660, 3900	1050–1600, 1700–2600, 2700–4100
10022-55	—	1050–1960, 2620–4170
10057-45	3720, 4140, 4290, 4490	1050–1950, 2600–3160
10048-36	2100, 2550, 2740, 2760, 2845, 3280, 3840, 4040	1050–1700, 2580–4320
10048-37	1500, 1745, 2625, 2655, 2820, 3540, 4140	1220–1760
Terrestrial:		
Granite	1240, 1320, 1500, 1570, 2040, 2070, 2820, 3120, 3150	2540–3060, 3420–4500
Gabbro	1330, 1490, 1770, 2020, 2100, 2320, 2570, 2910, 3840	1050–2080, 2720–3140, 3300–4230
Willemite	1500, 3470, 4070	2520–3160

both as isolated strong lines and as groups of lines of higher intensity than the comparison spectrum. These data are tabulated in Table 2.

DISCUSSION

The outstanding feature of the lunar sample luminescence is the low values of the efficiencies. These results agree with those of GEAKE *et al.* (1970) and NASH *et al.* (1970), who found no luminescence in the lunar rocks with middle and near ultraviolet excitation. The efficiencies are comparable to or less than the ones for terrestrial rocks that we and Nash measured with protons and that we measured with electrons and X-rays; they are also much lower than those we estimated for terrestrial rocks with the 1800–2200 Å excitation band by a less refined filter method (GREENMAN *et al.*, 1965; NASH, 1966).

In our earlier study, on the assumption of a one per cent efficiency for the 1800–2200 Å excitation band, we calculated that the level of lunar luminescence would be five per cent of the reflected background in the 2200–2500 Å band. This was the average intensity observed around 3950 Å by GRAINGER (1963), who made the most accurate line-depth measurements of the moon. The efficiencies we measured in this study of the Apollo 11 lunar samples are more than two orders of magnitude lower than that we assumed earlier; in a similar calculation they would predict a level of luminescence that would be undetectable by the line-depth technique. If our further studies with excitation at other ultraviolet wavelengths and with proton, electron, and X-ray excitation show no greater efficiencies than these, the Apollo 11 landing area can be considered to contribute nothing to the luminescence reported from the line-depth observations. GRAINGER's observations did not include the Apollo 11 landing area; if correct, they imply higher luminescence efficiencies on other areas of the moon.

Terrestrial gabbros, which are similar in composition to the Apollo 11 rocks, are found to possess low luminescence efficiency as compared to granites; this is evident also from the data in Table 1. Thus, other lunar areas, especially in the highlands, could contain rocks of higher efficiency than those from Apollo 11. For example, the Surveyor 7 alpha-scattering analysis measured less than half as much iron, a luminescence-quenching element, at the Tycho site than was measured at the Surveyor 5 and 6 mare sites (TURKEVICH *et al.*, 1969). Therefore, samples from many areas of the moon need to be studied in order to characterize the luminescence of the lunar rocks and to understand its significance.

Acknowledgments—We wish to thank M. W. WEGNER, W. M. HANSEN and A. D. PINKUL for their assistance. This work was supported by NASA Contract NAS9-7966.

REFERENCES

- ADAMS J. B. and JONES R. L. (1970) Spectral reflectivity of lunar samples. *Science* **167**, 737-739.
- DUBOIS J. (1959) Contributions a l'étude de la luminescence lunaire. *Roz. Cesk. Akad. Ved* **60**, 1-42.
- GEAKE J. E., DOLLEFUS A., GARLICK G. F. J., LAMB W., WALKER C., STEIGMANN A. S. and TITULAER C. (1970) Luminescence, electron paramagnetic resonance and optical properties of lunar material. *Science* **167**, 717-720.
- GRAINGER J. F. (1963) Lunar luminescence investigations. *Astron. Contrib. Univ. Manchester, Series III*, No. 104.
- GREENMAN N. N., BURKIG V. W., GROSS H. G. and YOUNG J. F. (1965) Feasibility study of the ultraviolet spectral analysis of the lunar surface. Douglas Aircraft Co. Rep. SM-48529.
- GREENMAN N. N. and MILTON W. B. (1968) Silicate luminescence and remote compositional mapping. Proceedings of the Sixth Annual Meeting of the Working Group on Extraterrestrial Resources, NASA SP-177, 55-63.
- KOZYREV N. A. (1956) The luminescence of the lunar surface and the intensity of solar corpuscular radiation. *Izv. Crimean Astrophys. Obs.* **16**, 148-158.
- LINK F. (1946) Sur la luminescence lunaire. *Compt. Rend.* **223**, 976.
- LSPET (LUNAR SAMPLE PRELIMINARY EXAMINATION TEAM) (1969) Preliminary examination of lunar samples from Apollo 11. *Science* **165**, 1211-1227.
- NASH D. B. (1966) Proton-excited silicate luminescence: experimental results and lunar implications. *J. Geophys. Res.* **71**, 2517-2534.
- NASH D. B., CONEL J. E. and GREER R. T. (1970) Luminescence and reflectance of Tranquillity samples: effects of irradiation, and vitrification. *Science* **167**, 721-724.
- SPINRAD H. (1964) Lunar luminescence in the near ultraviolet. *Icarus* **3**, 500-501.
- TURKEVICH A. L., ANDERSON W. A., ECONOMOU T. E., FRANZGROTE E. J., GRIFFIN H. E., GROTCHE S. L., PATTERSON J. H. and SOWINSKI K. P. (1969) The alpha-scattering chemical analysis experiment on the Surveyor lunar missions. Surveyor Program Results, NASA SP-184, 271-350.